UNIVERSITY OF CALIFORNIA

Los Angeles

An essential role for heme in miRNA processing

A dissertation submitted in partial satisfaction

of the requirements for the degree

Doctor of Philosophy in Molecular, Cellular, and Integrative Physiology

by

Sara Hillary Weitz

2015

ABSTRACT OF THE DISSERTATION

An essential role for heme in miRNA processing

by

Sara Hillary Weitz

Doctor of Philosophy in Molecular Cellular and Integrative Physiology

University of California, Los Angeles, 2015

Professor Shimon Weiss, Chair

MicroRNAs (miRNAs) are essential regulatory molecules that function to block translation as part of the miRNA-Induced Silencing Complex. Mature miRNAs are produced through a series of cleavage steps following transcription of the primary miRNA transcript (pri-miRNA). pri-miRNAs are recognized and cleaved by the Microprocessor complex that is composed of the RNA-binding protein DiGeorge Critical Region gene 8 (DGCR8) and the ribonuclease III enzyme Drosha. Biochemical characterization of recombinant DGCR8 expressed in E. coli indicated a Fe(III) heme cofactor. However, it is not clear whether this interaction is biologically relevant. Work described in this dissertation concerns the development of a live-cell fluorescence-based assay for measuring the cleavage efficiency of pri-miRNAs. I extensively validate the assay and show that it faithfully indicates intracellular activity of DGCR8. I then use this assay to answer a series of questions about pri-miRNA processing that in the past was not easily addressed in mammalian cells. I show that heme is required for DGCR8 activity in

cells. DGCR8 binds this cofactor through its RNA-binding heme domain (Rhed) that also directly contacts the pri-miRNA hairpin. My work indicates that the RNA-binding interface is important for pri-miRNA processing in cells. Biochemical screens of metalloporphyrins indicated that Co(III) protoporphyrin IX (PPIX) binds and activates DGCR8. My work clearly indicates that Co(III) activates pri-miRNA processing in HeLa cells. I have also studied a variety of Fe(III) protoporphyrins with modifications at the vinyl group on the ring. Only the porphyrins with small modifications, such as Fe(III) mesoprotoporphyrin IX and 2,4-dimethyldeuteroproporphyrin IX, retain the high potency of activating processing, suggesting that the vinyl group is involved in contacting DGCR8. Finally, by testing the activity of DGCR8 mutants with reduced affinity for heme to various degrees, and under various heme stressed cell culture conditions, I estimate that cellular Fe(III) heme availability is very low, likely to be in the picomolar range. This estimate is consistent with the high affinity of DGCR8 for Fe(III) heme. A detailed description of how to perform the cellular miRNA processing assay is also included. My study demonstrates that the cellular pri-miRNA processing assay is a powerful tool to understand the mechanism of pri-miRNA processing and how processing may be regulated by small molecules.

This dissertation of Sara Hillary Weitz is approved.

Feng Guo

William M Gelbart

Xinshu Xiao

Shimon Weiss, Committee Chair

University of California, Los Angeles

2015

Dedicated to my Mom and Dad,

who always believed I could do

anything I set my mind to.

TABLE OF CONTENTS

LIST OF FIGURES

ACKNOWLEDGEMENTS

This work would not have been possible without the tremendous support of both Feng Guo and Shimon Weiss. Though Feng began as a collaborator, his enthusiasm for the imaging tools used in Shimon's lab and willingness to support my work and training shifted his role to that of co-mentor. This collaboration was extremely fruitful in both our collective scientific advancement and in my own personal training. I am deeply grateful for everything that both Shimon and Feng taught me.

Chapter 2 is a reprint of the original article published in PNAS in January 2014. Based on the updated copyright terms of the PNAS journal, because I am an author on the paper, I am allowed to reprint the article without further permission. I would like to acknowledge my co-authors on this paper Ming Gong and Ian Barr. Their specific contributions are detailed in the chapter. I would also like to thank Phil Sharp at MIT for providing us with the bi-directional reporter plasmid.

Chapter 3 is a reprint of the original article published in Cell Reports in June 2014. Because this article was published as open access, permission to reprint was not needed. Jen Quick-Cleveland spearheaded this project. Other co-authors on this project include Jose Paul Jacob, Grant Shoffner, and Rachel Senturia and their specific contributions are described in the chapter.

Chapter 4 is the unpublished manuscript describing the use of Co(II)PPIX to activate DGCR8 *in vitro*, in human cells, and in mouse neurons. Ian Barr performed all *in vitro* analyses. I performed the work in human cells. Talia Atkin and PeiKen Hsu from Joseph Gogos and Maria and Maria Karayiorgou groups at Columbia University performed the mouse neuron work.

Chapter 5 is the unpublished work describing how derivatives of the protoporyrin ring in Fe(III) heme can activate DGCR8. Jose Paul Jacob is the lead on this project and he performed all of the biochemical characterization of the heme derivatives. Chapter 6 describes my work to determine cellular Fe(III) heme availability using the cellular pri-miRNA processing assay. Jen Quick-Cleveland helped tremendously with this study by characterizing DGCR8 mutants *in vitro*. Jose Paul Jacob performed *in vitro* processing assays and provided technical support. Ian Barr contributed the heme on-rate measurements.

During my graduate career I had three amazing undergrads Msgana Tamrat, Antione Kohl and Neha Prakash whom I thank for technical assistance. I was supported by the NIH Chemistry-Biology Interface Training Grant (T32GM008496) and the UCLA Dissertation Year Fellowship. This dissertation was also supported by grants from the National Institutes of Health to Feng Guo (GM080563) and Shimon Weiss (GM069709).

VITA

B.S. with Honors, Biochemistry/Chemistry 2004 - 2008

University of California-San Diego, *San Diego, CA*

PUBLICATIONS

Sara H. Weitz, Ming Gong, Ian Barr, Shimon Weiss and Feng Guo. Processing of microRNA primary transcripts requires heme in mammalian cells. *Proceedings of the National Academy of Science USA* 111, 1861-1866 (2014).

Jen Quick-Cleveland, Jose P. Jacob, **Sara H. Weitz**, Grant Shoffner, Rachel Senturia and Feng Guo. The DGCR8 RNA-binding heme domain recognizes primary microRNAs by clamping the hairpin. *Cell Reports* 7, 1994-2005 (2014).

Ian Barr, **Sara H. Weitz**, Talia Atkin, PeiKen Hsu, Maria Karayiorgou, Joseph Gogos, Shimon Weiss, and Feng Guo. Cobalt (III) protoporphyrin activates the DGCR8 protein and can compensate microRNA processing deficiency (under review).

Sara H. Weitz, Jen Quick-Cleveland, Jose P. Jacob, Ian Barr, Rachel Senturia, Shimon Weiss, and Feng Guo. The pool of available Fe(III) heme in mammalian cells (submitted).

AWARDS and GRANTS

NIH Chemistry-Biology Interface Training Grant 2010 - 2013

University of California-Los Angeles

Outstanding Poster Award, *Molecular Biology Institute* Oct 2010

Annual Retreat

Prof. R. Rahamimoff Travel Grant Jan 2012

Binational Science Foundation

Dissertation Year Fellowship 2014

University of California-Los Angeles

Outstanding Student Talk, *Molecular Cellular and Integrative* Feb 2014

Physiology Retreat

CHAPTER 1

Introduction

Processing of miRNA

MicroRNA (miRNA) are small non-coding RNAs (~22nt long) that regulate genes via mRNA degradation or translation inhibition[1,2]. The first miRNA was discovered in *C. elegans* by Victor Ambrose in 1993[3]. Since then, research on miRNAs has expanded tremendously. It is now estimated that there are ~2000 miRNAs in humans that regulate nearly every protein-coding gene[4]. Their function extends to many biological systems from development to immunology to circadian rhythm and their dysregulation can lead to diseases including cancer[5–9]. miRNA are produced from transcription of a miRNA gene or an intron of a protein-coding gene followed by two cleavage steps in the nucleus and the cytoplasm respectively (Fig. 1-1).

Transcription of a miRNA gene produces the primary miRNA transcript (pri-miRNA) with the mature miRNA residing in its hairpin structure[10]. The pri-miRNA hairpin is recognized by the RNA-binding protein DGCR8 (DiGeorge critical region gene 8) or Pasha (the fly and worm homologs of DGCR8) and is then cleaved at two staggered sites about 10bp from the base of the hairpin by the ribonuclease Drosha[11–15]. The resulting precursor miRNA (pre-miRNA) is exported into the cytoplasm by Exportin-5 where it is processed further by another ribonuclease Dicer, which cleaves off the top of the hairpin[16,17]. One strand is then selectively loaded into the miRNA-induced silencing complex (miRISC) while the other strand is typically degraded[18]. Using residues 2 – 7 of the miRNA (called the seed region), miRISC binds to complementary mRNA and targets them for

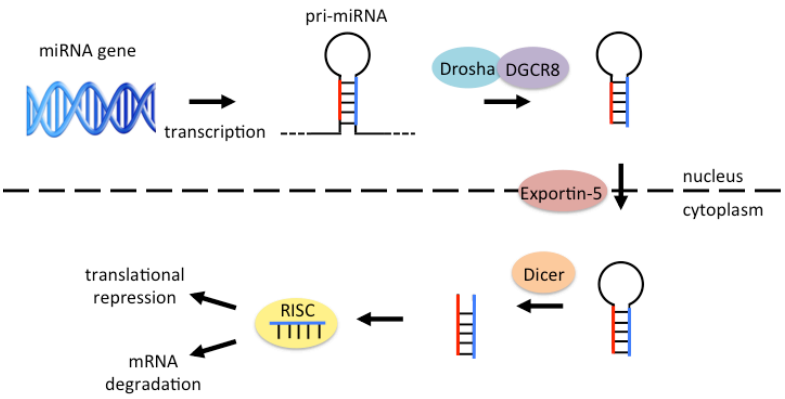

Figure 1-1. Schematic of miRNA processing

degradation or translational inhibition[19]. There is still some debate in the field as to which mechanism is predominating but recent evidence suggests that mRNA destabilization is more prevelent[20].

Regulation of pri-miRNA processing

Because miRNAs function in such a wide array of biological processes, their production is tightly regulated. pri-miRNA processing is crucial for determining miRNA abundance and several mechanisms exist for controlling pri-miRNA cleavage by Drosha and DGCR8[21]. One mechanism is the cross-regulation between Drosha and DGCR8[22,23]. *DGCR8* mRNA contains two pri-miRNA-like hairpins, which can be cleaved by Drosha. The cleavage results in a reduction of DGCR8 protein expression. Conversely, DGCR8 stabilizes Drosha through protein-protein interactions. This auto-regulatory pathway for Microprocessor balances the efficiency and specificity of its activity by effectively tuning Microprocessor levels to those of its pri-miRNA substrates[24].

The activity of Drosha and DGCR8 can also be controlled by post-translational modifications. Deacetylation of DGCR8 by histone deacetylase 1 (HDAC1) increases the affinity of DGCR8 for pri-miRNAs[25]. Acetylation of Drosha stabilizes the protein and inhibits its degradation[26]. DGCR8 can also be phosphorylated at numerous sites, which increases its stability[27]. In addition, Drosha requires phosphorylation for its nuclear import[28,29].

Several RNA-binding proteins have been identified as regulatory proteins of miRNA processing. Interestingly, many of these proteins only support the processing of a specific subset of miRNA. The DEAD box helicase protein DDX1 interacts with Drosha and promotes expression of a subset of miRNAs including all members of the miR-200 family[30]. SMAD proteins are able to

control processing of miR-21 through their interaction with the RNA helicase p68[31,32]. More recently, the RNA-binding protein Rbfox3 was shown to either promote or block processing of a subset of pri-miRNAs by binding to different positions on the pri-miRNA hairpin[33].

Assays for studying pri-miRNA

One of the most common ways to study pri-miRNA processing is *in vitro*. The components of the pri-miRNA processing machinery can either be immunoprecipitated from cellular nuclear extracts or overexpressed and purified from *E. coli*. Either immunoprecipitated or purified protein components are then added to a radiolabeled pri-miRNA and the resulting cleavage is observed on a gel. Though this technique is quite powerful, the field was missing a reproducible assay for studying miRNA processing in cells.

Studying pri-miRNA processing in cells has been technically challenging. Mature miRNAs are generally long-lived molecules, thus the abundance of miRNAs does not change dramatically unless cells grow during proliferation or differentiation. Furthermore, the Drosha-cleavage step is coupled to cell growth in certain cell types[34]. Finally, unprocessed pri-miRNAs seem to be degraded quickly via a pathway not well understood, and hence do not greatly accumulate. Two cellular reporter assays for pri-miRNA processing have been previously described; one is based on a fluorescent protein while the other luciferases[35,36]. The fluorescence assay is composed of a GFP-pri-miRNA fusion construct that is infected into various cell lines[35]. This assay suffers from the lack of a normalization factor to overcome variability in fluorescent protein expression due to processes unrelated to pri-miRNA processing. The second system utilizes a firefly luciferase-pri-miRNA fusion and normalizes the firefly luciferase signal to that of Renilla luciferase expressed from a co-transfected plasmid[36]. However, single cell resolution and the

possibility for real time experiments are lost with the use of luciferase assays. This dissertation describes my development of a cellular pri-miRNA assay using a bi-directional fluorescence reporter that allows robust data analyses at single-cell resolution. This assay has become incredibly useful and I will describe herein its many applications. In Chapter 7, I also provide a detailed protocol on how to perform the assay.

DGCR8 binds heme

Processing of the pri-miRNA transcript has been shown to occur co-transcriptionally[37,38]. How cells recognize the pri-miRNA hairpin with so many other RNA molecules within a cell, many of which also have a hairpin structure, has been the subject of debate[39–41]. The first pri-miRNA processing enzyme, Drosha, is unable to recognize and cleave pri-miRNAs without its binding partner DGCR8. It is thought that DGCR8 is responsible for recognizing and binding pri-miRNAs and for directing Drosha to the proper cleavage sites, making DGCR8 an essential component of the canonical miRNA biogenesis pathway.

DGCR8 is 773 amino acids long. The Guo lab made a truncated form of DGCR8 (called NC1, amino acid 276-751) that has the nuclear localization signal and low complexity regions deleted (Fig. 1-2)[42]. When purified NC1 had a yellow color, which indicated the presence of a cofactor. Further analysis of NC1 demonstrated that this cofactor was heme. The Guo lab performed extensive biochemical characterization of DGCR8 and its heme cofactor. The DGCR8 protein forms a dimer with the heme held by the two DGCR8 subunits[43]. DGCR8 associates with Fe(III) heme and only Fe(III) heme not

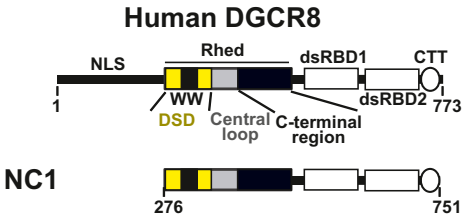

Figure 1-2. Domain structure of full-length human DGCR8 and the truncation construct NC1

Fe(II) heme is able to activate DGCR8 activity[44]. DGCR8's interaction with Fe(III) heme is very stable. When DGCR8 was incubated at room temperature with an large excess of heme scavenger protein apomyoglobin, DGCR8 held onto its heme even after 4 days making the off-rate unable to be measured (Fig. 1-3)[45].

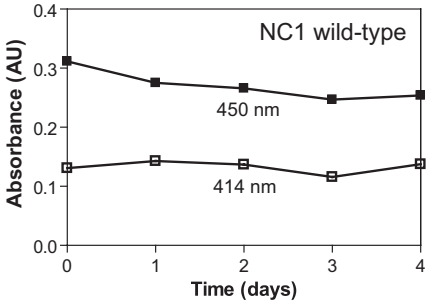

Figure 1-3. Incubation of apomyoglobin with DGCR8 to measure heme off-rate. 450 nm is the peak for heme bound DGCR8. 414 nm is the peak for heme bound myoglobin. Even after 4 days no change in absorbance at 450 nm is observed. This data was originally published by Ian Barr et. al.[45]

DGCR8 binds the heme cofactor using Cys352 residues from each subunit of the dimer. The Guo lab was able to produce crystals and solve the structure of a portion of the protein, the dimerization sub-domain (a.a. 276-353) at 1.7Å resolution[46,47]. Interestingly, four residues, Cys352 and Trp329 from both subunits, cluster on a common surface in the structure, suggesting a direct binding site for heme. The heme-free C352A, W329A and W329H mutants in the context of NC1 display substantially reduced pri-miRNA processing activity *in vitro*. There was a pressing need to demonstrate an *in vivo* function of heme in pri-miRNA processing.

In Chapter 2, I use my live-cell pri-miRNA processing assay to show that heme is required for pri-miRNA processing in cells. DGCR8 uses the binding motif "IPCL" to ligate the heme and mutation of any of these residues results in an elimination of cellular activity. In Chapter 3, we demonstrate that DGCR8 contains an independently folded domain that binds both heme and pri-miRNA, which we've named the RNA-binding heme domain (Rhed). The Rhed domain recognizes key structural features of pri-miRNA hairpins and is required for pri-miRNA processing in cells. In Chapters 4 and 5, I study heme derivatives, with substitutions of the metal

or modifications at the protoporphyrin ring, to determine which are able to activate pri-miRNA processing in cells.

Biology of heme

Heme is both synthesized within cells and imported from the external environment[48,49]. The synthesis of heme in eukaryotes is a multistep process occurring both in the cytoplasm and in the mitochondria. The pathway is initiated by the rate-limiting condensation of succinyl-CoA and glycine by the enzyme δ-aminolevulinic acid synthase (ALAS). Less is known about how heme moves across the cellular membrane. Some believe there is a specific heme transporter that is responsible for bringing heme into the cell whereas others think heme passively moves into the cell since it is hydrophobic. One likely candidate for a heme transporter is HRG-1 (Heme Responsive Gene 1)[50]. Depletion of HRG-1 in *C. elegans* results in altered heme sensing and accumulations of heme analogues. Human HRG-1 is highly expressed in the brain, kidney, heart and skeletal muscle and is important for heme transport in macrophages[51]. Heme is degraded by heme oxygenase (HO) to produce biliverdin[52]. Excess amount of free heme in a cell is toxic so the pathway of synthesis and degradation is highly regulated. It is also thought that specific heme transporters exist in the cell to protect against the formation of free radicals from free heme. Because of the complexity of heme synthesis, transport, and degradation, little is known about how much heme is available to be loaded onto newly synthesized heme proteins. In Chapter 6, I use DGCR8 mutants and my cellular processing assay to address the question of cellular heme availability.

Single molecule imaging of RNA

In the final chapter of this thesis, I describe my effort to develop a single molecule assay for visualizing pri-miRNA in live cells. By visualizing single pri-miRNA we hoped to track single processing events and measure the rate of processing in cells. There are three main strategies when trying to label RNA in cells: synthetic dyes attached to complementary RNA or DNA, fusing a fluorescent protein with RNA-binding proteins that recognize specific RNA sequences, or the more recently developed fluorescent RNA Spinach[53–56]. Synthetic dyes are bright and the RNA/DNA hybridization is stable and specific but cells have to be microinjected so the throughput is very low. RNA-binding proteins can be fused to fluorescent proteins and the respective RNA binding site attached to the RNA of interest. This technique benefits from being endogenously expressed. However, to get a strong enough signal some 24 copies of binding sites have to be attached to the RNA of interest so the construct is bulky and runs the risk of interfering with endogenous machinery. The newest developed strategy, Spinach, solves the bulkiness problem because the RNA tag itself is fluorescent. However, this method has not been extensively characterized for use in live mammalian cells. Considering the pros and cons of each of these methods we decided to use the RNA-binding protein strategy because it has been used successfully by multiple groups to label and track single molecules of RNA in live cells. In Chapter 8, I will describes the specific design of our strategy, the technical difficulties I encountered while developing the method, and the current status of the project.

References

1. Guo, H., Ingolia, N. T., Weissman, J. S. & Bartel, D. P. Mammalian microRNAs predominantly act to decrease target mRNA levels. *Nature* **466,** 835–40 (2010).

2. Fabian, M. R., Sonenberg, N. & Filipowicz, W. Regulation of mRNA translation and stability by microRNAs. *Annu. Rev. Biochem.* **79,** 351–79 (2010).

3. Lee, R., Feinbaum, R. & Ambros, V. The C. elegans heterochronic gene lin-4 encodes small RNAs with antisense complementarity to lin-14. *Cell* **75,** 843–854 (1993).

4. Friedländer, M. R. *et al.* Evidence for the biogenesis of more than 1,000 novel human microRNAs. *Genome Biol.* **15,** R57 (2014).

5. Croce, C. M. Causes and consequences of microRNA dysregulation in cancer. *Nat. Rev. Genet.* **10,** 704–14 (2009).

6. Ambros, V. MicroRNAs and developmental timing. *Curr. Opin. Genet. Dev.* **21,** 511–7 (2011).

7. Yi, R. *et al.* DGCR8-dependent microRNA biogenesis is essential for skin development. *Proc. Natl. Acad. Sci. U. S. A.* **106,** 498–502 (2009).

8. Ambros, V. The functions of animal microRNAs. *Nature* **431,** 350–5 (2004).

9. Pegoraro, M. & Tauber, E. The role of microRNAs (miRNA) in circadian rhythmicity. *J. Genet.* **87,** 505–511 (2008).

10. Kim, V. N., Han, J. & Siomi, M. C. Biogenesis of small RNAs in animals. *Nat. Rev. Mol. Cell Biol.* **10,** 126–39 (2009).

11. Lee, Y. *et al.* The nuclear RNase III Drosha initiates microRNA processing. *Nature* **425,** 415–9 (2003).

12. Denli, A. M., Tops, B. B. J., Plasterk, R. H. A., Ketting, R. F. & Hannon, G. J. Processing of primary microRNAs by the Microprocessor complex. *Nature* **432,** 231–5 (2004).

13. Han, J. *et al.* The Drosha-DGCR8 complex in primary microRNA processing. *Genes Dev.* **18,** 3016–27 (2004).

14. Landthaler, M., Yalcin, A. & Tuschl, T. The human DiGeorge syndrome critical region gene 8 and Its D. melanogaster homolog are required for miRNA biogenesis. *Curr. Biol.* **14,** 2162–7 (2004).

15. Gregory, R. I. *et al.* The Microprocessor complex mediates the genesis of microRNAs. *Nature* **432,** 235–40 (2004).

16. Yi, R., Qin, Y., Macara, I. G. & Cullen, B. R. Exportin-5 mediates the nuclear export of pre-microRNAs and short hairpin RNAs. *Genes Dev.* **17,** 3011–6 (2003).

17. Hutvágner, G. *et al.* A cellular function for the RNA-interference enzyme Dicer in the maturation of the let-7 small temporal RNA. *Science* **293,** 834–8 (2001).

18. Bernstein, E., Caudy, A. A., Hammond, S. M. & Hannon, G. J. Role for a bidentate ribonuclease in the initiation step of RNA interference. *Nature* **409,** 363–6 (2001).

19. Gregory, R. I., Chendrimada, T. P., Cooch, N. & Shiekhattar, R. Human RISC couples microRNA biogenesis and posttranscriptional gene silencing. *Cell* **123,** 631–40 (2005).

20. Eichhorn, S. W. *et al.* mRNA Destabilization Is the Dominant Effect of Mammalian MicroRNAs by the Time Substantial Repression Ensues. *Mol. Cell* **56,** 104–115 (2014).

21. Ha, M. & Kim, V. N. Regulation of microRNA biogenesis. *Nat. Rev. Mol. Cell Biol.* **15,** 509–524 (2014).

22. Han, J. *et al.* Posttranscriptional crossregulation between Drosha and DGCR8. *Cell* **136,** 75–84 (2009).

23. Triboulet, R., Chang, H.-M., Lapierre, R. J. & Gregory, R. I. Post-transcriptional control of DGCR8 expression by the Microprocessor. *RNA* **15,** 1005–11 (2009).

24. Barad, O. *et al.* Efficiency and specificity in microRNA biogenesis. *Nat. Struct. Mol. Biol.* **19,** 650–2 (2012).

25. Wada, T., Kikuchi, J. & Furukawa, Y. Histone deacetylase 1 enhances microRNA processing via deacetylation of DGCR8. *EMBO Rep.* **13,** 142–9 (2012).

26. Tang, X. *et al.* Acetylation of drosha on the N-terminus inhibits its degradation by ubiquitination. *PLoS One* **8,** e72503 (2013).

27. Herbert, K. M., Pimienta, G., DeGregorio, S. J., Alexandrov, A. & Steitz, J. A. Phosphorylation of DGCR8 increases its intracellular stability and induces a progrowth miRNA profile. *Cell Rep.* **5,** 1070–81 (2013).

28. Tang, X., Li, M., Tucker, L. & Ramratnam, B. Glycogen synthase kinase 3 beta (GSK3β) phosphorylates the RNAase III enzyme Drosha at S300 and S302. *PLoS One* **6,** e20391 (2011).

29. Tang, X., Zhang, Y., Tucker, L. & Ramratnam, B. Phosphorylation of the RNase III enzyme Drosha at Serine300 or Serine302 is required for its nuclear localization. *Nucleic Acids Res.* **38,** 6610–9 (2010).

30. Han, C. *et al.* The RNA-Binding Protein DDX1 Promotes Primary MicroRNA Maturation and Inhibits Ovarian Tumor Progression. *Cell Rep.* **8,** 1447–60 (2014).

31. Davis, B. N., Hilyard, A. C., Lagna, G. & Hata, A. SMAD proteins control DROSHA-mediated microRNA maturation. *Nature* **454,** 56–61 (2008).

32. Hata, A. & Davis, B. N. Regulation of pri-miRNA Processing Through Smads. *Adv. Exp. Med. Biol.* **700,** 15–27 (2011).

33. Kim, K. K., Yang, Y., Zhu, J., Adelstein, R. S. & Kawamoto, S. Rbfox3 controls the biogenesis of a subset of microRNAs. *Nat. Struct. Mol. Biol.* **21,** 901–910 (2014).

34. Peric, D., Chvalova, K. & Rousselet, G. Identification of microprocessor-dependent cancer cells allows screening for growth-sustaining micro-RNAs. *Oncogene* **31,** 2039–48 (2012).

35. Tsutsui, M. *et al.* Establishment of cells to monitor Microprocessor through fusion genes of microRNA and GFP. *Biochem. Biophys. Res. Commun.* **372,** 856–61 (2008).

36. Allegra, D. & Mertens, D. In-vivo quantification of primary microRNA processing by Drosha with a luciferase based system. *Biochem. Biophys. Res. Commun.* **406,** 501–5 (2011).

37. Morlando, M. *et al.* Primary microRNA transcripts are processed co-transcriptionally. *Nat. Struct. Mol. Biol.* **15,** 902–909 (2008).

38. Pawlicki, J. M. & Steitz, J. A. Primary microRNA transcript retention at sites of transcription leads to enhanced microRNA production. *J. Cell Biol.* **182,** 61–76 (2008).

39. Zeng, Y., Yi, R. & Cullen, B. R. Recognition and cleavage of primary microRNA precursors by the nuclear processing enzyme Drosha. *EMBO J.* **24,** 138–48 (2005).

40. Zeng, Y. & Cullen, B. R. Efficient processing of primary microRNA hairpins by Drosha requires flanking nonstructured RNA sequences. *J. Biol. Chem.* **280,** 27595–603 (2005).

41. Han, J. *et al.* Molecular basis for the recognition of primary microRNAs by the Drosha-DGCR8 complex. *Cell* **125,** 887–901 (2006).

42. Faller, M., Matsunaga, M., Yin, S., Loo, J. A. & Guo, F. Heme is involved in microRNA processing. *Nat. Struct. Mol. Biol.* **14,** 23–9 (2007).

43. Faller, M. *et al.* DGCR8 recognizes primary transcripts of microRNAs through highly cooperative binding and formation of higher-order structures. *RNA* **16,** 1570–83 (2010).

44. Barr, I. *et al.* Ferric, not ferrous, heme activates RNA-binding protein DGCR8 for primary microRNA processing. *Proc. Natl. Acad. Sci. U. S. A.* **109,** 1919–24 (2012).

45. Barr, I. *et al.* DiGeorge critical region 8 (DGCR8) is a double-cysteine-ligated heme protein. *J. Biol. Chem.* **286,** 16716–25 (2011).

46. Senturia, R. *et al.* Structure of the dimerization domain of DiGeorge critical region 8. *Protein Sci.* **19,** 1354–65 (2010).

47. Senturia, R., Laganowsky, A., Barr, I., Scheidemantle, B. D. & Guo, F. Dimerization and heme binding are conserved in amphibian and starfish homologues of the microRNA processing protein DGCR8. *PLoS One* **7,** e39688 (2012).

48. Thöny-meyer, L. in *Tetrapyrroles: Birth, Life, and Death* (Warren, M. & Smith, A.) 149–159 (Springer, 2009).

49. Dailey, H. A. The terminal steps of heme biosynthesis. *Biochem. Soc. Trans.* **4,** 590–595 (2002).

50. Hamza, I. & Dailey, H. A. One ring to rule them all: trafficking of heme and heme synthesis intermediates in the metazoans. *Biochim. Biophys. Acta* **1823,** 1617–32 (2012).

51. White, C. *et al.* HRG1 is essential for heme transport from the phagolysosome of macrophages during erythrophagocytosis. *Cell Metab.* **17,** 261–70 (2013).

52. Kozakowska, M. *et al.* Heme oxygenase-1 inhibits myoblast differentiation by targeting myomirs. *Antioxid. Redox Signal.* **16,** 113–27 (2012).

53. Schifferer, M. & Griesbeck, O. Application of aptamers and autofluorescent proteins for RNA visualization. *Integr. Biol. (Camb).* **1,** 499–505 (2009).

54. Singer, R. H., Lawrence, D. S., Ovryn, B. & Condeelis, J. Imaging of gene expression in living cells and tissues. *J. Biomed. Opt.* **10,** 051406 (2005).

55. Bao, G., Rhee, W. J. & Tsourkas, A. Fluorescent probes for live-cell RNA detection. *Annu. Rev. Biomed. Eng.* **11,** 25–47 (2009).

56. Paige, J. S., Wu, K. Y. & Jaffrey, S. R. RNA mimics of green fluorescent protein. *Science* **333,** 642–6 (2011).

CHAPTER 2

Processing of microRNA primary transcripts requires heme in mammalian cells

(*Proceedings of the National Academy of Science USA* 111, 1861-1866.)

This chapter presents my initial characterization of the live-cell pri-miRNA processing assay. I use the assay to show that DGCR8 requires heme for its activity in cells. Combining cellular data together with biochemical analysis of DGCR8, we identify a new heme-binding motif "IPCL." Importantly, I identify cellular growth conditions that deplete cellular heme content and result in a decrease in pri-miRNA processing efficiency. Initial formulation of the project and cloning of several of the mammalian DGCR8 expression vectors were the work of Ming Gong. Ian Barr aided in this project by performing the biochemical analysis of DGCR8 mutants.

Processing of microRNA primary transcripts requires heme in mammalian cells

Sara H. Weitz[a], Ming Gong[b], Ian Barr[b], Shimon Weiss[c,d,1], and Feng Guo[b,1]

[a]Interdepartmental Program in Molecular, Cellular, and Integrative Physiology, [b]Department of Biological Chemistry, David Geffen School of Medicine, [c]Department of Chemistry and Biochemistry, and [d]Department of Physiology, David Geffen School of Medicine, University of California, Los Angeles, CA 90095

Edited by David P. Bartel, Massachusetts Institute of Technology, Cambridge, MA, and approved December 24, 2013 (received for review May 29, 2013)

DiGeorge syndrome critical region gene 8 (DGCR8) is the RNA-binding partner protein of the nuclease Drosha. DGCR8 and Drosha recognize and cleave primary transcripts of microRNAs (pri-miRNAs) in the maturation of canonical microRNAs (miRNAs) in animals. We previously reported that human, frog, and starfish DGCR8 bind heme when expressed in *Escherichia coli* and that Fe (III) heme activates apoDGCR8 in reconstituted pri-miRNA processing assays. However, the physiological relevance of heme in miRNA maturation has not been clear. Here, we present a live-cell pri-miRNA processing assay that produces robust signals and faithfully indicates DGCR8 and Drosha activities. We demonstrate that all known heme-binding–deficient DGCR8 mutants are defective in pri-miRNA processing in HeLa cells. DGCR8 contains a previously uncharacterized heme-binding motif, "IPCL," that is also required for its activity. Heme availability and biosynthesis in HeLa cells positively affect pri-miRNA processing and production of mature miRNA. These results establish an essential function for heme in pri-miRNA processing in mammalian cells. Our study suggests that abnormal heme biosynthesis and degradation may contribute to diseases via miRNA-mediated gene regulation networks.

iron | protoporphyrin IX | RNA processing | noncoding RNA | fluorescence microscopy

MicroRNAs (miRNAs) are small noncoding RNAs (~20–22 nt) that regulate gene expression via specific targeting of mRNAs for degradation and translation inhibition (1–3). A miRNA is initially produced as a long primary transcript (pri-miRNA), which is processed by the Microprocessor, a complex composed of the ribonuclease Drosha and an RNA-binding protein DiGeorge syndrome critical region gene 8 (DGCR8) (or Pasha, the fly and worm homologs of DGCR8) (4–11). The resulting precursor miRNA (pre-miRNA) is exported into the cytoplasm by Exportin-5 where it is processed further by Dicer and subsequently loaded into RISC (RNA-induced silencing complex) (12, 13). Abundant evidence indicates that pri-miRNA processing is highly regulated during development and is often dysregulated in diseases (1, 14, 15). For example, p53, lin-28B, and SMAD proteins have been shown to directly regulate the Microprocessor complex (16–18). In addition, DiGeorge syndrome is caused by the chromosomal deletion 22q11.2, a section that includes DGCR8 (19). A mouse model for this deletion shows that haploinsufficiency of *Dgcr8* results in abnormal miRNA biogenesis in the brain that contributes to the neurological and behavioral defects associated with DiGeorge syndrome (20, 21).

Studying pri-miRNA processing in cells has been technically challenging. Mature miRNAs are generally believed to be long-lived molecules although accelerated decay for individual microRNAs has been reported (22). Thus, the abundance of miRNAs often does not change dramatically unless cells grow by proliferation or differentiation. Furthermore, the Drosha-cleavage step is coupled to cell growth in certain cell types (23). Finally, unprocessed pri-miRNAs seem to be degraded quickly via a pathway not well understood, and thus do not greatly accumulate. Two cellular reporter assays for pri-miRNA processing have been previously described. A fluorescence-based assay comprises a GFP–pri-miRNA fusion construct that is stably integrated into various cell lines (24). This assay suffers from the lack of a normalization factor to overcome variability in fluorescent protein expression due to processes unrelated to pri-miRNA processing. The second system uses a firefly luciferase–pri-miRNA fusion and normalizes the firefly luciferase signal to that of Renilla luciferase expressed from a cotransfected plasmid (25). However, as the luciferase expression levels are measured enzymatically in cell lysates, single-cell resolution and real-time experiments cannot be achieved.

An outstanding question about miRNA maturation concerns a potential role for heme in pri-miRNA processing. We previously found that a truncated form of the 773-residue DGCR8 called NC1 (amino acids 276–751) overexpressed in *Escherichia coli* stably associates with heme (26). Each DGCR8 dimer associates with one heme molecule using a heme-binding domain (HBD) located in its central region (amino acids 276–498) and ligates to the heme iron using the Cys352 residues from both subunits (27, 28). Through mutagenesis analyses, Cys352 and Trp329 have been identified to be important for association with heme (27). We also identified the N-terminal region of the HBD as a dimerization domain (amino acids 276–353) and determined the crystal structures of this domain from human and frog DGCR8 (27). The structures show that DGCR8 makes an unconventional use of its WW motif for mediating an extensive dimerization interface. Interestingly, Cys352 and Trp329 from both subunits cluster on a common surface, which is likely to serve as a direct binding site for heme. The heme-free C352A, W329A, and W329H NC1 mutants display reduced but still substantial pri-miRNA processing activity in vitro (26, 27). It is

Significance

MicroRNAs (miRNAs) have important functions in development and cell physiology. The vast majority of mature miRNAs are produced from primary transcripts of microRNAs (pri-miRNAs) by a multi-step pathway. The first step, cleavage of pri-miRNAs by the Microprocessor complex, is highly regulated but technically challenging to study. We have developed a robust method that faithfully measures pri-miRNA processing efficiency in live cells. Using this assay, we establish an essential function of heme in miRNA maturation, a provocative idea suggested by previous biochemical studies. Our study reveals a previously unknown cellular function of this central biological cofactor, linking metal ion biology with the regulation of noncoding RNAs. Our method should be widely useful for studying RNA processing in biology and diseases.

Author contributions: S.H.W., S.W., and F.G. designed research; S.H.W., M.G., and I.B. performed research; S.H.W. and I.B. analyzed data; and S.H.W. and F.G. wrote the paper.

The authors declare no conflict of interest.

This article is a PNAS Direct Submission.

[1]To whom correspondence may be addressed. E-mail: sweiss@chem.ucla.edu or fguo@mbi.ucla.edu.

This article contains supporting information online at www.pnas.org/lookup/suppl/doi:10.1073/pnas.1309915111/-/DCSupplemental.

not clear that, in compartmentalized eukaryotic cells where heme is synthesized in the mitochondrion and DGCR8 functions in the nucleus, heme can really affect pri-miRNA processing.

Here, we report a live-cell pri-miRNA processing assay using a ratiometric fluorescence reporter that allows robust data analyses at single-cell resolution. Using this assay in combination with results from heme-binding analyses, we provide clear evidence that heme is essential for pri-miRNA processing in human cells.

Results

A Fluorescence-Based Live-Cell Pri-miRNA Processing Reporter. We designed a ratiometric reporter construct based on a plasmid that simultaneously expresses two fluorescent proteins, mCherry and eYFP, driven by a bidirectional tetracycline-inducible promoter (Fig. 1*A*). This plasmid was generated by Sharp, Mukherji, and co-workers for examining interactions between mature miRNAs and 3′-untranslated regions (UTRs) of target messenger RNAs (29). In our reporter, pri-miRNA sequences were inserted into the 3′-UTR of the mCherry expression cassette whereas the eYFP 3′-UTR was left unaltered. Thus, this construct expresses an mCherry–pri-miRNA fusion RNA. Cleavage of the pri-miRNA moiety of the fusion RNA by Drosha/DGCR8 results in removal of the polyadenylation (poly-A) tail along with a portion of the 3′-UTR, which leads to degradation of the mCherry mRNA and reduction of mCherry protein expression and its fluorescent signal. The eYFP fluorescence signal allows changes of individual cells' transcriptional and translational activities to be normalized. Thus, the mCherry/eYFP ratio should negatively correlate with pri-miRNA processing activity. In this study, we chose to use the reciprocal, the eYFP/mCherry ratio, as it is a positive indicator for pri-miRNA processing efficiency.

As a starting point, we engineered human pri-miR-9-1 and pri-miR-30a into our fluorescent reporter. HeLa cells transiently transfected with either the pri-miR-9-1 or pri-miR-30a fluorescent reporter showed expression of eYFP and mCherry (Fig. 1*B*). Not surprisingly, there was a large intrinsic variation in the expression levels of eYFP and mCherry among cells. The eYFP and mCherry intensities of individual cells had a linear relationship over the range of reporter expression levels achieved, indicating that the reporters make proportional responses to the pri-miRNA processing machinery (Fig. 1*C*). No plateauing was observed, suggesting that the reporter system had not saturated the endogenous processing machinery. We calculated the slope from linear regression of the data to measure the overall efficiency of pri-miRNA processing.

We validated the fluorescent reporters by ectopically expressing DGCR8. HeLa cells express DGCR8 at a relatively low level (30); thus, we expected that expression of functional DGCR8 protein from a plasmid would increase the efficiency of pri-miRNA processing. Cells were cotransfected with a reporter and a plasmid expressing an N-terminal flag-tagged DGCR8 protein (N-flag-DGCR8) (Fig. 1*D*). The C-terminal tail of DGCR8 has been shown to be required for pri-miRNA processing (31, 32), and a mutant with the C-terminal tail deleted (ΔCTT) was used as an inactive control (Fig. 1*D*). When N-flag-DGCR8 was ectopically expressed, we continually observed a 90% increase in the slope (Fig. 1*E* and Fig. S1 *A*, *B*, *D*, and *E*). In contrast, no significant changes in slope were observed in cells expressing the ΔCTT mutant.

We next tested whether the fluorescent signals faithfully indicate the processing of pri-miRNAs in cells. We used quantitative RT-PCR (qRT-PCR) to determine the abundance of the mCherry–pri-miRNA fusion RNAs, the eYFP mRNA and mature miRNA. Consistent with the fluorescence measurements, the eYFP/mCherry–pri-miRNA RNA expression ratio increased by about twofold in cells expressing N-flag-DGCR8 (Fig. 1*F* and Fig. S1*F*). The levels of mature miR-9 and miR-30a in cells ectopically expressing N-flag-DGCR8 increased to 1.7- and 1.6-fold of those in cells transfected with reporters only (Fig. 1*G* and Fig. S1*G*). HeLa cells do not naturally express miR-9 so the reporter solely contributes the signal, whereas the mature miR-30a detected here originates from both the highly expressed endogenous gene and the reporter. We confirmed the mature miR-9 qRT-PCR results using Northern blots (Fig. S1*C*). Additionally, we observed an increase in the pre-miR-9 after N-flag-DGCR8 expression, which is consistent with an increase in pri-miR-9-1 processing (Fig. S1*C*). In contrast to the wild-type N-flag-DGCR8, expression of ΔCTT did not cause large changes to the abundance of mCherry–pri-miRNA fusion, mature miR-9, or miR-30a relative to the "reporter only" transfection. Additionally, we tested a pri-miR-9-1 reporter in which the Drosha cleavage site was mutated, and this reporter was unresponsive to N-flag-DGCR8 expression (*SI Text* and Fig. S2). These results clearly demonstrate that the fluorescence reporter expression responds to changes in bona fide pri-miRNA processing activity, can detect the processing potential of mutant pri-miRNA, and reflects the function of ectopically expressed N-flag-DGCR8 proteins. The latter observation will be used to examine DGCR8 mutants.

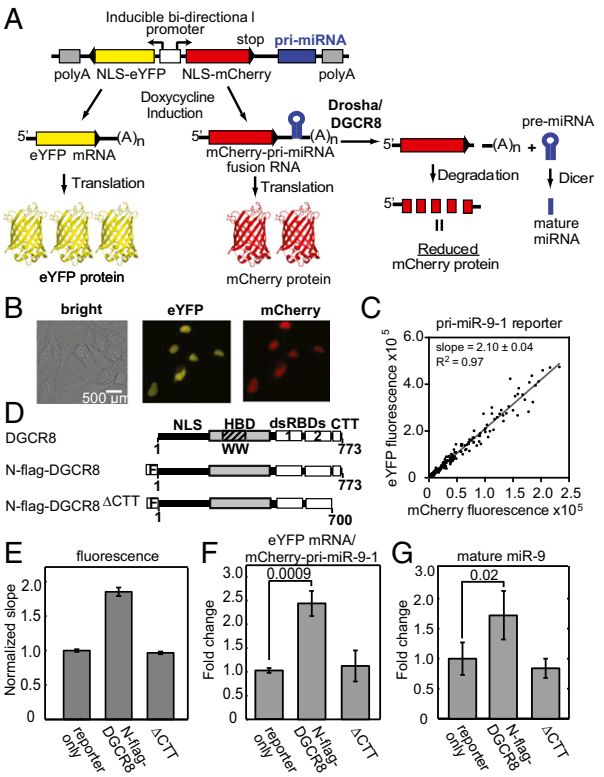

Fig. 1. Live-cell pri-miRNA processing reporter assay. (*A*) Schematic depiction of the assay. NLS, nuclear localization signal. (*B*) Exemplary cell images showing nuclear expression of eYFP and mCherry via transfection of the pri-miR-9-1 reporter. (*C*) eYFP and mCherry fluorescence signals from transfection with the pri-miR-9-1 reporter are plotted for each cell. Slope from a linear regression is shown on the graph, with $R^2 = 0.97$. (*D*) Schematics of human DGCR8 and the expression constructs used in the study. (*E*) Normalized fluorescence slopes for HeLa cells transfected with the pri-miR-9-1 reporter, either alone or with N-flag-DGCR8 expression plasmids. Error bars represent 95% confidence interval (95% CI) of the linear fit. The eYFP vs. mCherry scatter plots are in Fig. S1. (*F* and *G*) The abundance of the eYFP mRNA, the mCherry–pri-miRNA fusion RNA (*F*), and mature miR-9 (*G*) expression levels from *E* was measured using qRT-PCR (mean ± SD, $n = 3$). *P* values are labeled on the graphs.

The Reporter Assay Detects Alteration of Endogenous DGCR8 Activity. We next tested whether our reporter assay was sensitive to perturbation of DGCR8 expression via RNA interference. We

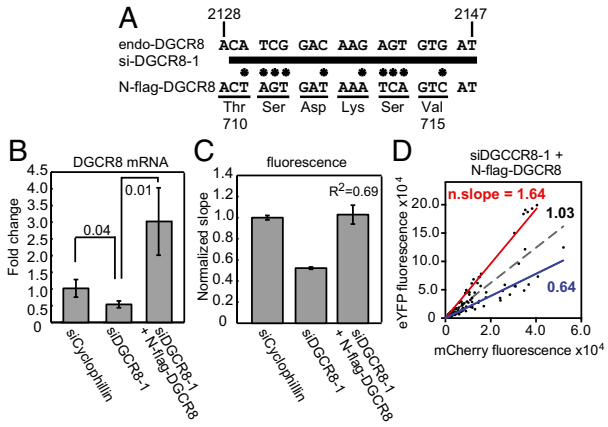

Fig. 2. The reporter assay detects alteration of endogenous DGCR8 activity. HeLa cells were cotransfected using Dharmafect duo with the pri-miR-9-1 reporter and siRNAs as indicated. Knockdown of endogenous DGCR8 was rescued via inclusion of pN-flag-DGCR8. (*A*) Schematic of the siDGCR8-1 binding site in the endogenous DGCR8 coding sequence. siDGCR8-1 is represented by the thick bar. Asterisks designate the location of mutations. (*B*) DGCR8 expression levels as measured using qRT-PCR. Shown are averages ± SD ($n = 3$). *P* values are labeled on the graph. (*C*) The mCherry vs. eYFP slopes (± 95% CI) normalized to siCyclophilin. The eYFP vs. mCherry scatter plots for cotransfections of pri-miR-9-1 reporter with either siCyclophilin or siDGCR8-1 are shown in Fig. S3 *A* and *B*, and that for the cotransfection of the reporter with siDGCR8-1 and pN-flag-DGCR8 is displayed in *D*. Dashed gray line is the linear regression for all data points. The red and blue lines are the linear regressions for the data points that lie above or below the dashed line, respectively. n. slope, normalized slope.

synthesized an siRNA, siDGCR8-1, that had been previously shown to reduce DGCR8 expression and decrease pri-miRNA processing and the abundance of mature miRNAs (10) (Fig. 2*A*). HeLa cells were cotransfected with siDGCR8-1 and the pri-miR-9-1 reporter. siCyclophilin was used as a normalization control. siDGCR8-1 reduced the expression of endogenous DGCR8 mRNA by 50% (Fig. 2*B*) and resulted in a 48% decrease in the fluorescence slope (Fig. 2*C*). This result indicates that our reporter is sensitive enough to detect a change in pri-miRNA processing efficiency caused by a modest reduction of endogenous DGCR8 expression. Note that the reduction of DGCR8 expression achieved here by RNA interference is similar to the ~50% decrease observed in a DiGeorge syndrome mouse model (20, 21).

We also tested whether the pri-miRNA–processing defect caused by siDGCR8-1 could be rescued by expressing N-flag-DGCR8. siDGCR8-1 targets a coding sequence in the C-terminal region of endogenous DGCR8; the N-flag-DGCR8 expression plasmid (pN-flag-DGCR8) contains 10 silent mutations within the siDGCR8-1 targeting site so that siDGCR8-1 does not affect the expression of this exogenous DGCR8 (Fig. 2*A*). Cotransfection of pN-flag-DGCR8 with the reporter and siDGCR8-1 enhanced the total DGCR8 expression to three times the level of the siCyclophilin control (Fig. 2*B*) and resulted in an overall eYFP/mCherry slope twice that of siDGCR8-1 only (Fig. 2*C*). This result is consistent with a rescue of pri-miRNA processing by expression of N-flag-DGCR8. The siDGCR8-1/pN-flag-DGCR8 data have a large deviation from the fitted line, with an R^2 value of 0.69, much lower than the >0.86 values obtained from most other experiments (Figs. 2 *C* and *D*). In fact, there appeared to be two cell populations, which can be roughly separated by the fit curve (gray dashed line in Fig. 2*D*). The lower cell population has a normalized eYFP/mCherry slope of 0.64 ($R^2 = 0.89$), which is close to that of the siDGCR8-1, whereas the upper cell population displays a normalized slope of 1.64 ($R^2 = 0.97$), which is close to the slope of N-flag-DGCR8 overexpression, 1.90 (Figs. 2*D* and 1*E*). A control transfection with a fluorescein-labeled siRNA indicated that the siRNA got into most cells. Thus, it is likely that the lower cell population took up the reporter and siDGCR8-1 whereas the upper population received the reporter, pN-flag-DGCR8, and siDGCR8-1. This interpretation is supported by further experiments, in which the amount of pN-flag-DGCR8 used in the transfection was increased from 0.1 to 0.3 μg and the percentage of cells present in the upper population increased correspondingly (Fig. S3 *C* and *D*). These results demonstrate that a benefit of our fluorescence imaging-based assay is to allow pri-miRNA processing efficiency of different cell populations to be detected.

Overexpression of Drosha Does Not Enhance Pri-miRNA Processing. We showed that pri-miRNA processing is sensitive to both overexpression and RNAi knockdown of DGCR8. As Drosha and DGCR8 are known to function together, we compared the pri-miRNA processing efficiency of HeLa cells ectopically expressing either Drosha-flag, N-flag-DGCR8, or both. Fluorescence measurements showed that transfection of pCK-Drosha-flag did not increase processing activity, in contrast to the pN-flag-DGCR8 transfection; and coexpression of Drosha and DGCR8 resulted in pri-miRNA processing efficiency either higher than (pri-miR-9-1 reporter) or similar to (pri-miR-30a reporter) N-flag-DGCR8 expression alone (Figs. S4 *A* and *B* and S5 *A* and *B*). Similarly, mature miR-9 expression did not increase after Drosha-flag expression but did increase to threefold that of the reporter only after N-flag-DGCR8 expression, and to 6.8-fold after coexpression (Fig. S4*C*). qRT-PCR analyses indicate that Drosha expression was successful with its mRNA level doubled in the cotransfection with the pri-miR-9-1 reporter and quadrupled with the pri-miR-30a reporter (Figs. S4*E* and S5*D*). These changes are modest compared with the 45- to 85-fold increase observed for DGCR8 (Figs. S4*D* and S5*C*) but are comparable with the DGCR8 expression level achieved in the cotransfection with siDGCR8-1 where large changes in pri-miRNA processing efficiency were observed (Fig. 2). Overall, our results seem to suggest that, in HeLa cells, DGCR8, not Drosha, is the rate-limiting factor for pri-miRNA processing. This notion is consistent with the previous reports that the DGCR8 protein is subjected to multiple layers of regulation (5, 30, 33–36).

All Known Heme-Binding–Deficient DGCR8 Mutants Are Defective in Pri-miRNA Processing in HeLa Cells. We used our cellular assay to investigate the role of heme in DGCR8 function. Cys352 is conserved in all DGCR8 family members and serves as the coaxial ligand to the Fe(III) in heme (28). Mutation of Cys352 to an alanine, serine, or histidine residue completely abolishes heme binding to the NC1 protein and reduces its pri-miRNA processing activity in vitro. Therefore, we tested the C352A mutant to examine the importance of heme binding in live cells. We set up a series of cotransfections of the pri-miR-9-1 reporter with pN-flag-DGCR8, either wild type or the ΔCTT or C352A mutants. Compared with the wild type, we observed a 51% decrease in the eYFP/mCherry fluorescence slope for the C352A transfection, which corresponds to a decrease in the processing activity (Fig. 3*A*). Similarly, the eYFP/mCherry–pri-miRNA fusion RNA ratio and the mature miR-9 level decreased in the C352A transfection (Fig. 3 *B* and *C*). In contrast, the fluorescence slope, the mCherry–pri-miR-9-1 fusion RNA and mature miR-9 levels for C352A are very similar to those for the inactive ΔCTT (Fig. 3 *A*–*C*). Furthermore, C352A was expressed at a similar level as the wild type, as shown by Western blotting (Fig. 3*D*). Thus, the lack of pri-miRNA processing activity observed for C352A is not due to reduced expression of the mutant protein. Altogether, these results clearly indicate that the DGCR8 C352A mutant is inactive in pri-miRNA processing in HeLa cells.

We subsequently tested additional heme-binding–deficient DGCR8 mutants. The crystal structures of the DGCR8 dimerization domains show that Cys352 and Trp329 cluster on a putative heme-binding surface (27, 37). Mutation of Trp329 to either alanine (the residue at the equivalent position in fly Pasha)

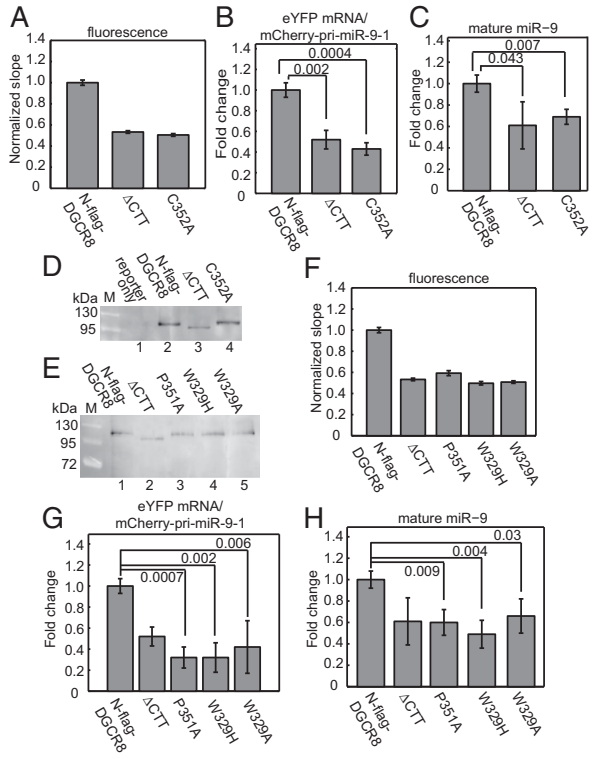

Fig. 3. All known heme-binding–deficient point mutants of DGCR8 are defective in pri-miRNA processing. HeLa cells were cotransfected with the pri-miR-9-1 reporter and N-flag-DGCR8 expression plasmids as indicated. (*A*) The normalized eYFP/mCherry slope (± 95% CI) of N-flag-DGCR8 C352A. (*B* and *C*) qRT-PCR analyses (mean ± SD, $n = 3$) of the (*B*) mCherry–pri-miRNA fusion RNA and (*C*) the mature miR-9 of the cotransfections in *A*. (*D* and *E*) Anti-flag immunoblots with equal amounts of nuclear extracts loaded. (*F*) Normalized fluorescence slopes (± 95% CI) for transfections with the DGCR8 mutants. (*G* and *H*) qRT-PCR analyses of (*G*) mCherry–pri-miRNA fusion RNA and (*H*) mature miR-9 for the transfections in *F*. Error bars represent SD ($n = 3$). *P* values are labeled on the graphs. The eYFP vs. mCherry fluorescence scatter plots are shown in Fig. S6 *A–D*.

or histidine (the residue in worms) in NC1 results in heme-free proteins after overexpression; and both mutants have reduced pri-miRNA processing activity in vitro (27). In addition to Trp329, Pro351 is also important for DGCR8 heme binding. Mutation of Pro351 to Ala greatly reduces the affinity of DGCR8 for heme (28). We therefore tested the activity of P351A, W329A, and W329H using our cellular pri-miRNA processing assay. In our initial experiments, equal amounts of wild-type and mutant plasmids were used in transfections; however, the three mutant proteins were expressed at slightly lower levels than the wild type. Thus, we doubled the amounts of the mutant plasmids in the transfections and achieved protein expression levels nearly equal to that of the wild type (Fig. 3*E*). Under the latter condition, all three mutants displayed normalized fluorescence slopes and eYFP/mCherry–pri-miR-9-1 fusion RNA ratios significantly lower than that of N-flag-DGCR8 but similar to ΔCTT (Fig. 3 *F* and *G*). Mature miR-9 levels decreased an average of 50% for all mutants relative to the wild type, again similar to that of ΔCTT (Fig. 3*H*). We tested these heme-binding–deficient mutants using the pri-miR-30a reporter construct and obtained similar results (Fig. S6 *E–K*). Altogether, these data clearly demonstrate that all known heme-binding–deficient DGCR8 mutants are defective in pri-miRNA processing in HeLa cells.

An "IPCL" Motif Is Required for Heme Binding and for Pri-miRNA Processing. The unique properties of DGCR8 encouraged us to search for motifs that are important for heme binding. The residues in the vicinity of Pro351 and Cys352 show a high degree of conservation among DGCR8 family members (Fig. 4*A*). Ile350 and Leu353 are invariable, Ser349 is conserved except in shrimp and insects, and His354 is conserved except in shrimp, insects, and worms. We mutated Ser349, Ile350, Leu353, and His354 to alanine in the context of NC1 and examined their heme-binding properties through overexpression in *E. coli* and purification using our routine procedures. The I350A and L353A mutations nearly abolished the presence of heme in purified NC1 proteins, and the mutant heme-free proteins cannot bind heme in vitro to reconstitute the complexes (Fig. S7 and Table S1). In contrast, purified S349A and H354A NC1 dimer proteins were occupied by heme, resembling the wild type. We then introduced these mutations to pN-flag-DGCR8 and tested their activity using the pri-miR-9-1 reporter. We found that S349A and H354A were active and that I350A and L353A were inactive in HeLa cells, as judged by the eYFP/mCherry fluorescence ratios (Fig. 4*B* and Fig. S8) and mature miR-9 levels (Fig. 4*C*). All DGCR8 point mutants were expressed at roughly equal levels as determined by qRT-PCR except for L353A, which had a higher expression level similar to the ΔCTT mutant (Fig. 4*D*). The nearly perfect correlation between heme binding, pri-miRNA processing, and sequence conservation observed in our mutagenesis analyses strongly supports an essential function of heme in the miRNA maturation pathway in animals.

Heme Availability and Biosynthesis in HeLa Cells Affects Pri-miRNA Processing. We tested whether cellular heme availability affects pri-miRNA processing activity using our cellular reporter assay. We cultured HeLa cells in heme-depleted media and compared their pri-miRNA processing efficiency with and without 10 μM hemin as supplement. The eYFP/mCherry fluorescence slope for cells grown under the heme-replenished condition had a modest but statistically significant increase (normalized slope = 1.11, $P = 0.0012$), which indicates an increase in pri-miRNA processing efficiency (Fig. 5*A*). Importantly, the mature miR-9 level nearly

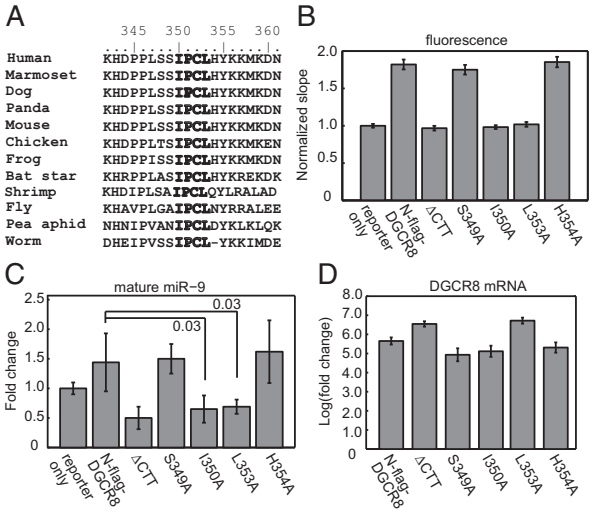

Fig. 4. The IPCL heme-binding motif is required for pri-miRNA processing. (*A*) Sequence alignment of DGCR8 homologs. (*B*) HeLa cells were cotransfected with the pri-miR-9-1 reporter and N-flag-DGCR8 expression plasmids as indicated. The normalized mCherry/eYFP slopes (± 95% CI) are shown. The eYFP vs. mCherry scatter plots are shown in Fig. S8. (*C*) qRT-PCR analyses (mean ± SD, $n = 3$) of mature miR-9 expression and (*D*) DGCR8 expression. *P* values are labeled on the graphs.

doubled in the presence of hemin, suggesting that alteration in heme availability in cellular environments can make large differences in mature miRNA levels (Fig. 5*B*). We also measured the amount of newly synthesized heme and observed a 60% reduction upon hemin treatment (Fig. 5C). This result is not surprising, as heme biosynthesis is known to be regulated via a feedback mechanism. Measurements of eYFP mRNA levels suggest that increase in miR-9 abundance by hemin was not caused by an enhanced rate of transcription (Fig. 5*D*).

We next examined the effects of inhibiting endogenous heme biosynthesis on pri-miRNA processing. We cultured HeLa cells under the heme-depleted condition, as described above, and treated them with 1 mM succinylacetone (SA). SA is a cell-permeable inhibitor of aminoluvelinic acid dehydratase, an enzyme responsible for the second step in the heme biosynthesis pathway (38). In a parallel experiment, the heme deficiency was rescued via addition of 10 μM hemin. To reduce secondary effects, we limited the duration of heme biosynthesis inhibition to 10 h. SA effectively reduced the amount of newly synthesized heme to about 25% that of no-treatment cells (Fig. 5*C*) and resulted in a 12% decrease in the eYFP/mCherry fluorescence slope, which corresponds to a decrease in pri-miRNA processing activity (Fig. 5*A*). The addition of SA did not decrease the levels of mature miR-9 compared to that with no treatment (Fig. 5*B*). However, we observed an increase in eYFP mRNA level after SA treatment, which suggests that the mCherry–pri-miR-9 transcription is likely to have increased under this condition (Fig. 5*D*). The lack of change in miR-9, despite the increased pri-miR-9-1 transcription, suggests that processing efficiency decreased after SA treatment. The lack of changes in miR-9 could also be contributed by a reduction of cell growth, an effect known to associate with inhibition of heme biosynthesis (39). The addition of exogenous hemin along with SA reversed the change in eYFP/mCherry fluorescence slope to a 17% increase relative to SA-treated cells (Fig. 5*A*), and the abundance of mature miR-9 doubled relative to those under both no-treatment and SA conditions (Fig. 5*B*). Because the changes of pri-miRNA processing efficiency caused by hemin and SA treatments were relatively small, we repeated these experiments and analyzed the RNAs using Northern blots. The trends in mature miR-9 levels were confirmed (Fig. S9*E*). Additionally, we observed an increase of the mCherry–pri-miR-9-1 fusion RNA upon SA treatment, which was reversed by hemin (Fig. S9*E*). Based on these observations, we conclude that both heme availability from extracellular environments and endogenous heme biosynthesis positively affect pri-miRNA processing. These effects are most likely to be exerted via the DGCR8–heme interaction. As the reduced pri-miRNA processing caused by inhibition of endogenous heme biosynthesis can be rescued by addition of hemin to the media, the origin of heme does not seem to be critical.

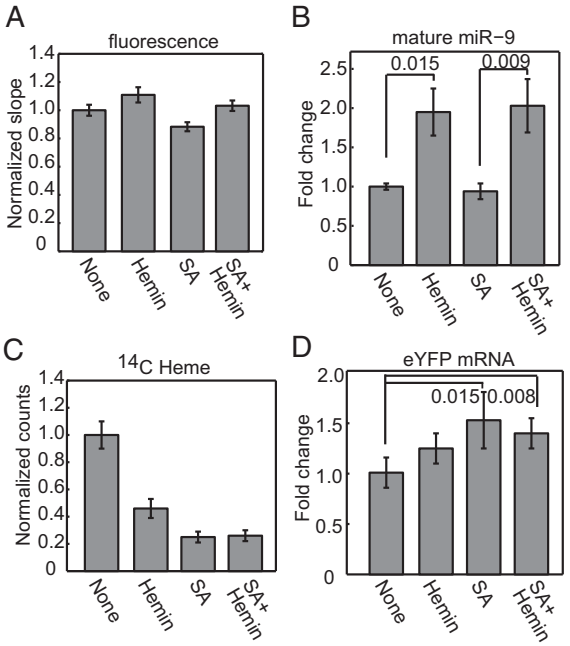

Fig. 5. Heme availability and biosynthesis in cells affects pri-miRNA processing. HeLa cells, grown in heme-depleted media and transfected with the pri-miR-9-1 reporter, were treated for 10 h with either hemin (10 μM) or succinylacetone (1 mM) or both. (*A*) Normalized eYFP/mCherry fluorescence slopes (± 95% CI). The eYFP vs. mCherry scatter plots are shown in Fig. S9 *A–D*. (*B*) Mature miR-9 expression (mean ± SEM, $n = 7$). (*C*) HeLa cells were treated with ^{14}C-labeled aminolevulinic acid, heme was extracted, and the radioactivity was measured. Measurements were normalized to the no-treatment (none) condition (mean ± SD, $n = 3$). (*D*) qRT-PCR analyses of eYFP expression (mean ± SD, $n = 4$). *P* values are labeled on the graphs.

Discussion

Here, we present a robust cellular assay for monitoring pri-miRNA cleavages. The assay is sensitive to both ectopic expression and RNA interference of the pri-miRNA processing machinery and thus can detect both increases and decreases in processing efficiency. The use of single-cell analyses and normalization with eYFP results in a sensitive and accurate reporter. Our assay enables us to isolate pri-miRNA processing efficiency from complex biological processes and diseases. With this technical advance, a multitude of questions about the Microprocessor complex could be investigated, including regulation of the Microprocessor and structural features of pri-miRNAs required for efficient processing (40, 41).

Using this assay we have analyzed the function of heme in miRNA maturation. Through a series of mutagenesis, we found that the six heme-binding–deficient DGCR8 mutants are defective in pri-miRNA processing. This correlation between heme binding and pri-miRNA processing in DGCR8 strongly argues for an essential function of heme in miRNA maturation. This conclusion is further strengthened by the observation that hemin activates pri-miRNA processing in HeLa cells cultured in heme-depleted media; and a heme biosynthesis inhibitor decreases processing. Because the heme-binding residues are highly conserved in animals (37), we speculate that the heme is also required in DGCR8 homologs.

We identified a previously uncharacterized heme-binding motif, IPCL. This motif shares similarity to the heme regulatory motif (HRM), which contains Cys-Pro, but in the opposite order. HRM directly binds heme and is found in repeats in a range of heme- regulated proteins such as the yeast transcription activator HAP1, the human δ-aminolevulenic acid synthase, and heme oxygenase-2 (42). It is possible that, in both motifs, the proline helps position the cysteine side chain in an appropriate geometry for ligation and for catalytic or regulatory functions. The conserved motif IPCL is essential but not sufficient for DGCR8 to associate with heme, as the dimerization subdomain, including Trp329 in the WW motif, and the C-terminal region of the HBD are also required for high-affinity association with heme. A bioinformatics search of protein sequences that contain both WW motif and IPCL yielded only DGCR8 homologs.

We show that heme is necessary for DGCR8 activity in live cells. What is the function of the DGCR8–heme interaction? There are two major possibilities that are not mutually exclusive. First, DGCR8 may be directly regulated by the availability of heme (43). In support of this possibility, we have shown previously that Fe(III) heme, but not the Fe(II) form, activates the pri-miRNA processing activity of DGCR8 in vitro (34) and here that heme availability and biosynthesis affect pri-miRNA processing efficiency in HeLa cells. Furthermore, heme oxygenase-1 (HO-1) was shown to reduce the total pool of cellular mature miRNAs and pre-miRNAs, in addition to blocking the induction of muscle-specific miRNA in myoblasts (44). HO-1 degrades heme in response to

various stress conditions. Although the increased miRNA level was attributed to decreases in DGCR8 protein levels, this observation is also consistent with reduced activation of the DGCR8 protein caused by increased heme degradation. As heme is synthesized in cells as the Fe(II) form, oxidation of the heme iron may also affect pri-miRNA processing.

The second possibility is that the heme bound to DGCR8 serves a structural purpose. We have shown that DGCR8 binds Fe(III) heme very tightly, making it hard to act as a reversible sensor of heme. Although the observation that reduction of the heme bound to DGCR8 to the Fe(II) state renders the protein inactive in pri-miRNA processing suggests a redox regulation, the reduction requires long incubation (30–60 min) with a strong reductant dithionite (34). Thus, reversible redox switch of the DGCR8-bound heme is unlikely to occur under physiological conditions. Additionally, the dual-cysteine ligation of the Fe(III) heme by DGCR8 makes the heme unavailable for potential catalytic functions. These hypotheses should be tested in the future.

Materials and Methods

Additional procedures can be found in *SI Materials and Methods*.

Vectors and Cloning. The pri-miRNA processing reporters were engineered based on the bidirectional tetracycline-inducible vector containing mCherry and eYFP (pTRE-BI-red/yellow) (29). Fragments of pri-miR-9-1 (143 nt) and pri-miR-30a (148 nt) were PCR-amplified from human genomic DNA and subsequently cloned into pTRE-BI-red/yellow.

Cell Culture and Transfection. The HeLa Tet-On cell line was purchased from Clontech. HeLa Tet-On cells were cultured in DMEM (Life Technologies) with 5% Tet-system approved FBS (Clontech) in 5% CO_2 at 37 °C. Cells were transfected with Effectene (Qiagen) following manufacturer's instructions.

Imaging and Analysis. All imaging was performed using a Nikon Eclipse Ti microscope equipped with an EMCCD camera (Andor iXon). We wrote a program based on the Matlab software package (The MathWorks) for integrating fluorescence intensities of individual cells, which is described in *SI Materials and Methods*.

ACKNOWLEDGMENTS. We thank P. Sharp for sharing the pTRE-BI-red/yellow plasmid long before publication, L. Zhang for advice on measurements of heme biosynthesis and for sharing ^{14}C-ALA, J. Feigon for sharing equipment, Y. Chen for technical support, and R. Senturia for sharing experience and discussion. This work was supported by National Institutes of Health Grants GM080563 (to F.G.), T32GM008496 (to S.H.W.), and GM069709 (to S.W.).

1. Ambros V (2011) MicroRNAs and developmental timing. *Curr Opin Genet Dev* 21(4): 511–517.
2. Guo H, Ingolia NT, Weissman JS, Bartel DP (2010) Mammalian microRNAs predominantly act to decrease target mRNA levels. *Nature* 466(7308):835–840.
3. Fabian MR, Sonenberg N, Filipowicz W (2010) Regulation of mRNA translation and stability by microRNAs. *Annu Rev Biochem* 79:351–379.
4. Kim VN, Han J, Siomi MC (2009) Biogenesis of small RNAs in animals. *Nat Rev Mol Cell Biol* 10(2):126–139.
5. Guo F (2012) *The Enzymes: Eukaryotic RNases and their Partners in RNA Degradation and Biogenesis, Part B*, eds Guo F, Tamanoi F (Elsevier Academic, Amsterdam), pp 101–121.
6. Lee Y, Jeon K, Lee J-T, Kim S, Kim VN (2002) MicroRNA maturation: Stepwise processing and subcellular localization. *EMBO J* 21(17):4663–4670.
7. Lee Y, et al. (2003) The nuclear RNase III Drosha initiates microRNA processing. *Nature* 425(6956):415–419.
8. Denli AM, Tops BBJ, Plasterk RHA, Ketting RF, Hannon GJ (2004) Processing of primary microRNAs by the Microprocessor complex. *Nature* 432(7014):231–235.
9. Gregory RI, et al. (2004) The Microprocessor complex mediates the genesis of microRNAs. *Nature* 432(7014):235–240.
10. Han J, et al. (2004) The Drosha-DGCR8 complex in primary microRNA processing. *Genes Dev* 18(24):3016–3027.
11. Landthaler M, Yalcin A, Tuschl T (2004) The human DiGeorge syndrome critical region gene 8 and its D. melanogaster homolog are required for miRNA biogenesis. *Curr Biol* 14(23):2162–2167.
12. Hutvágner G, et al. (2001) A cellular function for the RNA-interference enzyme Dicer in the maturation of the let-7 small temporal RNA. *Science* 293(5531):834–838.
13. Bernstein E, Caudy AA, Hammond SM, Hannon GJ (2001) Role for a bidentate ribonuclease in the initiation step of RNA interference. *Nature* 409(6818):363–366.
14. Blahna MT, Hata A (2013) Regulation of miRNA biogenesis as an integrated component of growth factor signaling. *Curr Opin Cell Biol* 25(2):233–240.
15. Croce CM (2009) Causes and consequences of microRNA dysregulation in cancer. *Nat Rev Genet* 10(10):704–714.
16. Suzuki HI, et al. (2009) Modulation of microRNA processing by p53. *Nature* 460(7254): 529–533.
17. Piskounova E, et al. (2011) Lin28A and Lin28B inhibit let-7 microRNA biogenesis by distinct mechanisms. *Cell* 147(5):1066–1079.
18. Davis BN, Hilyard AC, Lagna G, Hata A (2008) SMAD proteins control DROSHA-mediated microRNA maturation. *Nature* 454(7200):56–61.
19. Shiohama A, Sasaki T, Noda S, Minoshima S, Shimizu N (2003) Molecular cloning and expression analysis of a novel gene DGCR8 located in the DiGeorge syndrome chromosomal region. *Biochem Biophys Res Commun* 304(1):184–190.
20. Stark KL, et al. (2008) Altered brain microRNA biogenesis contributes to phenotypic deficits in a 22q11-deletion mouse model. *Nat Genet* 40(6):751–760.
21. Fénelon K, et al. (2011) Deficiency of Dgcr8, a gene disrupted by the 22q11.2 microdeletion, results in altered short-term plasticity in the prefrontal cortex. *Proc Natl Acad Sci USA* 108(11):4447–4452.
22. Rüegger S, Großhans H (2012) MicroRNA turnover: When, how, and why. *Trends Biochem Sci* 37(10):436–446.
23. Peric D, Chvalova K, Rousselet G (2012) Identification of microprocessor-dependent cancer cells allows screening for growth-sustaining micro-RNAs. *Oncogene* 31(16):2039–2048.
24. Tsutsui M, et al. (2008) Establishment of cells to monitor Microprocessor through fusion genes of microRNA and GFP. *Biochem Biophys Res Commun* 372(4):856–861.
25. Allegra D, Mertens D (2011) In-vivo quantification of primary microRNA processing by Drosha with a luciferase based system. *Biochem Biophys Res Commun* 406(4):501–505.
26. Faller M, Matsunaga M, Yin S, Loo JA, Guo F (2007) Heme is involved in microRNA processing. *Nat Struct Mol Biol* 14(1):23–29.
27. Senturia R, et al. (2010) Structure of the dimerization domain of DiGeorge critical region 8. *Protein Sci* 19(7):1354–1365.
28. Barr I, et al. (2011) DiGeorge critical region 8 (DGCR8) is a double-cysteine-ligated heme protein. *J Biol Chem* 286(19):16716–16725.
29. Mukherji S, et al. (2011) MicroRNAs can generate thresholds in target gene expression. *Nat Genet* 43(9):854–859.
30. Gong M, et al. (2012) Caspases cleave and inhibit the microRNA processing protein DiGeorge Critical Region 8. *Protein Sci* 21(6):797–808.
31. Faller M, et al. (2010) DGCR8 recognizes primary transcripts of microRNAs through highly cooperative binding and formation of higher-order structures. *RNA* 16(8):1570–1583.
32. Yeom K-H, Lee Y, Han J, Suh MR, Kim VN (2006) Characterization of DGCR8/Pasha, the essential cofactor for Drosha in primary miRNA processing. *Nucleic Acids Res* 34(16): 4622–4629.
33. Wada T, Kikuchi J, Furukawa Y (2012) Histone deacetylase 1 enhances microRNA processing via deacetylation of DGCR8. *EMBO Rep* 13(2):142–149.
34. Barr I, et al. (2012) Ferric, not ferrous, heme activates RNA-binding protein DGCR8 for primary microRNA processing. *Proc Natl Acad Sci USA* 109(6):1919–1924.
35. Han J, et al. (2009) Posttranscriptional crossregulation between Drosha and DGCR8. *Cell* 136(1):75–84.
36. Triboulet R, Chang H-M, Lapierre RJ, Gregory RI (2009) Post-transcriptional control of DGCR8 expression by the Microprocessor. *RNA* 15(6):1005–1011.
37. Senturia R, Laganowsky A, Barr I, Scheidemantle BD, Guo F (2012) Dimerization and heme binding are conserved in amphibian and starfish homologues of the microRNA processing protein DGCR8. *PLoS ONE* 7(7):e39688.
38. Ebert PS, Hess RA, Frykholm BC, Tschudy DP (1979) Succinylacetone, a potent inhibitor of heme biosynthesis: Effect on cell growth, heme content and δ-aminolevulinic acid dehydratase activity of malignant murine erythroleukemia cells. *Biochem Biophys Res Commun* 88(4):1382–1390.
39. Ye W, Zhang L (2004) Heme deficiency causes apoptosis but does not increase ROS generation in HeLa cells. *Biochem Biophys Res Commun* 319(4):1065–1071.
40. Han J, et al. (2006) Molecular basis for the recognition of primary microRNAs by the Drosha-DGCR8 complex. *Cell* 125(5):887–901.
41. Zeng Y, Cullen BR (2005) Efficient processing of primary microRNA hairpins by Drosha requires flanking nonstructured RNA sequences. *J Biol Chem* 280(30):27595–27603.
42. Zhang L, Guarente L (1995) Heme binds to a short sequence that serves a regulatory function in diverse proteins. *EMBO J* 14(2):313–320.
43. Mense SM, Zhang L (2006) Heme: A versatile signaling molecule controlling the activities of diverse regulators ranging from transcription factors to MAP kinases. *Cell Res* 16(8):681–692.
44. Kozakowska M, et al. (2012) Heme oxygenase-1 inhibits myoblast differentiation by targeting myomirs. *Antioxid Redox Signal* 16(2):113–127.

Supporting Information

Weitz et al. 10.1073/pnas.1309915111

SI Text

Determining Processing Competency of Pri-miRNAs in Cells. We tested whether the reporter assay can distinguish a processing-incompetent primary transcript of microRNA (pri-miRNA) mutant from the wild type. Pairing interaction around the Drosha cleavage sites in pri-mRNAs has been shown to be critical for processing (1). We mutated four residues around the 5′ Drosha cleavage site in the pri-miR-9-1 reporter to generate the M1 construct (Fig. S4*A*). Cotransfection of the M1 reporter with pN-flag-DGCR8 did not show the large increase in slope that was observed for the wild type (Fig. S4 *B* and *C*). Cotransfection with ΔCTT also did not exhibit significant changes. The lack of changes in processing of pri-miR-9-1 M1 by ectopic expression of N-flag-DGCR8 was confirmed by measurements of mCherry–pri-miR-9–1 fusion and eYFP mRNA levels using quantitative RT-PCR (qRT-PCR) (Fig. S4*D*). These results indicate that our reporter assay detects legitimate pri-miRNA cleavage events and may be used to examine processing competency of pri-miRNAs in cells.

SI Materials and Methods

Reagents. Succinylacetone (synonym 4,6-Dioxoheptanoic acid), doxycycline, and horse skeletal muscle apomyoglobin were from Sigma-Aldrich. Hemin was from MP Biomedicals. δ-Aminolevulinic acid (δ-ALA) was from either MP Biomedicals or Frontier Scientific. The siRNAs were purchased from Dharmacon, Thermo Scientific. The 4-^{14}C-aminolevulinic acid was a gift from Li Zhang (University of Texas at Dallas). Mature miR-9 Locked Nucleic Acids (LNA) probe was obtained from Exiqon.

Vectors and Cloning. The pri-miRNA processing reporters were engineered based on the bidirectional tetracycline-inducible vector containing mCherry and eYFP (pTRE-BI-red/yellow), both fused to an N-terminal nuclear localization signal sequence (2). Fragments of pri-miR-9-1 (143 nt) and pri-miR-30a (148 nt) were PCR-amplified from human genomic DNA. The primers were as follows with the ClaI and NotI cloning sites underlined: pri-miR-9-1 forward (ACCATCGATGGCTGCGTGGAAGAGGCGG), pri-miR-9-1 reverse (TGCAGCGGCCGCCTGCAGCCCCTCTGCGCAGT), pri-miR-30a forward (ACCATCGATGGAAAGAAGGTATATTGCT), pri-miR-30a reverse (TGCAGCGGCCGCAAACAAGATAATTGCTCCT).

The amplified pri-miRNAs were initially cloned into the ptre2hyg-HA vector (Clontech) between the ClaI and NotI sites for the purpose of a different study. The pri-miRNAs were subsequently excised using ClaI and SalI and inserted into pTRE-BI-red/yellow. The pri-miR-9-1 M1 mutant was made using the QuikChange site-directed mutagenesis protocol (Qiagen). Mutagenesis of N-flag-DGCR8 and NC1 expression constructs was carried out using the standard four-primer PCR method. The RNA- and protein-coding sequences of all plasmids were confirmed by sequencing.

Cell Culture and Transfection. The HeLa Tet-On cell line was purchased from Clontech. HeLa Tet-On cells were cultured in DMEM (Life Technologies) with 5% Tet-system approved FBS (Clontech) in 5% CO_2 at 37 °C. For transfections without siRNAs, 4.8×10^5 cells were seeded on 35-mm glass-bottom plates. The following day, cells were transfected with 0.4 μg of total DNA or 0.8 μg for low expression constructs using the Effectene reagent (Qiagen). Cells were immediately induced with 2 μg/mL doxycycline and imaged 18–24 h later unless specified otherwise. Media with phenol red were used for transfection and induction and were exchanged for a clear medium without the dye and containing 2 μg/mL doxycycline immediately before imaging.

Cotransfection of reporter and siRNAs was performed using the DharmaFECT Duo transfection reagent (Thermo Scientific) following the manufacturer's instructions. The final concentrations of siRNA and plasmid were 100 nM and 2 μg/mL, respectively. The sequence of siDGCR8-1 was the same as reported by Kim and coworkers (3). Cells were passaged 1 d posttransfection, plated on 35-mm glass-bottom plates, and 4 h later induced with 2 μg/mL doxycycline. Cells were imaged 18–24 h postinduction.

Heme-depleted media was made by treating Tet-system approved FBS with 0.1 M ascorbic acid for 2 h (4). The absorbance spectrum of the FBS was recorded at the beginning and throughout the treatment to monitor the disappearance of the 405-nm heme peak. The ascorbic acid was removed by dialyzing against 1 L of phosphate buffered saline (PBS, containing 137 mM NaCl, 2.7 mM KCl, 10 mM Na_2HPO_4, and 1.8 mM KH_2PO_4) at room temperature using dialysis tubing with a molecular mass cutoff of 12,500 Da twice for 1 h each round. Heme-depleted FBS was added to DMEM, and the medium was sterile-filtered. Cells were cultured in heme-depleted media for 24 h and split into either six-well plates or glass-bottom imaging plates. For pri-miRNA processing reporter assays, cells were transfected with Effectene. Either 1 mM succinylacetone (dissolved in water), 10 μM hemin (dissolved in DMSO), or both was added to the cell cultures at the same time as doxycycline. After 10 h, cells were either imaged or lysed for RNA extraction.

Measuring Rates of Heme Biosynthesis. To measure reduction in heme synthesis during succinylacetone/heme treatments, we added to the media 0.4 μCi of 4-^{14}C-aminolevulinic acid and 20 μM unlabeled δ-ALA. After 10 h, cells were washed twice with PBS, scraped into a 2-mL tube, and spun down at $13{,}226 \times g$ for 1 min. Cells were resuspended in 0.3 mL of heme extraction buffer containing 80% (vol/vol) acetone and 0.5 M HCl. Then, 1.2 mL of diethyl ether was added, and the cells were spun down at $13{,}226 \times g$ for 5 min at 4 °C. Two additional rounds of extraction with 2 M HCl were performed, and the final aqueous layer was added to a scintillation vial and allowed to evaporate overnight. The following day, 5 mL of scintillation fluid was added, and the amounts of ^{14}C-labeled heme were measured using a Beckman LS6500 liquid scintillation counter. Three biological replicates were performed, and the counts were normalized to the average of "no-treatment" samples.

Imaging and Analysis. All imaging was performed using a Nikon Eclipse Ti microscope equipped with an EMCCD camera (Andor iXon). We used a 20× air objective (NA = 0.45, Olympus) and lamp illumination (Nikon) at full power, an exposure time of 100 ms and 0 gain. The fluorescence signal was detected using filter cubes for eYFP (510 ± 10 nm band pass excitation and 535 ± 15 nm band pass emission) and mCherry (535 ± 25 nm band pass excitation and 610 ± 10 nm band pass emission). Images were saved as 16-bit tiff files.

We wrote a program based on the Matlab software package (The MathWorks) for integrating fluorescence intensities of individual cells. To determine the perimeter of individual nucleus (segmentation), our program imports individual pairs of eYFP and mCherry images and converts them to binary maps using user-defined threshold values. A value of 1 in the map indicates that the pixel is inside the nucleus, and 0 indicates outside. We

usually choose threshold values that maximize the number of cells detected. The perimeter of the nucleus is determined for each image separately, and then an adequate perimeter is chosen for the two images based on the following criteria. If the same cell is found in both images, the smaller perimeter is chosen to avoid including cytosols, which sometimes have low fluorescent signals. If a cell is detected in only one image, the perimeter is kept, allowing for very dim cells that are not detected in both images to be included. The center of the final perimeter for each cell is determined. After the nuclear perimeters are determined, further analysis is done on the original images. A background fluorescence value is calculated for each image by averaging the intensities of the pixels outside the identified nuclei. The background is then subtracted from the intensities of all pixels. The total intensity of an individual cell is calculated as the sum of the pixel intensities within the perimeter. Users can use the center coordinates in the output to remove dead cells or multiple cells detected as one object.

A list of total eYFP and mCherry intensities for individual cells was compiled in Microsoft Excel. Scatter plots were made for eYFP versus mCherry signals. The data were sorted based on each point's distance from the origin. Ten percent of the data with the highest intensities were removed, as they tend to dominate and possibly skew the linear fit. The final datasets were imported into Matlab and fit using the curve fit toolbox. *P* values were determined using the linear fit function of PRISM (GraphPad, version 4).

qRT-PCR for RNA Analyses. Total RNAs were extracted using the miRNeasy Mini kit (Qiagen) and were digested on-column using the RNase-free DNase set (Qiagen). The reverse transcription (RT) reactions were set up using SuperScript II (Life Technologies), and the quantitative PCR (qPCR) was performed using Platinum SYBR Green qPCR Supermix-UDG (Life Technologies). Following are a list of primers used for RT and qPCR reactions: mCherry RT (*TGTCAGGCAACCGTATTCACC*GTTCGTACTGTTCCACGA), eYFP RT (*TGTCAGGCAACCGTATTCACC*-ACTCCAGCAGGACCATGTGAT), mCherry qPCR forward (ACTACGACGCTGAGGTCAA), eYFP qPCR forward (AAGATCCGCCACAACATCGA), and qPCR reverse for mCherry and eYFP (*TGTCAGGCAACCGTATTCACC).*

To prevent potential plasmid in the RNA samples from interfering with the qPCR reactions, the RT primers were designed to include a 21-nt 5′-overhang (shown above in italics). The qPCR reverse primer sequence was identical to this overhang whereas the forward primers were gene-specific. A three-step qPCR reaction was performed with an annealing temperature of 60 °C. qPCR results were analyzed using the MxPro software (Stratagene). We calculated the ΔC_t values of the mCherry and eYFP transcripts and determined the fold changes by normalizing to the reporter only control.

Mature miR-9 and miR-30a (miR-9-5p and miR-30a-5p in the current miRBase nomenclature) were detected using TaqMan miRNA reverse transcription and miRNA Assay kits (Life Technologies) following the manufacturer's instructions. Ten nanograms of total RNA was used in each reverse transcription. C_t values were subtracted by those of either U6 small nuclear RNA or β-actin mRNA. Fold changes were calculated and normalized to the reporter-only control. DGCR8 expression was detected using a Taqman gene expression assay (Life Technologies), with RT performed using a random primer set and SuperScipt II (Life Technologies). The C_t values were subtracted by those of β-actin mRNA, and the fold change was calculated and was normalized to that of the siCyclophillin control transfection. All *P* values were calculated using a two-tailed Student *t* test except in Fig. 2*B* where a one-tailed *t* test was used.

Northern Blotting. Total RNA samples were prepared using the TriZol reagent (Invitrogen) according to the manufacturer's instructions. RNA quality and relative concentrations were determined using 1% agarose gels. Three to 20 μg of RNAs were loaded onto 15% polyacrylamide gels containing 7 M urea and separated by electrophoresis. RNA was transferred to Hybond-N+ membranes (GE Healthcare) and was cross-linked using UV light. The probe for U6 snRNA is a DNA oligo with the sequence 5′-AACGCTTCACGAATTTGCGT-3′. The probes were 5′-labeled with γ-^{32}P- ATP and were hybridized to membranes in ULTRAhyb-Oligo hybridization buffer (Life Technology) at 42 °C overnight. The membranes were washed and exposed to phosphorimagers. The images were recorded using a Typhoon Variable Mode Imager, and the bands were quantified using the program Quantify One (version 4.4.1; Bio-Rad). The plotting was performed using the program PRISM (version 4.0; GraphPad).

Immunoblotting. HeLa cells were transfected with the wild-type and mutant pN-flag-DGCR8 plasmids using Effectene (Qiagen) following standard protocol. Twenty-four hours posttransfection, cells were washed twice with PBS, scraped into 200 μL of PBS, and pelleted by centrifugation at 1,000 × *g* for 2 min at 4 °C. The PBS was removed, and ∼1×10^6 cells were resuspended in 80 μL of cold Buffer A [10 mM Hepes-KOH (pH 7.9), 1.5 mM $MgCl_2$, 10 mM KCl, 0.5 mM DTT, 0.2 mM phenylmethylsulfonyl fluoride (PMSF)]. Cells were incubated on ice for 10 min and then vortexed for 10 s and pelleted by centrifugation at 16,000 × *g* for 10 s at 4 °C. The supernatant (cytoplasmic fraction) was transferred to a new tube. The pellet was resuspended in 50 μL of Buffer C [20 mM Hepes-KOH (pH 7.9), 25% glycerol, 420 mM NaCl, 1.5 mM $MgCl_2$, 0.5 mM DTT, 0.2 mM PMSF] and incubated on ice for 20 min. Cells were pelleted by centrifugation at 16,000 × *g* for 2 min at 4 °C. The supernatant (nuclear fraction) was transferred to a new tube and processed for immunoblotting following our standard procedure (5). The membranes were first incubated overnight with mouse anti-FLAG antibodies (Sigma; diluted 1:1,000) followed by a 2-h incubation at room temperature with anti-mouse antibodies conjugated with horseradish peroxidase (HRP) (Novagen) (1:30,000 dilution). The membrane was washed thoroughly in PBST (PBS with 0.2% Tween-20), and the ECL Plus Western Blotting Detection System (GE Healthcare) protocol was then used according to the manufacturer's instructions. The images were recorded using chemifluorescence and the Typhoon Variable Mode Imager (GE Healthcare).

Expression, Purification, and Characterization of Recombinant NC1 Proteins. Human NC1 (wild type and mutants) proteins were expressed and purified as previously described (6). Briefly, they were expressed in *Escherichia coli* BL21(DE3) CodonPlus cells (Stratagene) grown in LB media supplemented with 1 mM δ-ALA at the time of induction. These proteins were purified using cation exchange followed by size exclusion chromatography. The purified proteins were stored in a buffer containing 20 mM Tris, pH 8.0, 400 mM NaCl, and 1 mM DTT. Electronic absorption spectra were recorded on a Beckman-Coulter DU800 spectrophotometer at 25 °C.

Heme dissociation and association assays were performed as described (7), in a buffer containing 20 mM Tris, pH 8.0, 400 mM NaCl, and 1 mM DTT. Fe(III) heme-bound NC1 S349A and H354A mutants, at 5.75 and 4.0 μM dimer concentrations, respectively, were incubated at room temperature with eightfold molar excess of apomyoglobin, which has an extremely high affinity for heme, with K_D of 3×10^{-15} M, and serves as a heme sink. Electronic absorption spectra were recorded over a period of 24 h. No heme transfer from NC1 mutants to apomyoglobin was observed. For heme association with the heme-free NC1 mutant dimers, I350A and L353A, 5 μM of the proteins were titrated with up to 10 μM Fe(III) heme, and electronic absorption spectra were recorded. Hemin chloride was converted to Fe(III) heme by dissolving it in 1.4 M NaOH at 10 mM concentration and incubating in the dark at room temperature for >30 min.

This concentrated solution was then diluted in water to give a 100-μM stock solution. No absorption peaks were observed around 450 nm, where the signature DGCR8-Fe(III) heme Soret peak is located.

Sequence Alignment. The following National Center for Biotechnology Information (NCBI) accession numbers were used for the DGCR8 homolog alignment: Human, *Homo sapien* (NCBI accession no. NM_022720); Marmoset, *Callithrix jacchus* (XM_002806547); Dog, *Canis familiaris* (XM_543542.4); Panda, *Ailuropoda melanoleuca* (XM_002920581); Mouse, *Mus musculus* (NM_033324); Chicken, *Gallus gallus* (XM_415079); Frog, *Xenopus laevis* (BC070985); Bat star, *Patiria miniata* (GQ397480.1); Shrimp, *Litopenaeus vannamei* (HQ692889.1); Fly, *Drosophila melanogaster* (NM_143622); Pea aphid, *Acyrthosiphon pisum* (NW_003383706.1); and Worm, *Caenorhabditis elegans* (NM_060373).

1. Lee Y, et al. (2003) The nuclear RNase III Drosha initiates microRNA processing. *Nature* 425(6956):415–419.
2. Mukherji S, et al. (2011) MicroRNAs can generate thresholds in target gene expression. *Nat Genet* 43(9):854–859.
3. Han J, et al. (2004) The Drosha-DGCR8 complex in primary microRNA processing. *Genes Dev* 18(24):3016–3027.
4. Ye W, Zhang L (2004) Heme deficiency causes apoptosis but does not increase ROS generation in HeLa cells. *Biochem Biophys Res Commun* 319(4):1065–1071.
5. Gong M, et al. (2012) Caspases cleave and inhibit the microRNA processing protein DiGeorge Critical Region 8. *Protein Sci* 21(6):797–808.
6. Faller M, Matsunaga M, Yin S, Loo JA, Guo F (2007) Heme is involved in microRNA processing. *Nat Struct Mol Biol* 14(1):23–29.
7. Barr I, et al. (2011) DiGeorge critical region 8 (DGCR8) is a double-cysteine-ligated heme protein. *J Biol Chem* 286(19):16716–16725.

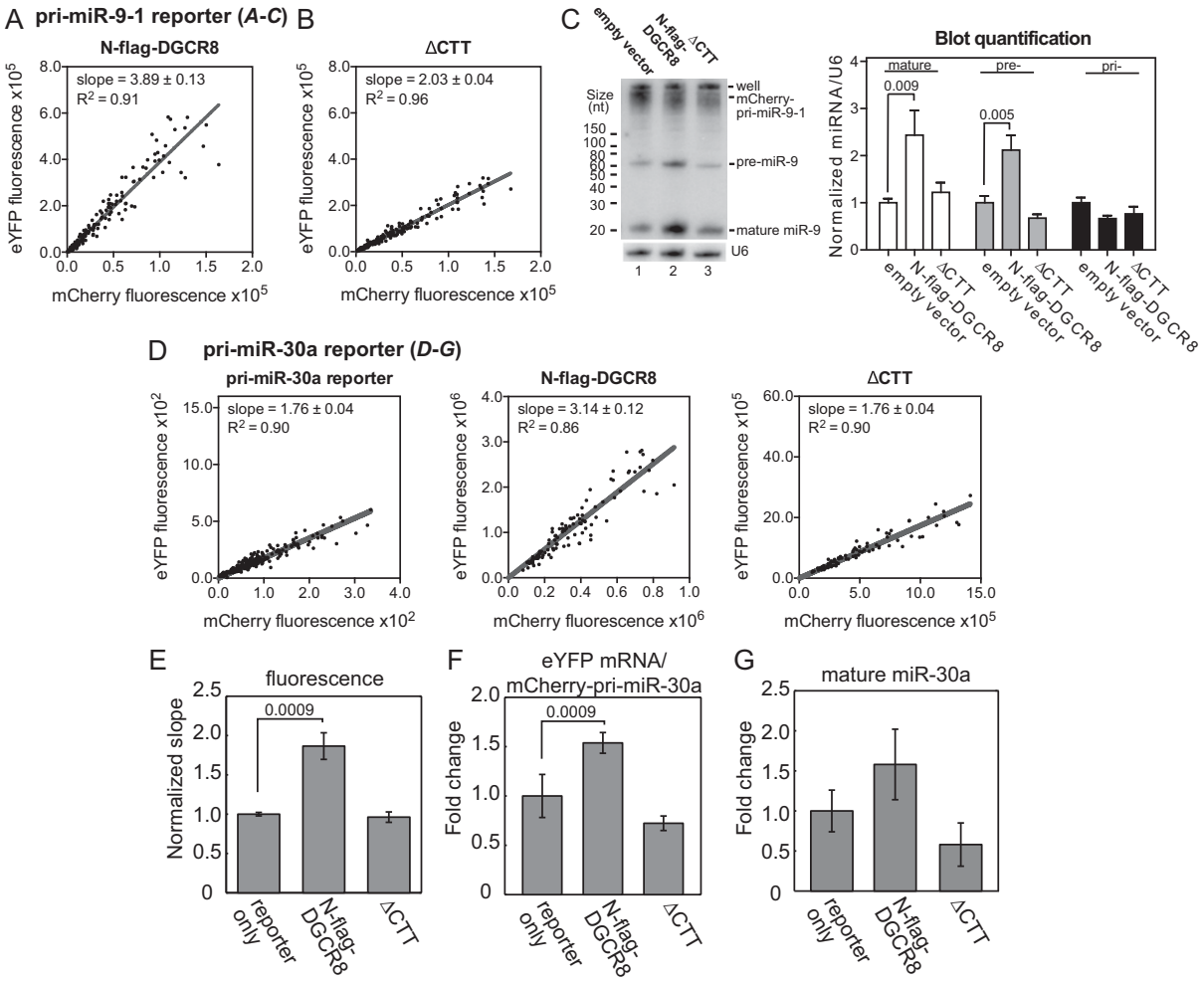

Fig. S1. Validation of the pri-miR-9–1 and pri-miR-30a reporters. (*A*–*C*) Validation of the pri-miR-9-1 reporter. Shown are additional data for the experiments described in Fig. 1*E*. Scatter plots of eYFP vs. mCherry fluorescent intensities of individual cells from cotransfection of the pri-miR-9-1 reporter with either wild-type N-flag-DGCR8 expression plasmid (*A*) or the ΔCTT mutant (*B*). The lines are from linear regression, with slope and R^2 shown on the graph. The ratio of *y* and *x* axes was set at 4:1 for all scatter plots. (*C*) Northern blotting analyses of total RNA samples. The pri-, pre-, and mature miR-9 intensities, after normalization by those of U6 snRNA, are indicated on the graph (mean ± SD, $n = 3$). (*D*–*G*) Validation of the pri-miR-30a reporter. HeLa cells were transfected with the pri-miR-30a reporter either alone or with N-flag-DGCR8 expression plasmid (wild type or ΔCTT). (*D*) Scatter plots of eYFP vs. mCherry fluorescence intensities of individual cells. The lines are from linear regression, with slope and R^2 shown on the graph. (*E*) Normalized eYFP/mCherry fluorescence slopes. Error bars represent 95% confidence interval (CI) of the linear fit. (*F* and *G*) qRT-PCR analyses of the mCherry-pri-miR-30a fusion RNA (*F*) and mature miR-30a (*G*). Error bars represent SD ($n = 3$). *P* values are labeled on the graphs.

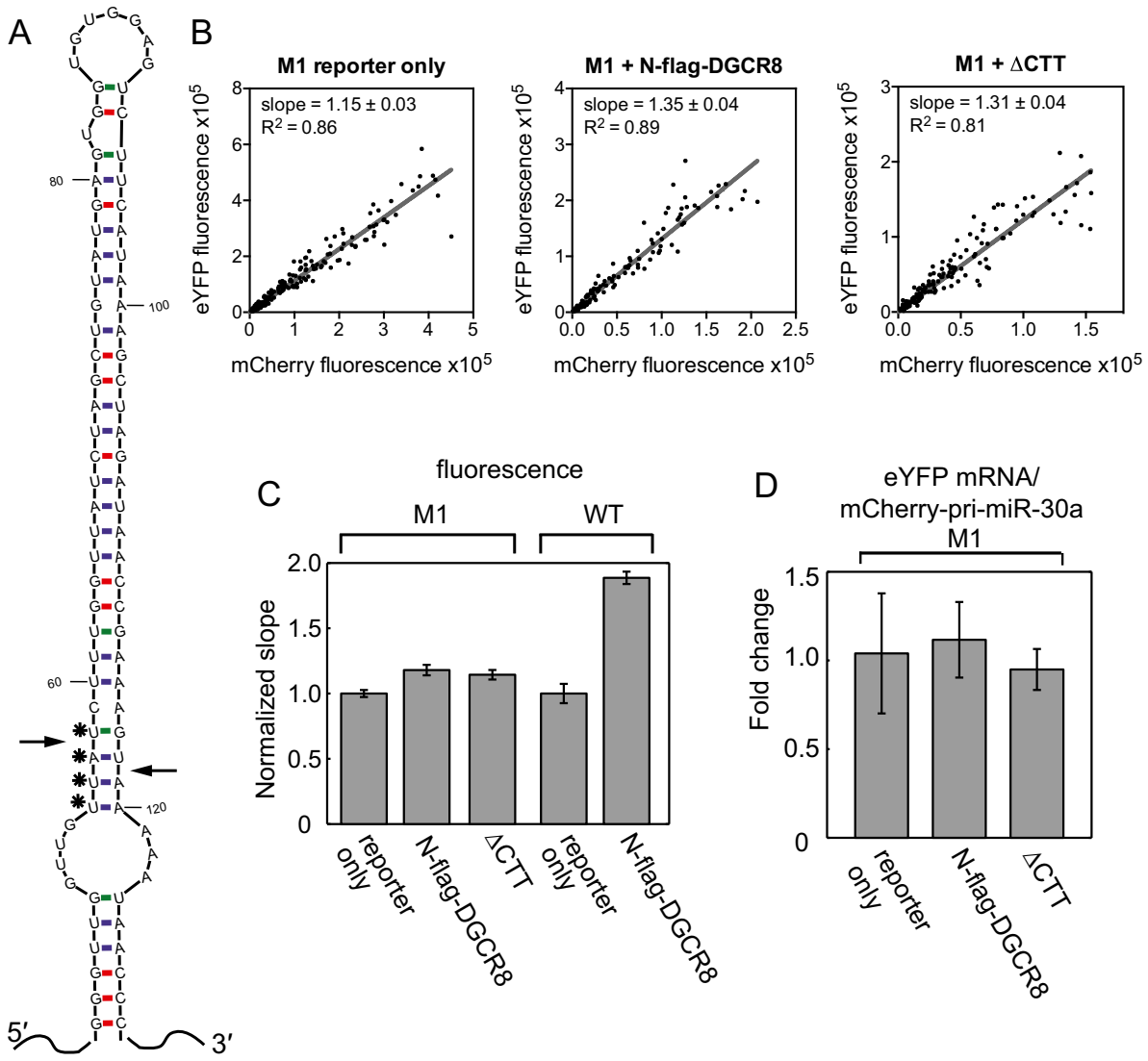

Fig. S2. Mutant pri-miR-9-1 reporter does not respond to ectopic expression of N-flag-DGCR8. (*A*) Secondary structure of the pri-miR-9-1 hairpin as predicted using MFOLD (1). Arrows indicate the expected Drosha cleavage sites. Residues marked by asterisks are mutated to AAUA (5′ to 3′) in the M1 mutant. (*B*) HeLa cells were transfected with the pri-miR-30a M1 or wild-type reporter, and pN-flag-DGCR8 plasmids as indicated. The eYFP and mCherry fluorescence signals are plotted for each cell. Slope and R^2 from linear regression are shown on the graph. The ratio of *y* and *x* axes was set at 1.6:1 for all plots. These experiments were performed together with those shown in Fig. 1*E*. (*C*) The normalized eYFP/mCherry fluorescence slopes are shown. Error bars are 95% CI from the linear fit. (*D*) qRT-PCR analyses of eYFP and mCherry-pri-miR-9-1 fusion RNAs from the experiments using the M1 reporter. Shown are average ± SD ($n = 3$). The slight changes, relative to the reporter-only control, are not statistically significant, with *P* value(N-flag-DGCR8) = 0.63 and *P* value(ΔCTT) = 0.93.

1. Zuker M (2003) Mfold web server for nucleic acid folding and hybridization prediction. *Nucleic Acids Res* 31(13):3406–3415.

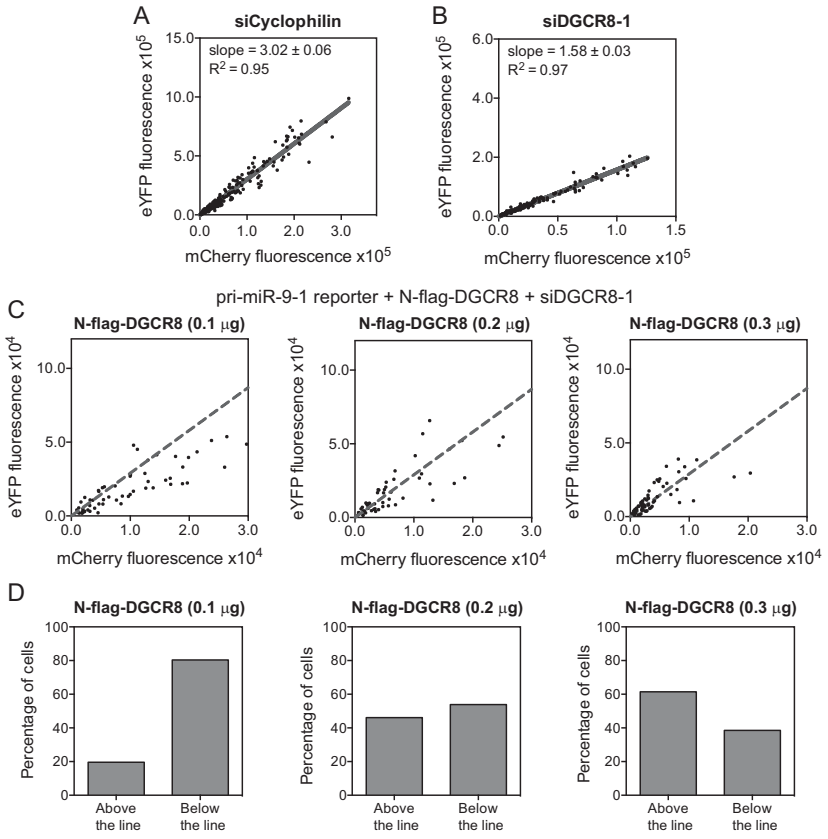

Fig. S3. Additional data to show that the reporter assay detects alteration of endogenous DGCR8 activity. (*A* and *B*) Scatter plots of eYFP vs. mCherry fluorescent intensities from the cotransfection of the pri-miR-9-1 reporter with siCyclophilin (*A*) or siDGCR8-1 (*B*), as described in Fig. 2*C*. The ratio of *y* and *x* axes was set at 4:1 for all scatter plots. (*C*) Scatter plots for cotransfections of the pri-miR-9-1 reporter, siDGCR8-1, and pN-flag-DGCR8. The amount of pN-flag-DGCR8 was varied whereas the amount of reporter was changed correspondingly to keep the total mass of plasmids to 0.4 μg, as required by the Effectene transfection protocol. The cells were assigned to the two groups based on the same gray dashed line as the linear regression fit for the data shown in Fig. 2*D* (slope = 2.9). (*D*) The percentage of data points that fell above and below the gray dashed line in *C*. We believe that cells above the line received pN-flag-DGCR8 whereas those below did not.

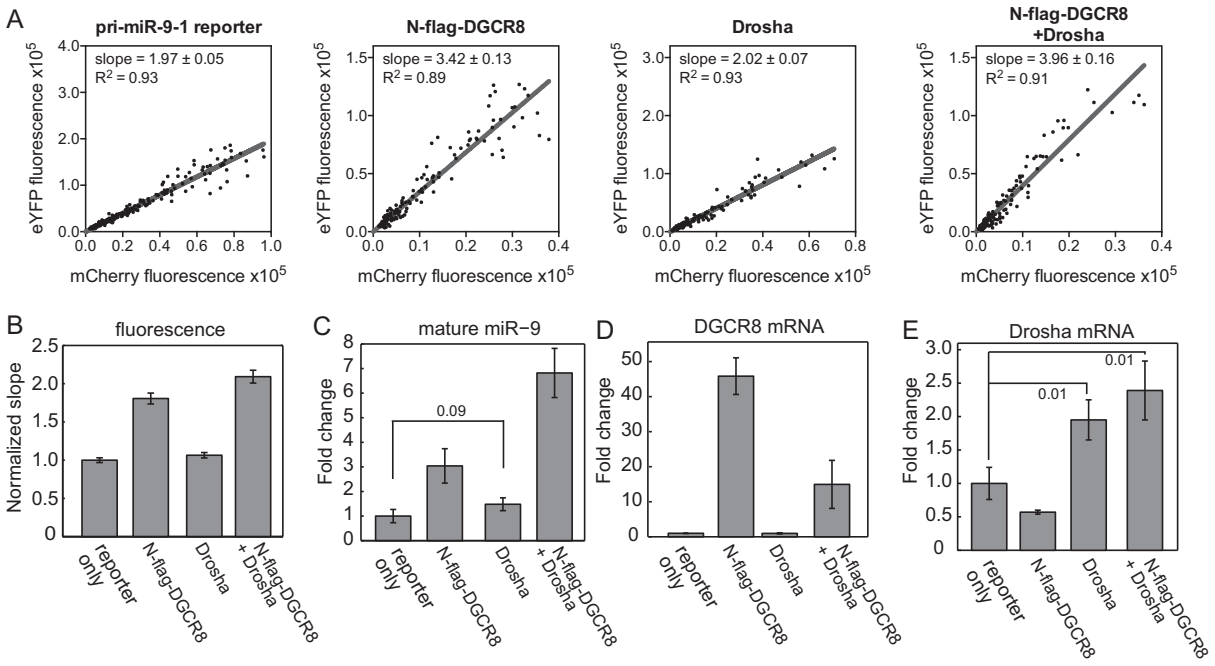

Fig. S4. Overexpression of Drosha does not enhance pri-miR9-1 processing. The pri-miR-9-1 reporter was transfected to HeLa cells either alone or with pN-flag-DGCR8, pCK-Drosha-Flag, or both. Cells were imaged, and RNA was extracted 18–20 h posttransfection. (*A*) Scatter plots showing the eYFP and mCherry fluorescence signals for individual cells and corresponding linear fits. The ratio of *y* and *x* axes was set at 4:1. (*B*) The normalized eYFP/mCherry fluorescence slope. The error bars represent 95% CI. (*C*) Mature miR-9 expression levels were measured using qRT-PCR. Error bars show SD ($n = 3$), except for N-flag-DGCR8, and "N-flag-DGCR8 + Drosha" ranges from two experiments are indicated. Total DGCR8 (*D*) and Drosha (*E*) expression levels, including expression from both endogenous genes and the plasmids, were measured using qRT-PCR. Shown are averages ± SD ($n = 3$). *P* values are labeled on the graphs.

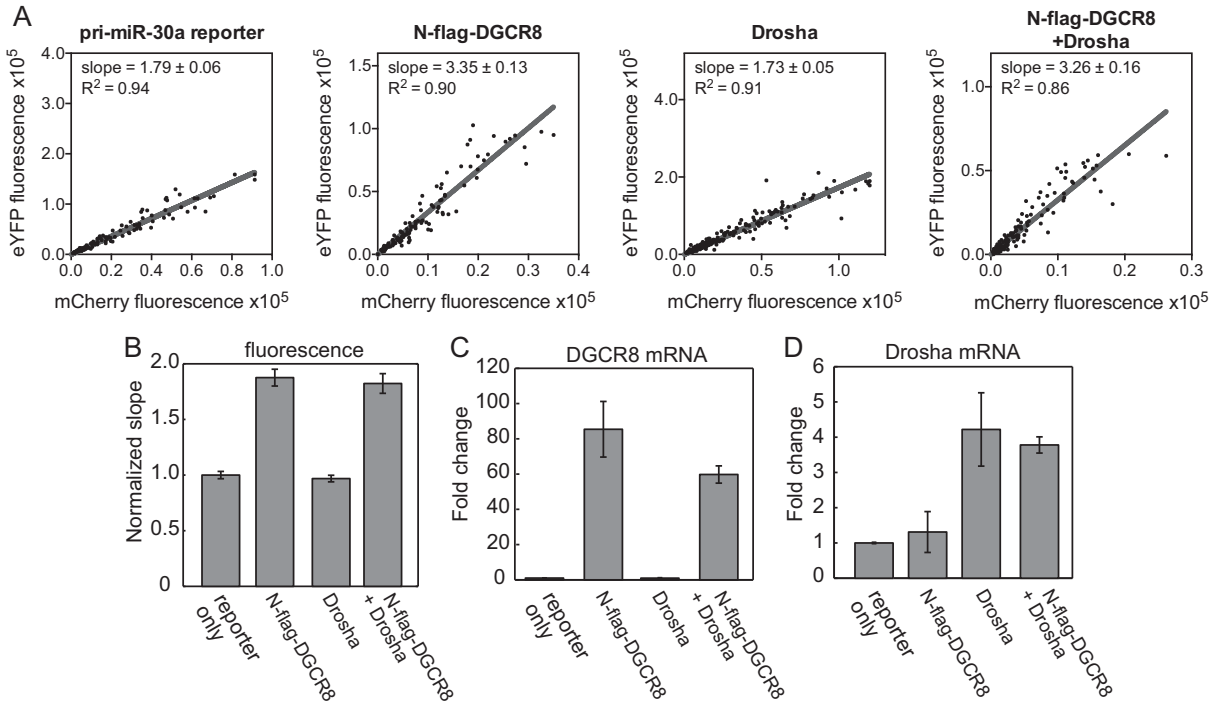

Fig. S5. Overexpression of Drosha does not enhance pri-miR-30a processing. The pri-miR-30a reporter was transfected to HeLa cells either alone or with pN-flag-DGCR8, pCK-Drosha-Flag, or both. (*A*) Scatter plots showing the eYFP and mCherry fluorescence signals for individual cells and corresponding linear fits. The ratio of *y* and *x* axes was set at 4:1. (*B–D*) The normalized eYFP/mCherry fluorescence slopes (*B*), DGCR8 (*C*), and Drosha (*D*) expression levels are plotted. Error bars in *A* represent 95% CI of the linear regression and in other panels show SD ($n = 3$).

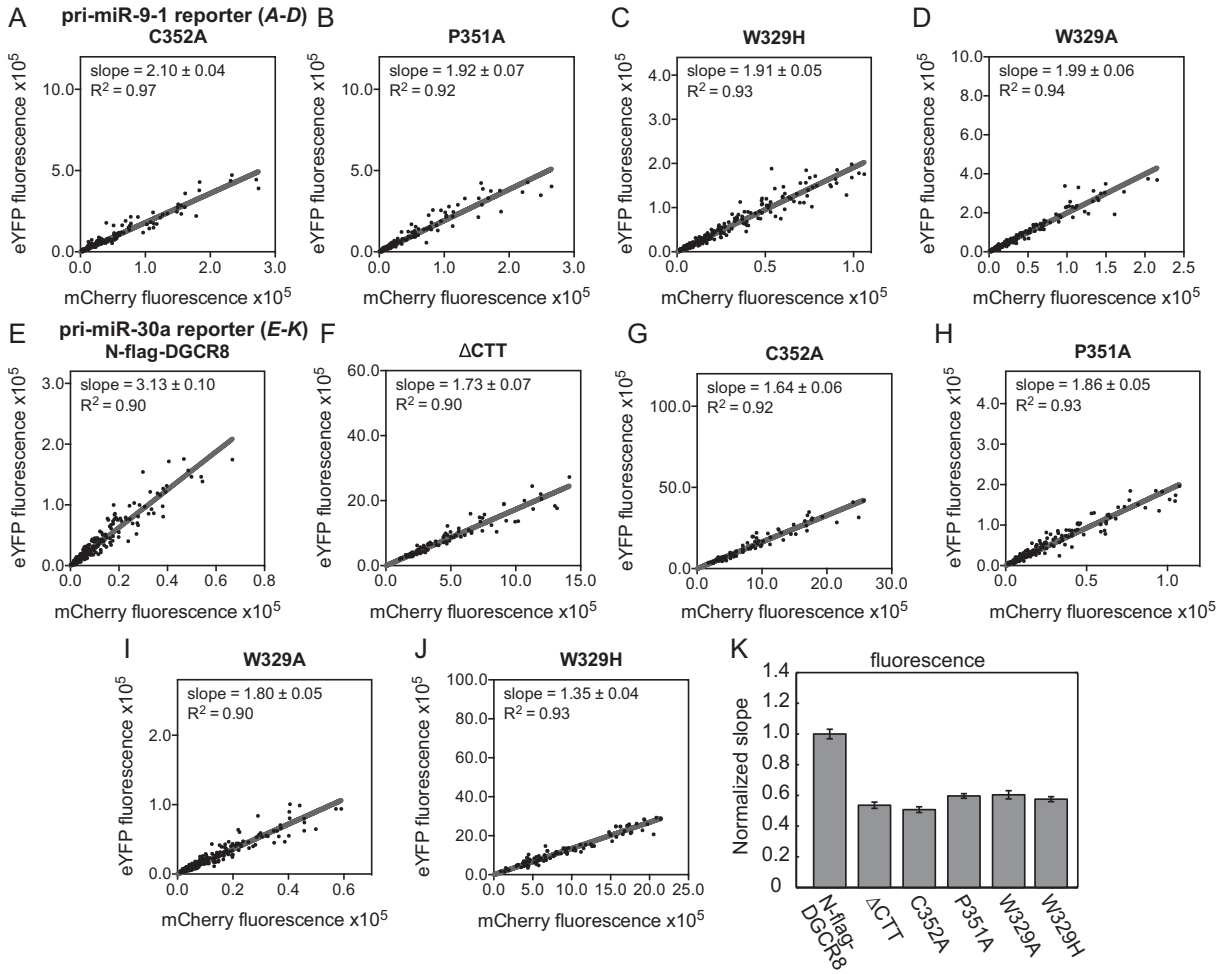

Fig. S6. All known heme-binding–deficient DGCR8 mutants are defective in cells. (*A–D*) Fluorescence scatter plots for the examination of heme-binding–deficient mutants as in Fig. 3 *A* and *F*. (*A*) C352A, (*B*) P351, (*C*) W329H, (*D*) W329A. The ratio of *y* and *x* axes was set at 4:1 for all scatter plots. Scatter plots for the corresponding N-flag-DGCR8 and ΔCTT transfections are shown in Fig. S1 *A* and *B*. (*E–K*) Examination of the DGCR8 mutants using the pri-miR-30a reporter confirms. Scatter plots of the eYFP and mCherry fluorescence signals for individual cells and corresponding linear fit for HeLa cells transfected with pri-miR-30a reporter and pN-flag-DGCR8 (*E*), ΔCTT (*F*), C352A (*G*), P351A (*H*), W329A (*I*), or W329H (*J*). (*K*) Shown are normalized eYFP/mCherry fluorescence slopes from transfections with the pri-miR-30a reporter and the indicated N-flag-DGCR8 expression plasmids. Error bars represent 95% CI from linear regression.

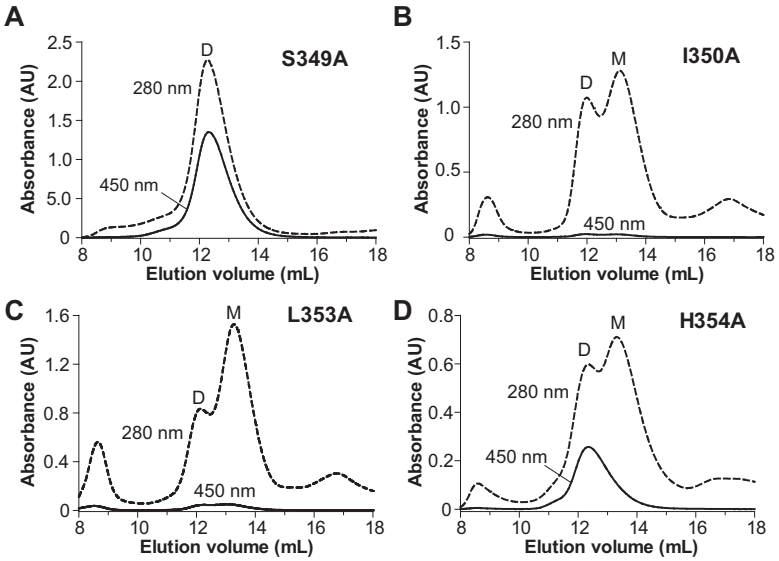

Fig. S7. Identification of a heme-binding motif in DGCR8. Mutant NC1 proteins were overexpressed in *E. coli* with 1 mM δ-ALA added at the time of induction. They were purified using a procedure described previously (5). The size exclusion chromatograms from the last step of the purification are shown. Before this step, the proteins were already over 90% pure. (*A*) S349A. (*B*) I350A. (*C*) L353A. (*D*) H354A. Dimer and "monomer" peaks are labeled as "D" and "M," respectively. The "monomer" species may not be biologically relevant, as it contains heterodimers in which one NC1 subunit is cleaved by bacterial proteases so that only the dimerization domain region remains, and the other NC1 subunit is intact.

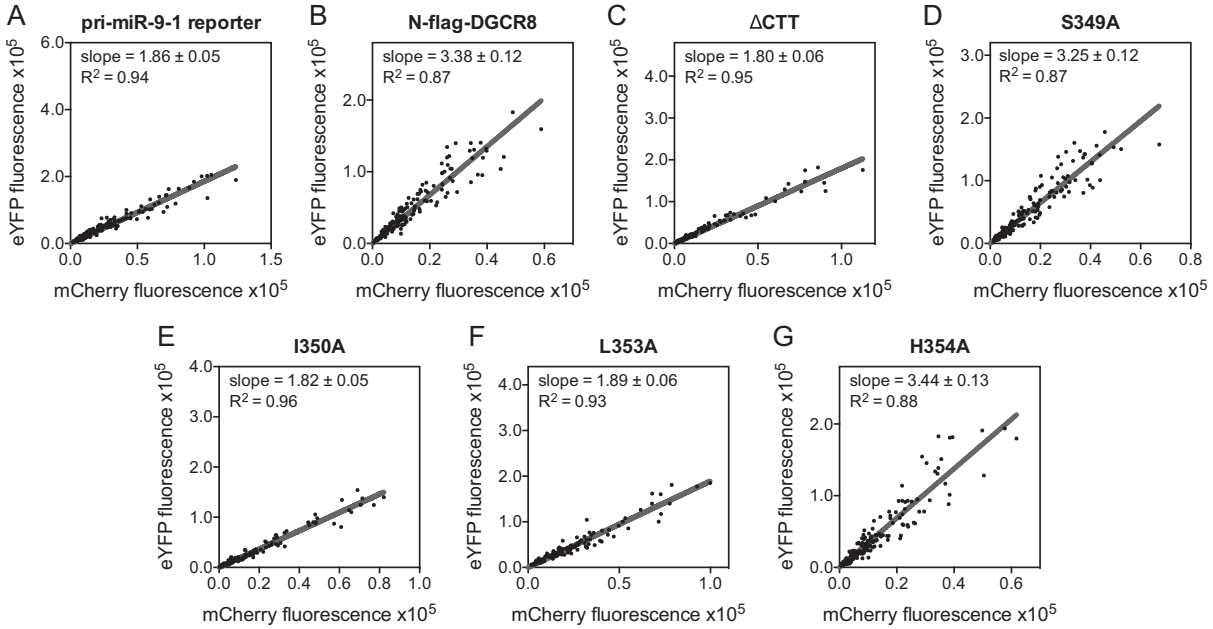

Fig. S8. Fluorescence scatter plots for the examination of DGCR8 mutations in or around the IPCL motif as in Fig. 4. The pri-miR-9-1 reporter was transfected to HeLa cells either alone (*A*) or with pN-flag-DGCR8 (*B*), ΔCTT (*C*), S349A (*D*), I350A (*E*), L353A (*F*), or H354A (*G*). The ratio of *y* and *x* axes was set at 4:1 for all plots.

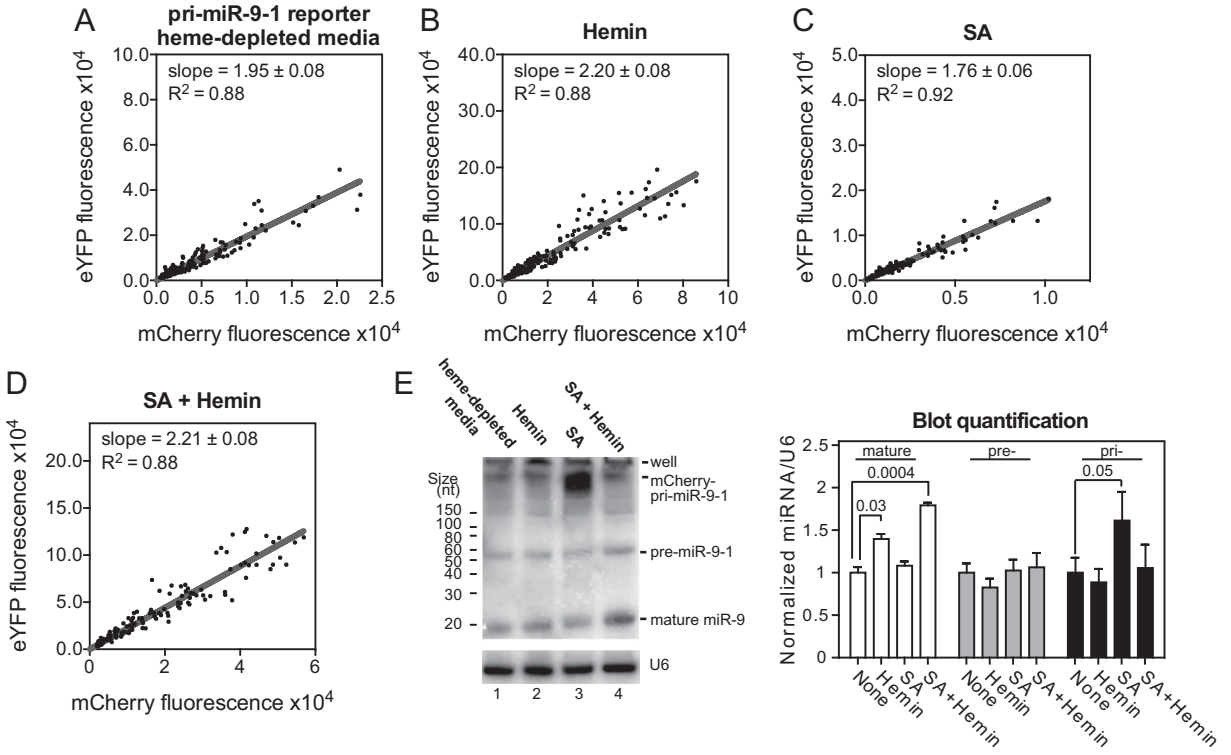

Fig. S9. Additional data to show that heme availability and biosynthesis in cells affect pri-miRNA processing. (*A*–*D*) Fluorescence scatter plots for Fig. 5*A*. HeLa cells were grown in heme-depleted media and transfected with the pri-miR-9-1 reporter, with no chemical treatment (*A*), or treated for 10 h with either hemin (*B*), or succinylacetone (*C*), or both (*D*). The ratio of *y* and *x* axes was set at 4:1 for all scatter plots. (*E*) Northern blot analyses of total RNAs. The pri-, pre-, and mature miR-9 levels, after normalization to those of U6 snRNA, are plotted on the *Right*.

Table S1. Identification of IPCL as a heme-binding motif

DGCR8 construct	Heme-bound	Heme removal by apomyoglobin	Reconstitution of heme complex
WT	Y	N	Y
S349A	Y	N	—
I350A	N	—	N
P351A	Y	Y	Y
C352A	N	—	N
L353A	N	—	N
H354A	Y	N	—

N, no; Y, yes; —, not tested.

CHAPTER 3

The DGCR8 RNA-binding heme domain recognizes primary microRNAs by clamping the hairpin

(Cell Reports, 7, 1994-2005.)

This chapter describes one of my applications of the live cell pri-miRNA processing assay. The project was initially started by Rachel Senturia who found that the heme binding domain was able to bind RNA. In this publication, Jen Quick-Cleavland continues the project, confirms that the heme-binding domain binds RNA and that it specifically recognizes the ss-ds RNA junctions in the pri-miRNA. As a result we rename the domain RNA-binding heme domain (Rhed). I use my cellular assay to prove that DGCR8 requires its RNA-binding heme domain (Rhed) for functional cellular activity. I also identify several basic residues, which are responsible for the DGCR8-RNA interaction. This was a highly collaborative project. Jose P. Jacob performed all of the *in vitro* processing assays. Grant Shoffner performed some of the initial DGCR8 RNA binding experiments.

The DGCR8 RNA-Binding Heme Domain Recognizes Primary MicroRNAs by Clamping the Hairpin

Jen Quick-Cleveland,[1] Jose P. Jacob,[1] Sara H. Weitz,[2] Grant Shoffner,[1] Rachel Senturia,[1] and Feng Guo[1,*]
[1]Department of Biological Chemistry, David Geffen School of Medicine, University of California, Los Angeles, Los Angeles, CA 90095, USA
[2]Molecular, Cell and Integrative Physiology, University of California, Los Angeles, Los Angeles, CA 90095, USA
*Correspondence: fguo@mbi.ucla.edu
http://dx.doi.org/10.1016/j.celrep.2014.05.013

SUMMARY

Canonical primary microRNA transcripts (pri-miRNAs) are characterized by a ~30 bp hairpin flanked by single-stranded regions. These pri-miRNAs are recognized and cleaved by the Microprocessor complex consisting of the Drosha nuclease and its obligate RNA-binding partner DGCR8. It is not well understood how the Microprocessor specifically recognizes pri-miRNA substrates. Here, we show that in addition to the well-known double-stranded RNA-binding domains, DGCR8 uses a dimeric heme-binding domain to directly contact pri-miRNAs. This RNA-binding heme domain (Rhed) directs two DGCR8 dimers to bind each pri-miRNA hairpin. The two Rhed-binding sites are located at both ends of the hairpin. The Rhed and its RNA-binding surface are important for pri-miRNA processing activity. Additionally, the heme cofactor is required for formation of processing-competent DGCR8-pri-miRNA complexes. Our study reveals a unique protein-RNA interaction central to pri-miRNA recognition. We propose a unifying model in which two DGCR8 dimers clamp a pri-miRNA hairpin using their Rheds.

INTRODUCTION

In the canonical microRNA (miRNA) maturation pathway in animal cells, miRNA primary transcripts (pri-miRNAs) are specifically recognized and cleaved by the Microprocessor to produce precursor miRNAs (pre-miRNAs) in the nucleus (Kim et al., 2009; Guo, 2012). Pre-miRNAs are exported to the cytoplasm, where they are cleaved by the ribonuclease Dicer, and mature miRNA strands are incorporated into the miRNA-induced silencing complexes. Previous studies have revealed fundamental features of pri-miRNAs, including a hairpin with mature miRNA strands located on either side of the stem (Lee et al., 2003) and unstructured regions flanking the hairpin (Zeng and Cullen, 2005; Han et al., 2006). The hairpin stems contain roughly 30 bp with internal loops and bulges at variable positions. Base-pairing interactions in the stem, especially the bottom third, are clearly important for processing (Lee et al., 2003). The basal junction of a pri-miRNA, where the stem and the flanking unstructured regions join, is required for processing (Han et al., 2006). It has been proposed that the basal junction serves as an anchoring point for the Microprocessor to determine the cleavage sites ~11 bp away (the basal junction anchoring model). There have also been reports that apical region of the hairpin, including a ≥10 nt terminal loop, is important for processing (Zeng et al., 2005; Zhang and Zeng, 2010). Recently, three short (2–4 nt) sequence motifs have been shown to be enriched in nonnematode pri-miRNAs and important for processing of some pri-miRNAs in human cells (Auyeung et al., 2013). Overall, pri-miRNAs are defined primarily by their structures, with some sequence elements involved.

The Microprocessor has to identify true pri-miRNA substrates out of the myriad of other RNAs, and DGCR8 (*Di*George *c*ritical *r*egion gene *8*, called Pasha in flies and worms) (Lee et al., 2003; Denli et al., 2004; Gregory et al., 2004; Han et al., 2004; Landthaler et al., 2004) plays a major role in this recognition. The 773-residue DGCR8 contains a nuclear localization signal (NLS) in the N-terminal region (Yeom et al., 2006; Shiohama et al., 2007), a central heme-binding domain, two double-stranded RNA-binding domains (dsRBDs), and a C-terminal tail (CTT) (Figure 1A). Prior to this study, the dsRBDs were shown to bind RNAs (Han et al., 2006; Faller et al., 2007; Sohn et al., 2007) and were defined as the "DGCR8 core" (Sohn et al., 2007). However, the dsRBDs alone bind pri-miRNAs with varying stoichiometry (Roth et al., 2013) and thus are unlikely to be the sole specificity determinant. DGCR8 has been shown to crosslink to pri-miRNA basal junction fragments (Han et al., 2006). However, the crosslinked protein and RNA residues have not been identified. It remains unknown how DGCR8 recognizes pri-miRNAs.

DGCR8 binds an essential heme (protoporphyrin IX in complex with iron) cofactor using a unique heme-binding domain. An active recombinant DGCR8 construct called NC1 (residues 276–751) and an isolated heme-binding domain (Figure 1A) both form constitutive dimers bound with one heme molecule (Faller et al., 2007; Senturia et al., 2010; Barr et al., 2011, 2012). Fe(III) heme directly binds the apo form of NC1 dimer and activates pri-miRNA processing in vitro (Barr et al., 2012). In HeLa cells, all known heme-binding-deficient DGCR8 mutants are inactive in pri-miRNA processing, and heme availability affects processing efficiency (Weitz et al., 2014). A WW-motif-containing dimerization subdomain (DSD) resides in the heme-binding domain and contributes a surface for heme binding (Senturia et al., 2010). Dimerization and heme binding appear

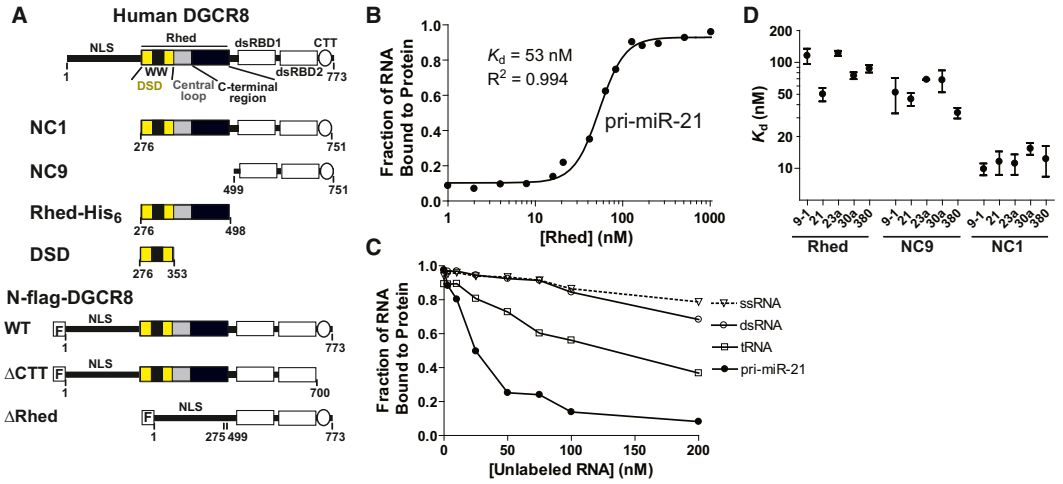

Figure 1. The Rhed Contributes to pri-miRNA Recognition by Directly Binding These RNAs and by Collaborating with the dsRBDs

(A) Recombinant human DGCR8 proteins used. "F" represents a FLAG tag.

(B) A representative curve from filter-binding assays showing that the Rhed binds pri-miRNAs. The data were fit using a cooperative-binding model. The K_d is defined as the Rhed dimer concentration at which half-maximal RNA binding is achieved.

(C) Competition filter-binding assays using unlabeled ssRNA, siRNA duplex, yeast tRNAs, or pri-miR-21 to compete with a trace amount of ^{32}P-labeled pri-miR-21 for association with 150 nM of Rhed dimer. An average molecular mass of 25 kDa was assumed in calculating molar concentrations of tRNAs.

(D) Comparison of the K_d values of Rhed, NC9, and NC1 for a panel of five pri-miRNAs. The average K_d values and SD are summarized in Table 1. Purity of the recombinant proteins is shown in Figure S1. The sequences and MFOLD-predicted secondary structures (Zuker, 2003) of these pri-miRNAs are shown in Table S1 and Figure S2.

to be conserved features of DGCR8 homologs (Senturia et al., 2012). Despite the body of evidence supporting the importance of the DGCR8 heme-binding domain, its function in pri-miRNA processing remains unclear.

In this work, we show that the heme-binding domain of DGCR8 plays a key role in pri-miRNA substrate recognition. Therefore, we have renamed this domain the RNA-binding heme domain (Rhed). The Rhed directly binds pri-miRNAs at the basal and apical junctions of the hairpin. Using cellular and biochemical pri-miRNA processing assays, we show that the Rhed and the Rhed-RNA interaction are important for DGCR8 activity. By collaborating with other domains, the Rhed allows full structural features of pri-miRNAs to be recognized.

RESULTS

The Rhed of DGCR8 Directly Binds pri-miRNAs, Contributing to Affinity and Specificity

Our biochemical analyses indicate a function of Fe(III) heme-bound Rhed in pri-miRNA recognition. Because the Fe(II) heme-bound and heme-free forms of the human Rhed are insoluble at pH 5–8, we exclusively use the Fe(III) heme-bound Rhed dimer in this study and refer to this form of the protein as the Rhed. Filter-binding assays showed that the Rhed binds a panel of five pri-miRNAs (Figure S2) with K_d values ranging from 50 to 120 nM under equilibrium conditions (Figure 1B; Table 1). These interactions appear to be specific to pri-miRNAs, as neither a 21 nt single-stranded RNA (ssRNA) nor an siRNA duplex can compete with pri-miR-21 for binding the Rhed in competition filter-binding assays (Figure 1C). tRNAs do compete, but not as efficiently as unlabeled pri-miR-21 (Figure 1C). Therefore, it is likely that the Rhed contributes to the pri-miRNA-binding specificity of DGCR8.

To estimate the relative contribution of the Rhed and dsRBDs to pri-miRNA binding, we measured the affinity of Rhed, NC1, and NC9 (=NC1 ΔRhed) for pri-miRNAs. The NC1 protein we used in this study is a Fe(III) heme-bound dimer unless stated otherwise. With deletion of the Rhed that is also responsible for dimerization, NC9 is a monomer. The affinity of the Rhed for each of the five pri-miRNAs (K_d = 50–120 nM) is comparable to that of the dsRBDs-containing NC9 (K_d = 30–70 nM) (Figure 1D; Table 1), indicating the importance of Rhed in RNA binding. Both the Rhed and NC9 have lower affinities for each of the pri-miRNAs compared to NC1 (K_d = 10–16 nM) (Figure 1D; Table 1), suggesting that these domains work together to achieve tight binding. The K_d values for NC1 and NC9 are in qualitative agreement with other measurements for similar constructs as previously reported (Faller et al., 2007, 2010; Sohn et al., 2007; Roth et al., 2013).

Each pri-miRNA Hairpin Contains Two Binding Sites for DGCR8

We analyzed the DGCR8-pri-miRNA-binding stoichiometry using size-exclusion chromatography (SEC), in which A_{450nm} (the Söret peak of the DGCR8-bound heme) and A_{260nm} (contributed mostly by RNA and to a lesser extent by the DGCR8-heme complex) were monitored simultaneously. Injection of NC1 mixed with pri-miR-23a or pri-miR-21 at 2:1 ratio resulted in single peaks (Figures 2A and 2B). Using a recently determined extinction coefficient (ϵ) of human DGCR8-bound heme (74 mM^{-1} cm^{-1} at

Table 1. Summary of K_d Values in nM Units Measured Using Filter-Binding Assays

Rhed and dsRBDs Working Together to Achieve High-Affinity Binding to pri-miRNA

pri-miRNA	Rhed	NC9	DSD	NC1
pri-miR-380	87 ± 7	33 ± 4	143 ± 13	12 ± 4
pri-miR-9-1	119 ± 18	52 ± 19	152 ± 51	10 ± 1
pri-miR-21	50 ± 7	45 ± 6	158 ± 10	12 ± 4
pri-miR-23a	121 ± 7	69 ± 0.6	208 ± 23	10 ± 1
pri-miR-30a	75 ± 6	72 ± 19	204 ± 3	16 ± 1

K_d of Rhed for Truncated pri-miRNAs

Apical Junctions	No. of bp in Stem	K_d	Basal Junctions	No. of bp in Stem	K_d
aj-miR-23a-C	24	102 ± 6	bj-miR-23a	9	232 ± 15
aj-miR-23a-D	20	191 ± 24			
aj-miR-23a-E	11	FB_{max} = 0.2–0.5			
aj-miR-23a-F	7	FB_{max} = 0.2–0.5			
aj-miR-21-D	18	178 ± 32	bj-miR-21	8	326 ± 32
aj-miR-21-E	10	FB_{max} = 0.2–0.5			

Mutations in the Rhed Region that Directly or Indirectly Affect the Affinity for pri-miRNAs

Mutants	R322A/R325A		R341A/K342A		K424A/K426A/K431A (G1)	
Context	NC1	DSD	NC1	Rhed	NC1	Rhed
pri-miR-380	25 ± 3	151 ± 16	32 ± 3	NB	50 ± 6*	57.3 ± 20
pri-miR-9-1	28 ± 5	116 ± 8	48 ± 5	NB	30 ± 5*	FB_{max} = 0.2–0.5
pri-miR-21	22 ± 1	240 ± 14	45 ± 3*	NB	19 ± 1*	FB_{max} = 0.2–0.5
pri-miR-23a	36 ± 20	128 ± 41	45 ± 5	NB	24 ± 5*	FB_{max} = 0.2–0.5

Errors are SD from three to nine repeats except those marked by "*," which indicate ranges from two replicates. In the binding reactions, the fraction of RNA bound (FB) to protein generally plateaued to >0.9. Those reactions in which the maximal FB only reaches 0.2–0.5 are marked as "FB_{max} = 0.2–0.5." The highest protein concentrations used were 1 or 3 μM. See also Figures S2 and S3 and Table S1. NB, no binding.

450 nm) (Senturia et al., 2012), we calculated the molar ratios of NC1 dimers and pri-miRNAs to be ~2:1 across the elution peaks (Figure 2B). These data suggest that there are two binding sites for DGCR8 dimers on each pri-miRNA hairpin.

The elution volume of the NC1-pri-miR-23a complex (8.3 ml) is close, but not identical, to the void volume (8.2 ml). We previously observed a similar elution volume for the NC1-pri-miR-30a complex (8.5 ml) (Figure 5D) (Faller et al., 2007). The 480 kDa apoferritin (one of the standard proteins used for calibration) also elutes in this region. These DGCR8-pri-miRNA complexes (including NC1-pri-miR-21) are expected to have molecular masses of ~260 kDa but greatly deviate from globular shapes and contain peripheral RNA strands of various lengths and structures. Therefore, it is not surprising that these complexes elute as if with higher molecular masses. Importantly, the protein-RNA ratios determined from the A_{450} and A_{260} measurements are independent of the elution volumes and shapes of the complexes.

The Rhed Determines the Stoichiometry of DGCR8-pri-miRNA Interaction

We performed similar SEC analyses using the Rhed. An input containing the Rhed and pri-miRNA (pri-miR-23a, pri-miR-21, or pri-miR-30a) at 2:1 molar ratio elutes in a single peak that is about 2 ml earlier than that of the free RNA (Figures 2C and S4A). Based on the A_{450} and A_{260} in the chromatograms, we calculated the Rhed:RNA ratio to be ~2:1 across the elution peak. Therefore, we conclude that there are two Rhed-binding sites on a pri-miRNA and that the Rhed is responsible for determining the DGCR8-pri-miRNA-binding stoichiometry. It is likely that the Rhed occupies similar pri-miRNA-binding sites whether it is in an isolated polypeptide or a part of processing-competent DGCR8 proteins.

We also analyzed the Rhed and pri-miR-30a complex at substoichiometric (1:1) input ratio. We observed an SEC elution peak at 11.4 ml, between those of the 2:1 complex (10.1 ml) and the free RNA (~12 ml) (Figure S4B). The Rhed:RNA ratio gradually changed from 2:1 to 0 across the elution peak, indicating the presence of multiple species at 2:1, 1:1, and 0:1 ratios that were partially resolved. This result suggests that, at least in the absence of the dsRBDs and CTT, the Rhed does not strongly prefer to bind one site versus the other.

The Rhed Binds Both Ends of a pri-miRNA Hairpin—The Apical and Basal Junctions

To locate the Rhed-binding sites on pri-miRNAs, we generated a series of truncated pri-miRNAs (Figures 2A and S3; Table S1) and analyzed their interactions with the Rhed using filter-binding assays and SEC. A pri-miR-23a truncation contains the 10 nt hairpin loop and 24 bp of the upper stem and thus includes the apical junction (aj-miR-23a-C; Figure S3A). The Rhed binds to aj-miR-23a-C with an affinity similar to that for pri-miR-23a (Table 1). Importantly, SEC analyses indicated that the Rhed dimer:aj-miR-23a-C molar ratio in their complex is reduced to ~1:1. When the Rhed:aj-miR-23a-C input ratio was 1:1, a single

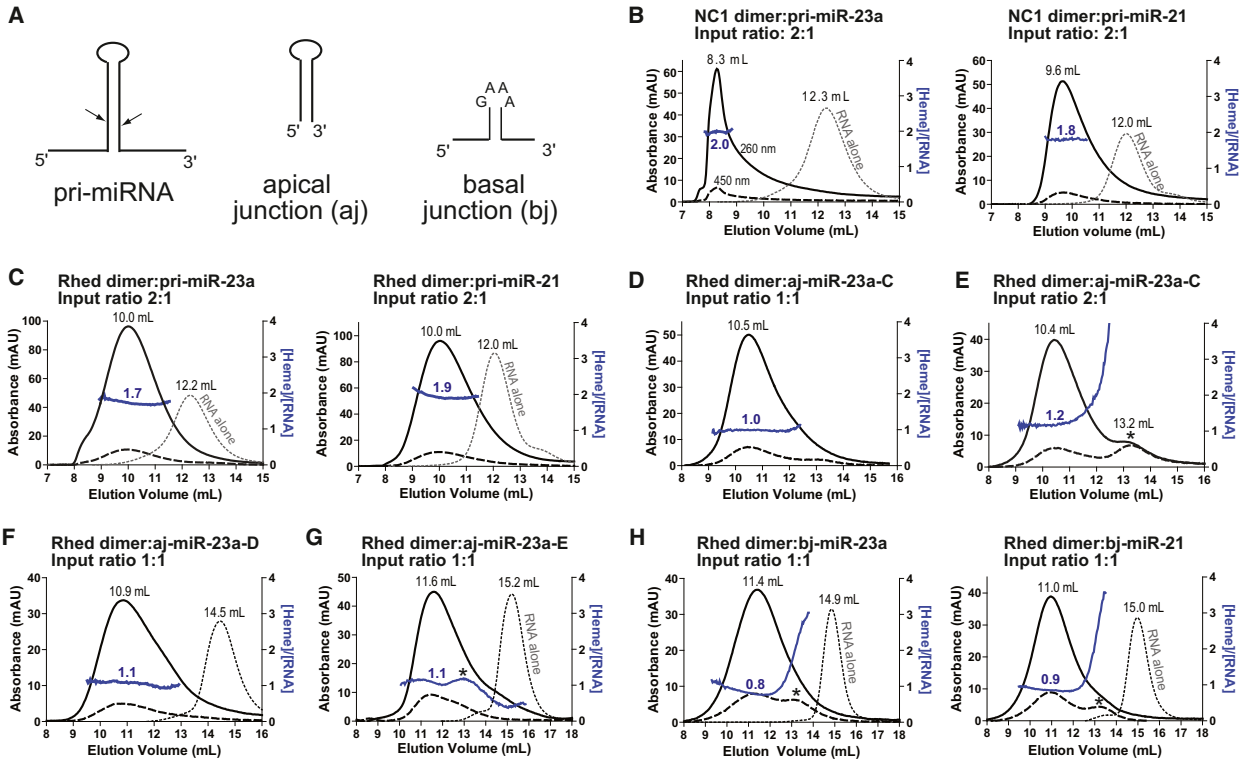

Figure 2. RNA Truncation and SEC Analyses Suggest that the Rhed Binds to pri-miRNA Junctions

(A) Schematics of pri-miRNA fragments. The arrows indicate the Drosha cleavage sites. The sequences and secondary structures are shown in Table S1 and Figures S2 and S3.

(B–H) Size-exclusion chromatograms of NC1 in complex with 2 μM pri-miRNAs (B), the Rhed with 2 μM pri-miRNAs (C), the Rhed with 4 μM of aj-miR-23a-C at varying input ratios (D and E), the Rhed with 4 μM of aj-miR-23a-D (F), the Rhed with 4 μM of aj-miR-23a-E (G), and the Rhed with 4 μM of indicated basal junctions (H). Solid black lines indicate A_{260}, dashed lines show A_{450}, and dotted lines are A_{260} of the RNA-only runs. Solid blue lines represent heme:RNA ratios calculated from A_{450} and A_{260}, following the scale on the right y axis. The asterisk in (E), (G), and (H) marks a peak of free Rhed.

See also Figures S1–S4 and Table S1.

peak was observed, whereas increasing the input ratio to 2:1 resulted in a chromatogram containing both free-Rhed and complex peaks with nearly equal A_{450} (Figures 2D and 2E). We further truncated pri-miR-23a-C at its basal segments to generate aj-miR-23a-D, aj-miR-23a-E, and aj-miR-23a-F, which contain 20 bp, 11 bp, and 7 bp (Figures S3B–S3D), respectively. SEC analyses show that the Rhed forms ~1:1 complexes with all three RNAs (Figures 2F, 2G, S4C, and S4D), suggesting that the apical junction region contains a core binding site for the Rhed. Filter-binding assays showed that the affinity of Rhed for these RNAs decreases over the truncations, with K_d values increased to 191 nM for aj-miR-23a-D and the fractions of aj-miR-23a-E and aj-miR-23a-F bound to 1 μM Rhed only reached 0.25–0.30 and 0.15–0.20, respectively (Table 1). The large reduction in affinity caused by the deletion of 9 bp from aj-miR-23a-D suggests that the central segment of the pri-miR-23a stem is also important for the Rhed to bind the apical hairpin. Furthermore, to evaluate the importance of the hairpin loop, we replaced the 10 nt loop of aj-miR-23a-C with a GAAA tetraloop (aj-miR-23a-C-GAAA; Table S1) and found that the affinity of Rhed for this RNA decreased dramatically with the fraction of RNA bound to 1 μM Rhed only reached ~0.20. We also engineered pri-miR-21 to produce apical hairpins aj-miR-21-D and aj-miR-21-E that contain 18 bp and 10 bp in their stems (Figures S3E and S3F). The Rhed binds these RNAs with 1:1 stoichiometry (Figure S4E) and decreasing affinities over the truncations (Table 1), similar to the pri-miR-23a aj series. Therefore, we conclude that a Rhed-binding site is located in the apical junction area and a high-affinity interaction requires both the hairpin loop and ~20 bp of the upper stem.

To identify the second Rhed-binding site, we deleted the apical hairpins from the pri-miRNAs and thereby produced basal junction models that include 8–9 bp of the lower stem and 7–9 nt of single-stranded regions on both sides of the hairpin (Figures 2A, S3G, and S3H). We linked the 5′ and 3′ strands using a GAAA tetraloop to stabilize the relatively short stem. The Rhed binds these bj-miRNAs, with affinities (K_d's of 232–326 nM) modestly lower than those for pri-miRNAs (K_d's of 50–120 nM) (Table 1), and the stoichiometry is ~1:1 (Figure 2H). As the bj RNAs are already quite short, we conclude that the second Rhed-binding site is located at the basal junction of a pri-miRNA.

Both the apical and basal Rhed-binding sites contain stem-ssRNA junctions, which are likely to be important features for Rhed to recognize. The stem and single-stranded regions of the junctions are all required for binding the Rhed, as neither ssRNA nor a duplex can compete with pri-miRNAs (Figure 1C) and substituting the hairpin loop of aj-miR-23a-C with GAAA disrupts the binding (see above). We also considered the possibility that certain pri-miRNA sequences drive the association with the Rhed. Three sequence motifs have recently been shown to be important for processing of some pri-miRNAs in human cells (Auyeung et al., 2013), including a "UG" at −14 position (14 nt upstream of the 5′ Drosha cleavage site), a "UGU" or "GUG" at P22–P44 positions (22–24 nt into the pre-miRNA), and a "CNNC" at positions 16–17 (16–17 nt downstream of the 3′ Drosha cleavage site). The −14 position is located at the basal junction, P22-P24 at the apical junction, and the 16–17 positions are close to the basal junction. We searched for these motifs in the five pri-miRNAs used in this study. pri-miR-30a has all three motifs, pri-miR-380 has none, and pri-miR-9-1, pri-miR-21, and pri-miR-23a each contain two (Figures S2). There is no clear correlation between the presence of these motifs and the affinity for Rhed (Table 1). Therefore, it is likely that the Rhed recognizes the structures of pri-miRNA junctions.

The Rhed Is Required for pri-miRNA Processing

We next tested if the Rhed and its RNA-binding activity are important for pri-miRNA processing using cellular and biochemical assays. We first employed a recently developed fluorescent live-cell assay for pri-miRNA processing (Weitz et al., 2014). In this assay, a reporter plasmid inducibly expresses two fluorescent proteins, mCherry and eYFP (Figure 3A). A pri-miRNA sequence is inserted into the 3′ UTR of the mCherry expression cassette, so that cleavage of the pri-miRNA reduces mCherry expression. The eYFP and mCherry fluorescent signals for individual cells have a linear relationship, and the slope faithfully indicates the efficiency of pri-miRNA processing but is not affected by subsequent steps of the miRNA maturation pathway (Weitz et al., 2014). Cotransfection of the reporter with the N-flag-DGCR8 expression plasmid (Figure 1A) increases pri-miRNA processing efficiency and the fluorescence slope (Figure 3B) and thus provides a robust method for measuring the activity of DGCR8 mutants. Endogenous DGCR8 is expressed at a very low level in HeLa cells and does not seem to interfere with the measurements as the N-flag-DGCR8 expression is typically 30- to 100-fold higher (Weitz et al., 2014).

Using live-cell reporters containing either pri-miR-9-1 or pri-miR-30a, we found that deletion of the Rhed renders DGCR8 inactive. Unlike the wild-type, expression of N-flag-DGCR8 ΔRhed (Figure 1A) fails to increase the eYFP versus mCherry slopes relative to the transfections either without exogenous DGCR8 expression or with an inactive DGCR8 mutant, ΔCTT, in which the CTT is deleted (Han et al., 2004; Faller et al., 2010) (Figure 3B). The lost activity of ΔRhed is further supported by quantitative RT-PCR (qRT-PCR) measurements of the eYFP mRNA (for normalization), mCherry-pri-miRNA fusions, and mature miRNAs (Figures 3C and 3D) and is not caused by reduced DGCR8 protein expression or lack of nuclear localization (Figure 3E). Altogether, our data suggest that the Rhed is required for pri-miRNA processing in human cells.

Two previous studies showed that recombinant DGCR8 proteins without the Rhed and NLS are active for processing pri-miR-16 and pri-miR-30a in vitro (Yeom et al., 2006; Faller et al., 2007). To clarify the functional importance of the Rhed, we compared the processing activity of NC1 and NC9 (Figure 1A) in vitro using four additional pri-miRNA substrates (Figures S2A–S2D; Table S1). Deletion of the Rhed from the highly active NC1 abolishes processing of pri-miR-380, pri-miR-9-1, and pri-miR-21 at all DGCR8 concentrations tested in vitro (Figures 3F–3H and 3K). The activity of NC9 is greatly reduced for pri-miR-23a compared to that of NC1, with some processing observed at high NC9 concentrations (100 nM in Figure 3I and 200 nM in Figure 3K). We also confirmed that NC9 has substantial pri-miR-30a processing activity (Figures 3J and 3K), similar to the previous report (Faller et al., 2007). The pri-miR-30a sequence used in in vitro processing assays is identical to the insert of the pri-miR-30a cellular reporter. It is possible that, in vitro, recombinant DGCR8 constructs with the Rhed deleted *can* assemble with certain pri-miRNAs into productive complexes that are not formed in vivo. Altogether, our cellular and biochemical results demonstrate that the Rhed is important for DGCR8 function. These observations also highlight the importance of using both biochemical and cellular assays in studying pri-miRNA processing mechanism.

The RNA-Binding Surface of Rhed Is Important for pri-miRNA Processing

We next analyzed the RNA-binding surface of the Rhed using truncation and site-directed mutagenesis. The Rhed can be roughly divided into three regions: the N-terminal DSD, a central acidic loop, and a C-terminal region (Figure 1A). The DSD is soluble when expressed in *E. coli* without the rest of Rhed (Senturia et al., 2010). Filter-binding assays show that the DSD binds pri-miRNAs but does not bind the 21 nt ssRNA or the siRNA duplex. The affinities of the DSD for the five pri-miRNAs (K_d = 150–300 nM) are only modestly lower than those of the Rhed (K_d = 50–120 nM) (Table 1). However, unlike the Rhed, the DSD binds the junction-less aj-miR-23a-C-GAAA, with a K_d of 518 ± 45 nM (mean ± range, n = 2). These results suggest that the DSD makes an important contribution to the Rhed-pri-miRNA interaction but does not retain all the affinity or exactly the same binding specificity.

Site-directed mutagenesis demonstrated that both the DSD and C-terminal regions of the Rhed contribute to pri-miRNA binding. The central loop is the least conserved among DGCR8 homologs and thus was not explored here. We previously determined crystal structures of the DSDs from human and frog DGCR8 (Senturia et al., 2010; Senturia et al., 2012). Inspection of the structures identified four surface-exposed basic residues (R322, R325, R341, and K342), which we mutated to alanine in pairs of spatial proximity (Figure 4A). The C-terminal region (residues 413–498) is rich in conserved basic residues (Senturia et al., 2012). Because no structure is available for this region, we systematically mutated them to alanine in groups with each containing two to three nearby mutations. These mutations were introduced to DGCR8 in a variety of contexts

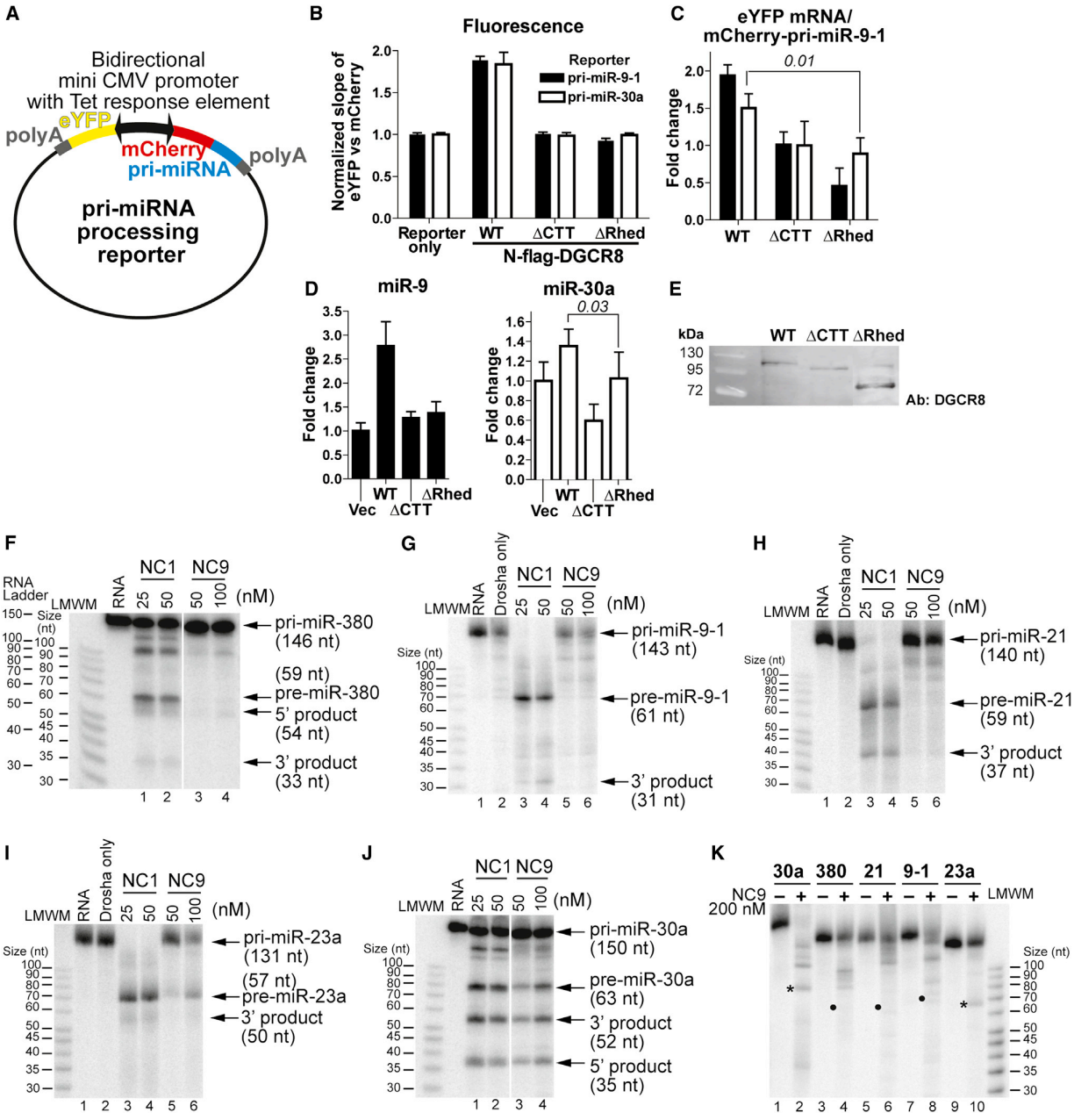

Figure 3. The DGCR8 Rhed Is Important for pri-miRNA Processing

(A) Schematic of the reporter plasmids.

(B–E) The reporters were transfected into HeLa cells either alone or with the indicated N-flag-DGCR8 expression plasmids. (B) Slopes of the eYFP and mCherry fluorescence intensities, after normalization to that of the reporter-only transfection, are plotted. Error bars represent 95% confidence intervals. (C) Ratios of eYFP mRNA and mCherry-pri-miRNA (mean ± SD, n = 3 or 4). (D) Abundance of mature miR-9 and miR-30a normalized by that of β-actin (mean ± SD, n = 3). Select p values are indicated in italics. miR-30a is highly expressed endogenously in HeLa cells, and thus the relative changes are modest. (E) An anti-DGCR8 immunoblot of nuclear extracts from the transfected cells. An equal amount of total proteins was loaded in each lane, as estimated using a Coomassie-stained SDS gel.

(F–K) Reconstituted pri-miRNA processing assays. LMWM, low-molecular-weight marker. Relationship between LMWM and a true RNA ladder in 15% gels is shown in (F). In (K), the asterisks mark a pre-miRNA band and the dots mark the position expected for a pre-miRNA product.

See also Figure S1.

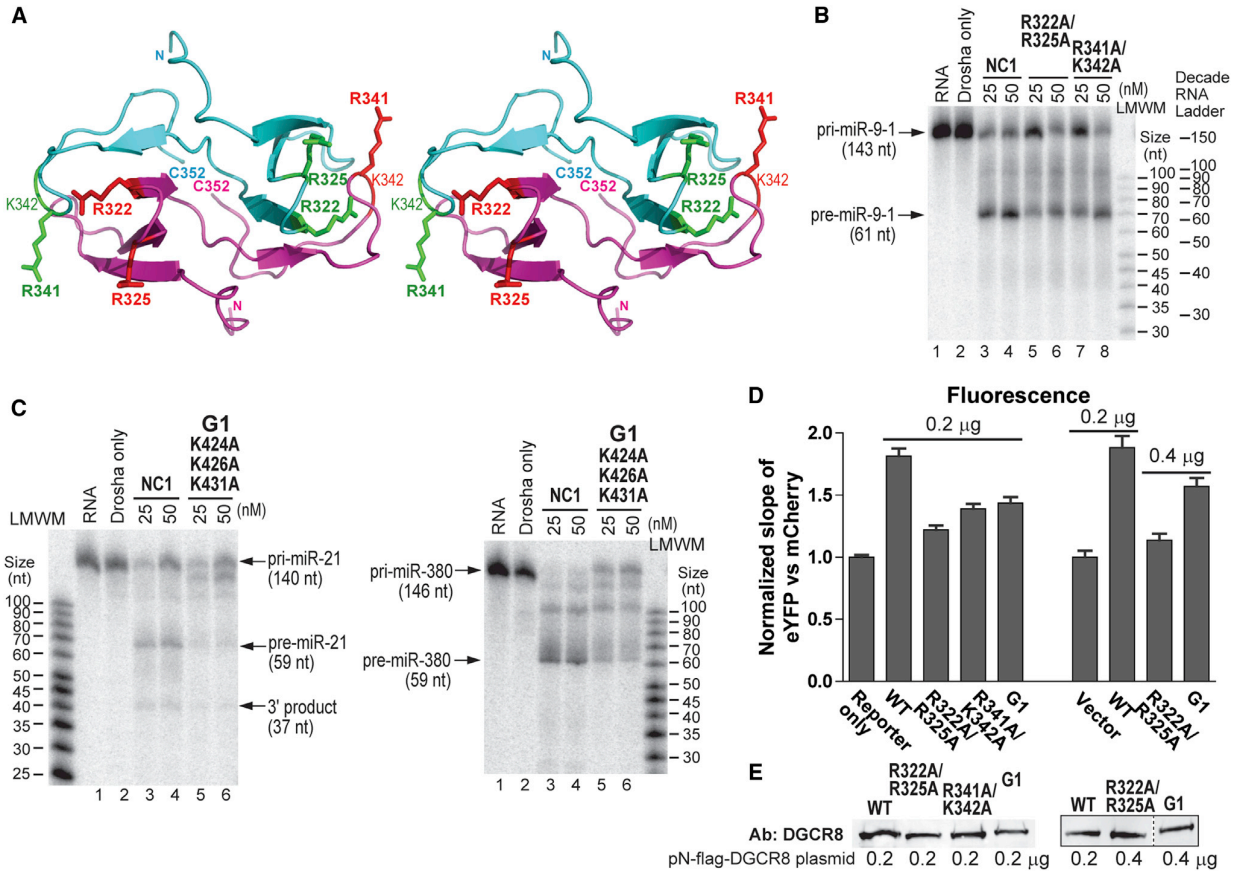

Figure 4. The pri-miRNA-Binding Surfaces of the Rhed Are Important for Processing

(A) Stereo diagram of the DSD crystal structure of human DGCR8 (Protein Data Bank accession code 3LE4) (Senturia et al., 2010), with the side chains of the mutated residues shown in sticks. The two subunits are drawn in cyan and magenta.

(B and C) Reconstituted pri-miRNA processing assays.

(D) Cellular assays using the pri-miR-9-1 reporter. The amounts of DGCR8 expression plasmids or the pCMV-Tag-2A vector are indicated on the graph. Error bars represent 95% confidence intervals. The presence of pCMV-Tag2A vector in the control transfection does not alter the fluorescence slope.

(E) Anti-DGCR8 immunoblots of nuclear extracts from transfected cells. Equal amount of total proteins was loaded in each lane.

See also Figures S1 and S5.

for pri-miRNA-binding and processing assays. Filter-binding assays indicated that the R341A/K342A mutations reduce the affinities by 3- to 5-fold for pri-miRNAs in the context of the NC1 and abolish pri-miRNA binding in the context of the Rhed (Table 1). The lack of pri-miRNA binding of Rhed R341A/K342A was confirmed using SEC analyses (Figure S5A). These results clearly indicate that R341 and K342 make a critical contribution to the Rhed-pri-miRNA interaction, most likely by directly participating at the RNA-binding interface. The modest affinity changes of the NC1 mutant are not surprising, as the dsRBDs are intact.

The R322A/R325A mutations reduce the affinity for pri-miRNAs by about 2- to 4-fold in the context of NC1 but make the Rhed protein insoluble and do not strongly alter the affinity for pri-miRNAs in the context of the DSD (Table 1). These observations suggest that R322 and R325 affect the Rhed-pri-miRNA interaction indirectly by partially disrupting the Rhed structure. The K424A/K426A/K431A mutations (G1) decreases the affinity for pri-miRNAs by 2- to 4-fold in the context of NC1 and render the Rhed protein incapable to plateauing to >50% occupancy of most pri-miRNAs in filter-binding assays (Table 1). These RNA-binding defects were not caused by failure of the Rhed G1 mutant to bind the nitrocellulose membrane used in filter-binding assays, regardless whether pri-miRNAs are present (data not shown). However, SEC analyses of the Rhed G1-pri-miRNA complexes, assembled at higher protein and RNA concentrations (4 and 2 μM, respectively), showed peaks similar to those of the complexes formed by the wild-type Rhed protein (Figure S5B). Overall, our data suggest that at least some of the mutated residues contribute to pri-miRNA binding but that the RNA-binding defects of the mutant are not as severe as those of R341A/K342A.

The R341A/K342A, R322A/R325A and G1 mutants in the context of NC1 demonstrate reduced pri-miRNA processing activity in vitro (Figures 4B and 4C). Their electronic absorption

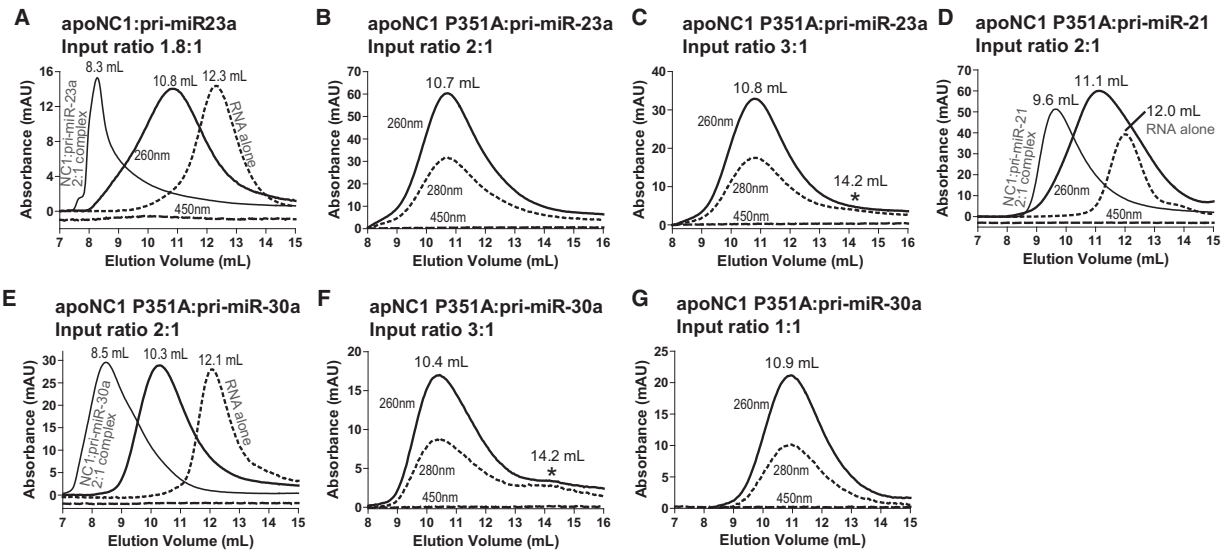

Figure 5. Fe(III) Heme Causes a Large Conformational Change to DGCR8-pri-miRNA Complexes

Size-exclusion chromatograms of (A) apoNC1 in complex with 0.45 μM pri-miR-23a and (B–G) apoNC1 P351A with 2 μM pri-miRNAs at the indicated input ratios. The asterisk in (C) and (F) marks a potential free protein peak.

spectra are indistinguishable from those of the wild-type (Figures S5C–S5F), ruling out the possibility that the pri-miRNA processing defects are caused by a heme-binding deficiency. Finally, these mutations were tested in the context of N-flag-DGCR8 using the live-cell reporter assay. The normalized eYFP versus mCherry slopes were 1.22 ± 0.03, 1.39 ± 0.04, and 1.44 ± 0.05 (±95% confidence interval, same below) for R322/R325A, R341A/K342A and G1, respectively (Figure 4D). These slopes are significantly lower (p values < 0.0001) than the 1.81 ± 0.06 for the wide-type N-flag-DGCR8 but also significantly higher (p values < 0.0001) than the 1.00 ± 0.02 for the reporter-only transfections. Immunoblotting analyses indicated that the N-flag-DGCR8 mutants were expressed at levels either similar to (R341A/R325A) or slightly lower than (R322A/K325A and G1) that of the wild-type (Figure 4E). We successfully compensated the lower expression levels of the N-flag-DGCR8 mutants by doubling the amounts of expression plasmids used in the transfections (Figure 4E) and observed no increase in the fluorescence slope for R322A/R325A (1.14 ± 0.05) and a slight increase of the fluorescence slope for G1 (1.57 ± 0.07) (Figure 4D). The G1 slope is still significantly lower than that of the wild-type control (1.88 ± 0.09) (p value < 0.0001). These results indicate that these mutations render the DGCR8 protein partially defective in cells. Altogether, our data demonstrate that the DSD and the C-terminal region of the Rhed contribute to pri-miRNA binding and that the RNA-binding surface is important for the pri-miRNA processing activity of DGCR8.

Fe(III) Heme Is Required for Formation of Proper DGCR8-pri-miRNA Complexes

To understand the role of heme in DGCR8-pri-miRNA interaction, we analyzed the interaction between the heme-free apoNC1 proteins and pri-miRNA. We previously showed that apoNC1 has affinity for pri-miRNAs similar to that of the Fe(III) heme-bound form (Barr et al., 2012). This is not surprising, as the DSD and dsRBDs are still expected to be well folded. SEC analysis of the apoNC1 dimer with pri-miR-23a at an input ratio of 2:1 resulted in a peak at 10.8 ml (Figure 5A). This elution volume is between those of free pri-miR-23a (12.3 ml) and the Fe(III) heme-bound NC1-pri-miR-23a complex (8.3 ml), suggesting that the apoNC1 binds pri-miR-23a but in a conformation and/or stoichiometry different from those of the heme-bound NC1-pri-miR-23a complex.

We further analyzed pri-miRNA complexes with the apo form of a NC1 mutant P351A. The wild-type apoNC1 dimer is difficult to produce, usually has ~10% of residual heme associated, and is not very soluble at pH 7 and above (Barr et al., 2012). In contrast, NC1 P351A is easily purified as a heme-free dimer and is soluble at pH 8, at which the binding assays are performed. apoNC1 P351A can bind Fe(III) heme to reconstitute a complex similar to the wild-type (Barr et al., 2011). SEC of apoNC1 P351A dimer and pri-miR-23a at 2:1 input ratio resulted in a single peak at 10.7 ml, similar to the complex containing wild-type apoNC1 (Figure 5B). apoNC1 P351A with pri-miR-21 and pri-miR-30a also yielded elution peaks between those of the free RNAs and the heme-bound NC1-RNA complexes (Figures 5D and 5E). Increasing the protein:RNA input ratio to 3:1 did not shift the elution peaks, suggesting that the binding sites have been saturated (Figures 5C and 5F). Additionally, an increase of A_{280} was observed at ~14.2 ml, implying the presence of excess protein. Decreasing the input ratio to 1:1 shifted the elution peak to a larger volume, but not as far as that of the free pri-miRNA (Figure 5G). These results suggest that apoNC1 binds a pri-miRNA with up to 2:1 stoichiometry. Overall, we

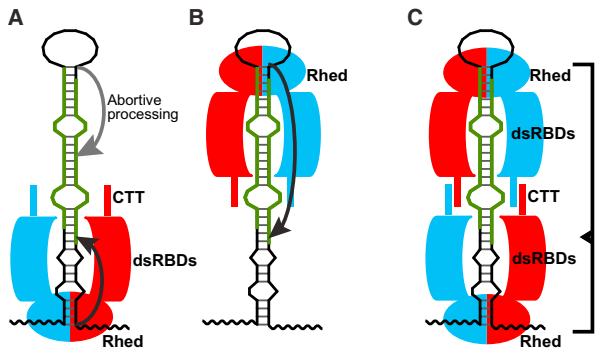

Figure 6. Models of How a pri-miRNA Is Recognized by the Microprocessor

(A) The basal junction anchoring model (Han et al., 2006).

(B) The apical junction anchoring model (Zeng et al., 2005).

(C) Our proposed molecular clamp model. See Discussion for details. The DGCR8 subunits in a dimer are shown in red and cyan. The thick avocado strands represent 5′ and 3′ mature miRNAs.

conclude that the association of DGCR8 with Fe(III) heme causes a large conformational change in its complex with pri-miRNAs. It is also possible that the shift of elution volume is caused by partially disassembly of the apoNC1-pri-miRNA complexes during the SEC experiments. As heme-free DGCR8 is inactive in cells (Weitz et al., 2014), the conformation and/or stability induced by heme must be important for recognition and cleavage of pri-miRNAs by the Microprocessor.

The Covalent Linkage between the Rhed and dsRBDs Is Required for Proper Assembly of DGCR8-pri-miRNA Complexes

To further dissect the relationship between the Rhed and dsRBDs in pri-miRNA recognition, we tested if the two components of NC1, namely the Rhed and NC9, can mediate pri-miRNA processing in *trans* or assemble into proper tertiary complexes with pri-miRNAs. As already shown in Figure 3, with NC9 alone, pri-miR-9-1 cannot be processed and pri-miR-23a is weakly processed in vitro. NC9 and Rhed together do not alter the pri-miRNA processing activity comparing to the NC9 alone (Figures S6A and S6B), indicating that the covalent linkage between the Rhed and dsRBDs is important for pri-miRNA processing. In SEC analyses with both the Rhed and NC9, the pri-miRNAs eluted at volumes smaller than those of the Rhed-pri-miRNA binary complexes but different from those of the NC1-pri-miRNA complexes (Figures S6C–S6E), suggesting that some (nonproductive) tertiary complexes have formed. These observations suggest that the Rhed is responsible for properly anchoring the dsRBDs to pri-miRNAs for processing.

DISCUSSION

Our study identifies the DGCR8 Rhed as the junction-binding domain that anchors the Drosha-DGCR8 complex to pri-miRNAs. It is expected that dsRBDs of DGCR8 associate with the stems of pri-miRNA hairpins (Sohn et al., 2007). The Rhed and dsRBDs together should make extensive contacts with pri-miRNAs, allowing high-affinity binding and specific recognition.

The Rhed-junction interaction provides a physical basis for previously proposed models regarding pri-miRNA recognition. For the basal junction anchoring model (Han et al., 2006), the Rhed binding to the basal junction allows the Microprocessor complex to measure ~11 bp and thereby determine the Drosha cleavage sites (Figure 6A). It was also suggested that the apical junction may serve as an alternative anchoring point for the Microprocessor and that this interaction leads to less efficient cleavages that are located in the middle of mature miRNA strands (called "abortive processing") (Figure 6A) (Han et al., 2006). The capability of the Rhed to bind the apical junction can explain the abortive processing. In a second model, the Microprocessor binds the hairpin loop (approximately equivalent to the apical junction) and measures ~22 bp to determine the Drosha cleavage sites (Zeng et al., 2005; Zhang and Zeng, 2010) (Figure 6B). For this "apical junction anchoring model," the Rhed-apical junction interaction results in productive processing. Common to both models is that association of DGCR8 with only one junction is sufficient to activate processing.

The stoichiometry of DGCR8 and pri-miRNAs in processing competent complexes has been investigated in several studies, but no clear consensus has been reached. It has been previously reported that there is more than one copy of the DGCR8 protomer within the Microprocessor complex (Han et al., 2004). This observation may be explained by the dimerization of DGCR8 and/or by the formation of higher-order structures of DGCR8 upon binding pri-miRNAs. The crystal structure of the monomeric DGCR8 core showed that the two domains adopt an α-β-β-α fold typical for dsRBDs and that these domains are held together by a relatively rigid interface involving an extra α helix at the C terminus of dsRBD2 (Sohn et al., 2007). The RNA-binding surfaces of dsRBD1 and dsRBD2 are expected to point to distinct directions. Based on this and other evidence, it was suggested that each DGCR8 core binds either one pri-miRNA hairpin that is severely bent or two separate hairpins. A recent nuclear magnetic resonance and biochemical study indicated that the DGCR8 core binds pri-miR-16 fragments with varying stoichiometry and that this interaction is reduced by competitor tRNAs (Roth et al., 2013). It was thereby concluded that the DGCR8-pri-miRNA interaction is nonspecific.

In contrast to the DGCR8 core, DGCR8 proteins containing the Rhed do bind pri-miRNAs with specificity (Han et al., 2006; Faller et al., 2010) (Figure 1C) and well-defined stoichiometry. Based on biochemical analyses of DGCR8-pri-miRNA complexes, we previously proposed that DGCR8 dimers form a cooperative higher-order oligomer upon binding to a pri-miRNA (Faller et al., 2010). Using a previously estimated ϵ_{450} of 58 mM^{-1} cm^{-1} for DGCR8-bound Fe(III) heme, we derived NC1 dimer: pri-miRNA ratios of ~3:1 in SEC peaks of their complexes (Faller et al., 2007, 2010). The ϵ_{450} was recently revised to 74 mM^{-1} cm^{-1}, using a widely accepted pyridine hemochromogen method (Senturia et al., 2012). Using this ϵ_{450} value, here we

consistently obtained an NC1 dimer:pri-miRNA ratio of ~2:1 for the previous and new data. Our study suggests that the Rhed is a major specificity and stoichiometry determinant. Any mechanism regarding pri-miRNA recognition must include the dimeric Rhed of DGCR8. Technically, it is important to use recombinant DGCR8 proteins with high heme content in the investigation (Barr and Guo, 2014).

The observation of simultaneous and cooperative binding of two NC1 dimers to a pri-miRNA suggests a "molecular clamp" model. In this model, two DGCR8 dimers grip both ends of the hairpin using their Rheds and interact with each other, making extensive contacts with the pri-miRNA stem (Figure 6C). While it remains to be determined whether binding of both DGCR8 dimers to a pri-miRNA is required for assembly of active tertiary complexes with Drosha, this model is supported by recent cellular data showing that both the apical and basal junctions of pri-miRNAs are important for determining Drosha cleavage sites (Ma et al., 2013). Furthermore, a previous negative-stain electron tomography study yielded a "fat butterfly" density for a DGCR8-pri-miR-30a complex (Faller et al., 2010). Compared to the trimer-of-dimers proposal, the molecular clamp model seems to be more consistent with this electron density in that the body of the butterfly may be the pri-miRNA hairpin and the four wings may be the DGCR8 subunits in the dimer of dimers.

The molecular clamp model allows the length of a full pri-miRNA stem to be measured through an interdimer interaction. The full stem length is one of the most important features of pri-miRNAs but is measured in neither the basal junction anchoring model nor the apical junction anchoring model. We previously showed that the CTT of DGCR8 contains an amphipathic α helix and that mutation of conserved hydrophobic residues on this α helix reduces binding cooperativity and abolishes pri-miRNA processing (Faller et al., 2010). This helix may be involved in the communication between the two DGCR8 dimers. The CTT is also required for binding Drosha (Han et al., 2006), possibly linking assembly of DGCR8 dimer of dimers to activation of RNA cleavage.

A DGCR8-pri-miRNA complex seems to contain built-in asymmetry, which should be able to help Drosha identify the correct cleavage sites that are closer to the basal junction. The apical junction of a pri-miRNA is next to a closed hairpin loop, whereas the single-stranded regions of the basal junction lead to the open ends of the RNA. This topological difference may contribute to the asymmetry of the complex. In fact, our data show different features in the Rhed interactions with the apical and basal junctions—the central region of the miRNA stem appears to be more important for Rhed association with the apical junctions than with the basal junctions (Table 1). Overall, the molecular clamp model unifies features of previous proposals, is consistent with most available experimental data, and explains how the full structural features of pri-miRNAs are recognized.

The mechanisms of substrate recognition by two ribonuclease III enzymes involved in miRNA maturation, Drosha and Dicer, bear interesting similarities and differences. Both Drosha and Dicer partner with dsRNA-binding proteins. However, Dicer-associated RNA-binding partners are not required for cleavage; instead, they modulate substrate affinity and cleavage rates as well as loading of small RNAs to RNA-induced silencing complexes (Doyle et al., 2012). The PAZ domain of Dicer anchors the enzyme to the open end of a pre-miRNA hairpin, allowing the cleavage sites to be determined at a fixed distance (Macrae et al., 2006; Ma et al., 2012). The helicase domain of Dicer binds to the pre-miRNA hairpin loop and enhances the cleavage of pre-miRNAs over other Dicer substrates such as long dsRNAs (Tsutsumi et al., 2011; Ma et al., 2012). The interaction between the DGCR8 Rhed and pri-miRNA basal junctions seems functionally analogous to that between the Dicer PAZ domain and pre-miRNA open end. Similarly, the interaction between the Rhed and pri-miRNA apical junction may be comparable to the contact between the Dicer helicase domain and pre-miRNA hairpin loop. Thus, Drosha and Dicer systems appear to utilize distinct domains for the same purpose of recognizing the ends of substrate RNA helices.

The Rhed is an example of a heme-binding domain that directly binds nucleic acids. A number of transcription factors contain regulatory heme-binding domains, but these domains are separate from their DNA-binding domains (Gilles-Gonzalez and Gonzalez, 2005; Yin et al., 2007; Marvin et al., 2009). We believe that DGCR8 uses the heme cofactor for structural stabilization and/or regulatory functions. Without heme, DGCR8 still binds pri-miRNAs, but their complexes do not adopt processing-competent conformations.

The Rhed appears to have evolved together with animal miRNAs, consistent with an essential function in pri-miRNA recognition. Neither the Rhed nor canonical miRNA is found in bacteria or archaea. Plants do not have the Rhed, and their miRNAs are processed from primary transcripts with longer hairpins by Dicer-like enzymes (Axtell et al., 2011). The Rhed is unique to DGCR8 homologs, whereas the dsRBDs are distributed among a wide range of organisms and in proteins involved in diverse biological functions (Masliah et al., 2013). Most canonical animal miRNAs are thought to originate from unstructured RNA sequences. Emergence of new canonical miRNAs requires successful processing and thereby the formation of junction-containing hairpin structures. Thus, the Rhed of DGCR8 imposes a strong constraint for a new miRNA gene and serves as a gatekeeper for miRNA maturation and subsequent gene-regulation pathways.

DGCR8 has been shown to bind many other RNAs in mammalian cells, including mRNAs, small nucleolar RNAs, and long noncoding RNAs (Macias et al., 2012; Heras et al., 2013). In the inherited neurodegenerative disorder fragile X-associated tremor/ataxia syndrome, the expanded CGG repeats in the fragile X mental retardation 1 (*FMR1*) mRNA bind DGCR8, sequester the pri-miRNA processing machinery, decrease mature miRNA levels, and cause neuronal cell dysfunction (Sellier et al., 2013). Furthermore, DGCR8 and Drosha are required for the function of a class of artificial pri-miRNAs called shRNA^{mir}. As a DNA vector-based RNAi technology, shRNA^{mir} is widely used in biomedical research and is being explored for its therapeutic potential (Silva et al., 2005; Ni et al., 2011). Our characterization of the previously unknown RNA-binding domain in DGCR8 should aid understanding of its role in both miRNA and non-miRNA pathways and enhance the rational design of artificial pri-miRNAs in the future.

EXPERIMENTAL PROCEDURES

Plasmids

Details regarding plasmids are provided in Supplemental Experimental Procedures.

Expression, Purification, and Characterization of Recombinant DGCR8 Proteins

Recombinant DGCR8 proteins were expressed, purified, and characterized as previously described (Faller et al., 2007; Barr et al., 2011, 2012). See Supplemental Experimental Procedures for details.

Transcription and Purification of pri-miRNAs

Details regarding the transcription and purification of pri-miRNAs are provided in Supplemental Experimental Procedures.

pri-miRNA-Binding and Processing Assays

These assays were performed as described previously (Faller et al., 2007). Briefly, for filter-binding assays, a trace amount of ^{32}P-labeled pri-miRNA was incubated with DGCR8 proteins at room temperature for 30 min. For competition filter-binding assays, unlabeled competitor RNAs were also included in the binding reactions (Faller et al., 2010). The mixtures were filtered through nitrocellulose (EMD Millipore) and positively changed nylon (GE Healthcare) membranes. The autoradiography images of the membranes were analyzed using Quantity One (Bio-Rad version 4.4.1). The data were fit and graphed using PRISM (GraphPad version 4).

SEC analyses were performed at room temperature. The NC1 or Rhed proteins were incubated with annealed pri-miRNAs at the indicated concentrations for >5 min; these binding reactions contained a total of 233 mM NaCl. The mixtures were analyzed using an ÄKTA Purifier chromatography system and a Superdex 200 10/300 GL column (GE Healthcare), with a running buffer containing 20 mM Tris (pH 8.0) and 80 mM NaCl. After baseline subtraction, A_{450} was used to calculate DGCR8-bound heme concentration. The contribution of heme-bound DGCR8 to A_{260} was calculated based on the A_{260}/A_{450} ratio of the protein and was subtracted from the A_{260} values in the chromatograms. The remaining A_{260} was used to calculate the RNA concentration. The chromatogram plots were generated using PRISM.

For reconstituted pri-miRNA processing assays (Barr and Guo, 2014), uniformly ^{32}P-labeled pri-miRNAs were annealed and incubated at 37°C for 30 or 45 min with purified recombinant His_6-Drosha$^{390\text{-}1374}$ and DGCR8 proteins. The reactions were analyzed using 7 M urea 15% PAGE and autoradiography.

Live-Cell pri-miRNA Processing Assays

Detailed procedures have been described previously (Weitz et al., 2014). Briefly, HeLa Tet-On cells (Clontech) were transfected with reporter and/or N-flag-DGCR8-expression plasmid. Cells were immediately induced with 2 μg/ml doxycycline and imaged 18–24 hr later. Total eYFP and mCherry intensities for individual cells were fit by linear regression (y = slope * x), and slopes were obtained. p values were determined using the linear regression function of PRISM. Expression levels of N-flag-DGCR8 were analyzed using immunoblotting (Gong et al., 2012). The mCherry-pri-miRNA fusion and the eYFP mRNA levels were determined using qRT-PCR as described (Weitz et al., 2014). The miRNA levels were measured using TaqMan assays (Life Technologies).

SUPPLEMENTAL INFORMATION

Supplemental Information includes Supplemental Experimental Procedures, six figures, and one table and can be found with this article online at http://dx.doi.org/10.1016/j.celrep.2014.05.013.

AUTHOR CONTRIBUTIONS

J.Q. performed most protein-RNA-binding assays (filter binding and SEC) and mutagenesis analyses. J.P.J. did most in vitro pri-miRNA processing assays. S.H.W. performed the live-cell assays. G.S. initiated the SEC analyses and purified the RNA truncations. R.S. initiated the project. F.G., J.Q., J.P.J., and S.H.W. designed most experiments. F.G., J.Q., and J.P.J. wrote the manuscript with input from other authors.

ACKNOWLEDGMENTS

We thank R. Johnson, D. Black, K. Yeom, and I. Barr for critical comments of the manuscript; S. Weiss for support; and Y. Chen, M. Gong, S. Griner, and N. Prakash for technical assistance. This work was partially supported by NIH grant GM080563 (to F.G.), Ruth L. Kirschstein National Research Service Award GM007185 (to J.Q. and G.S.), NIH grant T32GM008496 (to S.H.W.), and a Stein Oppenheimer Endowment Award (to F.G.).

Received: December 28, 2013
Revised: April 3, 2014
Accepted: May 6, 2014
Published: June 5, 2014

REFERENCES

Auyeung, V.C., Ulitsky, I., McGeary, S.E., and Bartel, D.P. (2013). Beyond secondary structure: primary-sequence determinants license pri-miRNA hairpins for processing. Cell *152*, 844–858.

Axtell, M.J., Westholm, J.O., and Lai, E.C. (2011). Vive la différence: biogenesis and evolution of microRNAs in plants and animals. Genome Biol. *12*, 221.

Barr, I., and Guo, F. (2014). Primary microRNA processing assay reconstituted using recombinant Drosha and DGCR8. Methods Mol. Biol. *1095*, 73–86.

Barr, I., Smith, A.T., Senturia, R., Chen, Y., Scheidemantle, B.D., Burstyn, J.N., and Guo, F. (2011). DiGeorge critical region 8 (DGCR8) is a double-cysteine-ligated heme protein. J. Biol. Chem. *286*, 16716–16725.

Barr, I., Smith, A.T., Chen, Y., Senturia, R., Burstyn, J.N., and Guo, F. (2012). Ferric, not ferrous, heme activates RNA-binding protein DGCR8 for primary microRNA processing. Proc. Natl. Acad. Sci. USA *109*, 1919–1924.

Denli, A.M., Tops, B.B., Plasterk, R.H., Ketting, R.F., and Hannon, G.J. (2004). Processing of primary microRNAs by the Microprocessor complex. Nature *432*, 231–235.

Doyle, M., Jaskiewicz, L., and Filipowicz, W. (2012). Dicer proteins and their role in gene silencing pathways. In The Enzymes: Eukaryotic RNases and Their Partners in RNA Degradation and Biogenesis, B. Part, F. Guo, and F. Tamanoi, eds. (Amsterdam: Academic Press), pp. 1–35.

Faller, M., Matsunaga, M., Yin, S., Loo, J.A., and Guo, F. (2007). Heme is involved in microRNA processing. Nat. Struct. Mol. Biol. *14*, 23–29.

Faller, M., Toso, D., Matsunaga, M., Atanasov, I., Senturia, R., Chen, Y., Zhou, Z.H., and Guo, F. (2010). DGCR8 recognizes primary transcripts of microRNAs through highly cooperative binding and formation of higher-order structures. RNA *16*, 1570–1583.

Gilles-Gonzalez, M.A., and Gonzalez, G. (2005). Heme-based sensors: defining characteristics, recent developments, and regulatory hypotheses. J. Inorg. Biochem. *99*, 1–22.

Gong, M., Chen, Y., Senturia, R., Ulgherait, M., Faller, M., and Guo, F. (2012). Caspases cleave and inhibit the microRNA processing protein DiGeorge Critical Region 8. Protein Sci. *21*, 797–808.

Gregory, R.I., Yan, K.P., Amuthan, G., Chendrimada, T., Doratotaj, B., Cooch, N., and Shiekhattar, R. (2004). The Microprocessor complex mediates the genesis of microRNAs. Nature *432*, 235–240.

Guo, F. (2012). Drosha and DGCR8 in microRNA biogenesis. In The Enzymes: Eukaryotic RNases and Their partners in RNA degradation and biogenesis, B. Part, F. Guo, and F. Tamanoi, eds. (Amsterdam, Netherlands: Elsevier Academic Press), pp. 101–121.

Han, J., Lee, Y., Yeom, K.H., Kim, Y.K., Jin, H., and Kim, V.N. (2004). The Drosha-DGCR8 complex in primary microRNA processing. Genes Dev. *18*, 3016–3027.

Han, J., Lee, Y., Yeom, K.H., Nam, J.W., Heo, I., Rhee, J.K., Sohn, S.Y., Cho, Y., Zhang, B.T., and Kim, V.N. (2006). Molecular basis for the recognition of primary microRNAs by the Drosha-DGCR8 complex. Cell *125*, 887–901.

Heras, S.R., Macias, S., Plass, M., Fernandez, N., Cano, D., Eyras, E., Garcia-Perez, J.L., and Cáceres, J.F. (2013). The Microprocessor controls the activity of mammalian retrotransposons. Nat. Struct. Mol. Biol. *20*, 1173–1181.

Kim, V.N., Han, J., and Siomi, M.C. (2009). Biogenesis of small RNAs in animals. Nat. Rev. Mol. Cell Biol. *10*, 126–139.

Landthaler, M., Yalcin, A., and Tuschl, T. (2004). The human DiGeorge syndrome critical region gene 8 and Its *D. melanogaster* homolog are required for miRNA biogenesis. Curr. Biol. *14*, 2162–2167.

Lee, Y., Ahn, C., Han, J., Choi, H., Kim, J., Yim, J., Lee, J., Provost, P., Rådmark, O., Kim, S., and Kim, V.N. (2003). The nuclear RNase III Drosha initiates microRNA processing. Nature *425*, 415–419.

Ma, E., Zhou, K., Kidwell, M.A., and Doudna, J.A. (2012). Coordinated activities of human dicer domains in regulatory RNA processing. J. Mol. Biol. *422*, 466–476.

Ma, H., Wu, Y., Choi, J.G., and Wu, H. (2013). Lower and upper stem-single-stranded RNA junctions together determine the Drosha cleavage site. Proc. Natl. Acad. Sci. USA *110*, 20687–20692.

Macias, S., Plass, M., Stajuda, A., Michlewski, G., Eyras, E., and Cáceres, J.F. (2012). DGCR8 HITS-CLIP reveals novel functions for the Microprocessor. Nat. Struct. Mol. Biol. *19*, 760–766.

Macrae, I.J., Zhou, K., Li, F., Repic, A., Brooks, A.N., Cande, W.Z., Adams, P.D., and Doudna, J.A. (2006). Structural basis for double-stranded RNA processing by Dicer. Science *311*, 195–198.

Marvin, K.A., Reinking, J.L., Lee, A.J., Pardee, K., Krause, H.M., and Burstyn, J.N. (2009). Nuclear receptors homo sapiens Rev-erbbeta and Drosophila melanogaster E75 are thiolate-ligated heme proteins which undergo redox-mediated ligand switching and bind CO and NO. Biochemistry *48*, 7056–7071.

Masliah, G., Barraud, P., and Allain, F.H. (2013). RNA recognition by double-stranded RNA binding domains: a matter of shape and sequence. Cell. Mol. Life Sci. *70*, 1875–1895.

Ni, J.Q., Zhou, R., Czech, B., Liu, L.P., Holderbaum, L., Yang-Zhou, D., Shim, H.S., Tao, R., Handler, D., Karpowicz, P., et al. (2011). A genome-scale shRNA resource for transgenic RNAi in Drosophila. Nat. Methods *8*, 405–407.

Roth, B.M., Ishimaru, D., and Hennig, M. (2013). The core microprocessor component DiGeorge syndrome critical region 8 (DGCR8) is a nonspecific RNA-binding protein. J. Biol. Chem. *288*, 26785–26799.

Sellier, C., Freyermuth, F., Tabet, R., Tran, T., He, F., Ruffenach, F., Alunni, V., Moine, H., Thibault, C., Page, A., et al. (2013). Sequestration of DROSHA and DGCR8 by expanded CGG RNA repeats alters microRNA processing in fragile X-associated tremor/ataxia syndrome. Cell Reports *3*, 869–880.

Senturia, R., Faller, M., Yin, S., Loo, J.A., Cascio, D., Sawaya, M.R., Hwang, D., Clubb, R.T., and Guo, F. (2010). Structure of the dimerization domain of DiGeorge critical region 8. Protein Sci. *19*, 1354–1365.

Senturia, R., Laganowsky, A., Barr, I., Scheidemantle, B.D., and Guo, F. (2012). Dimerization and heme binding are conserved in amphibian and starfish homologues of the microRNA processing protein DGCR8. PLoS ONE *7*, e39688.

Shiohama, A., Sasaki, T., Noda, S., Minoshima, S., and Shimizu, N. (2007). Nucleolar localization of DGCR8 and identification of eleven DGCR8-associated proteins. Exp. Cell Res. *313*, 4196–4207.

Silva, J.M., Li, M.Z., Chang, K., Ge, W., Golding, M.C., Rickles, R.J., Siolas, D., Hu, G., Paddison, P.J., Schlabach, M.R., et al. (2005). Second-generation shRNA libraries covering the mouse and human genomes. Nat. Genet. *37*, 1281–1288.

Sohn, S.Y., Bae, W.J., Kim, J.J., Yeom, K.H., Kim, V.N., and Cho, Y. (2007). Crystal structure of human DGCR8 core. Nat. Struct. Mol. Biol. *14*, 847–853.

Tsutsumi, A., Kawamata, T., Izumi, N., Seitz, H., and Tomari, Y. (2011). Recognition of the pre-miRNA structure by Drosophila Dicer-1. Nat. Struct. Mol. Biol. *18*, 1153–1158.

Weitz, S.H., Gong, M., Barr, I., Weiss, S., and Guo, F. (2014). Processing of microRNA primary transcripts requires heme in mammalian cells. Proc. Natl. Acad. Sci. USA *111*, 1861–1866.

Yeom, K.H., Lee, Y., Han, J., Suh, M.R., and Kim, V.N. (2006). Characterization of DGCR8/Pasha, the essential cofactor for Drosha in primary miRNA processing. Nucleic Acids Res. *34*, 4622–4629.

Yin, L., Wu, N., Curtin, J.C., Qatanani, M., Szwergold, N.R., Reid, R.A., Waitt, G.M., Parks, D.J., Pearce, K.H., Wisely, G.B., and Lazar, M.A. (2007). Rev-erbalpha, a heme sensor that coordinates metabolic and circadian pathways. Science *318*, 1786–1789.

Zeng, Y., and Cullen, B.R. (2005). Efficient processing of primary microRNA hairpins by Drosha requires flanking nonstructured RNA sequences. J. Biol. Chem. *280*, 27595–27603.

Zeng, Y., Yi, R., and Cullen, B.R. (2005). Recognition and cleavage of primary microRNA precursors by the nuclear processing enzyme Drosha. EMBO J. *24*, 138–148.

Zhang, X., and Zeng, Y. (2010). The terminal loop region controls microRNA processing by Drosha and Dicer. Nucleic Acids Res. *38*, 7689–7697.

Zuker, M. (2003). Mfold web server for nucleic acid folding and hybridization prediction. Nucleic Acids Res. *31*, 3406–3415.

CHAPTER 4

Cobalt (III) protoporphyrin activates the DGCR8 protein and can compensate microRNA processing deficiency

The work described in the chapter was initiated by Ian Barr. Ian used recombinately expressed and purified DGCR8 to test whether other metalloporphyrins were able to activate DGCR8 for processing. During his screening process he found that Co(III) protoporphyrin IX was able to activate DGCR8. I continued his study by testing Co(III) PPIX's activity in cells. I came to the same conclusion as Ian, that Co(III) PPIX can activate DGCR8's processing activity in cells. To test if Co(III) PPIX could rescue pri-miRNA processing deficiencies in mice, we collaborated with Maria Karayiorgou and Joseph Gogos's group at Columbia University. His students Talia Atkin and PeiKen Hsu, tested Co(III)PPIX's activity in mouse neurons from mice with a heterozygous deletion of DGCR8. Performing qPCR on endogenous mature miRNA, Talia and PeiKen found that Co could rescue the processing defect caused by DGCR8 deletion. This chapter is our unpublished manuscript.

ABSTRACT

Processing of microRNA primary transcripts (pri-miRNAs) is highly regulated and defects in the processing machinery play a key role in many human diseases. In DiGeorge syndrome, heterozygous deletion of DiGeorge critical region gene 8 (DGCR8) causes a processing deficiency, which contributes to abnormal brain development. The DGCR8 protein is the RNA-binding partner of Drosha ribonuclease, both essential for processing canonical pri-miRNAs. Here, to identify an agent that can compensate reduced DGCR8 expression, we screened for metalloporphyrins that can mimic the natural DGCR8 heme cofactor. We found that Co(III) protoporphyrin IX (PPIX) stably binds DGCR8 and activates it for pri-miRNA processing in vitro and in HeLa cells. Importantly, treating cultured Dgcr8+/- mouse neurons with Co(III)PPIX can compensate the pri-miRNA processing defects. Co(III)PPIX is effective at concentrations as low as 0.2 μM and is not degraded by heme degradation enzymes, making it useful as a research tool and a potential therapeutic.

INTRODUCTION

pri-miRNA processing defects have been reported in a range of human diseases including cancer and schizophrenia [1,2]. Critical contribution of such defects to pathogenesis has been demonstrated [3,4]. In DiGeorge syndrome, the *DGCR8* (called *Pasha* in *Drosophila* and *Pash-1* in *C. elegens*) gene is heterozygously deleted along with 30-60 other genes in chromosome 22q11 [5-9]. The haploinsufficiency of *DGCR8* reduces the abundance of DGCR8 protein, resulting in lower pri-miRNA processing efficiency and abnormal expression of a subset of miRNAs [10]. The miRNA deficiency has a pronounced effect on brain development and function, and contributes to the cognitive and behavioral deficits of DiGeorge syndrome [10-13]. The DGCR8 protein and Drosha form the Microprocessor complex. Together they cooperate to recognize and cleave pri-miRNAs, thereby producing precursor miRNAs (pre-miRNAs) as intermediates[3-6,11]. Following this initial step in the canonical miRNA maturation pathway, pre-miRNAs are exported to the cytoplasm and are further cleaved by the Dicer nuclease to generate mature miRNA strands, which are eventually incorporated into the miRNA-induced silencing complex (miRISC) and become functional in gene regulation [14].

To restore miRNA processing in DiGeorge syndrome and other diseases, it is highly desirable to enhance the activity of DGCR8 protein using small molecule agents, rather than engaging in risky gene therapies. DGCR8 has been shown to be regulated by cofactor binding, phosphorylation, acetylation and proteolytic cleavage [15-18]. These posttranslational modifications offer opportunities for intervention. This study takes advantage of the fact that DGCR8 is activated by the cofactor heme *b* [19-21]. A purified recombinant DGCR8 construct NC1 (a.a. 276-751 of the 773-aa full-length protein) forms a stable complex with Fe(III) heme, but binds Fe(II) heme with much weaker affinity [20,21]. Fe(III) heme in DGCR8 is coordinated by a unique two-

cysteine configuration [22]. DGCR8 binds heme using an RNA-binding heme domain (Rhed) that directly contacts pri-miRNAs and cooperates with two double-stranded RNA-binding domains to achieve high-affinity binding and specific recognition [23]. In cells, DGCR8 mutants that are unable to bind heme are unable to process pri-miRNAs[14]. Additionally, DGCR8 activity can be modulated by removing heme from the cell culture media, adding back exogenous heme, or inhibiting endogenous heme biosynthesis[14].

It is well known that excess amounts of freely available heme in cells are degraded by heme oxygenases [24], making heme less useful as a sustainable activator for pri-miRNA processing. In this study, we set out to identify heme analogs that are capable of binding and activating DGCR8. We either removed the central Fe of heme or substituted it with a diverse set of other metals. We successfully identified one such derivative, Co(III)PPIX, and demonstrated that it can rescue miRNA expression in *Dgcr8*$^{+/-}$ mouse neurons. CoPPIX is not degraded by heme oxygenases and thereby should be able to activate pri-miRNA processing for a prolonged period of time.

METHODS

Materials

Hemin and Co(III)PPIX were purchased from Sigma (St. Louis, MO, USA). All other metalloporphyrins were obtained from Frontier Scientific (Logan, UT, USA).

Expression and purification of recombinant DGCR8

Fe(III) NC1, apoNC1 and apoNC1 P351A proteins were purified as described previously [20,21]. Briefly, the constructs were expressed in the pET-24a^{+} vector in *E. coli* and purified using cation

exchange chromatography followed by size-exclusion chromatography (SEC). The SEC buffer contained 20 mM Tris pH 8.0, 400 mM NaCl, and 1 mM DTT. Reduction of the Fe(III) NC1 was accomplished using 2 mM sodium dithionite in 50 mM 2-(*N*-morpholino)ethanesulfonic acid (MES) pH 6.0, 400 mM NaCl, and 1 mM DTT.

DGCR8-porphyrin binding assay

All porphyrin solutions were made fresh on the day of use and stored at ≤ 4°C. Protoporphyrin IX was initially dissolved in 50% DMSO and 50% 0.1 M NaOH, concentration was measured (~1 mM), and diluted into the final binding buffer (pH 6 or 8). Metalloporphyrins were initially dissolved in 0.1 M NaOH, and then diluted to 100 μM stocks using binding buffer. The concentrations were determined either gravimetrically (Rh and In) or using published extinction coefficients. Several published absorbance peaks and extinction coefficient values are listed in Table 4-1.

The porphyrin-binding reaction buffer contained 1 mM DTT, 400 mM NaCl, and the buffer was either 50 mM MES pH 6.0 (for wild-type apoNC1) or 20 mM Tris pH 8.0 (for apoNC1 P351A). Absorbance spectra were collected using either a Varian Cary 300 Bio spectrophotometer with bandwidth set to 1 nm (Figs. 4-2A and 4-3A,C), or a DU800 spectrophotometer (Beckman-Coulter, bandwidth ≤ 1.8 nm) (Figs. S1, S2 and S3).

Reconstituted pri-miRNA processing assays

The assays were done as described previously [21]. The reactions were incubated at 37°C for either 30 min (pri-miR-23a and pri-miR-30a) or 45 min (pri-miR-21 and pri-miR-380), and were analyzed using 15% acrylamide, 7 M urea denaturing gels and autoradiography. The bands were quantified using the ImageQuant software (GE Healthcare). The intensities of pre-miRNAs were converted to the equivalents of pri-miRNAs by multiplying the ratio of the numbers of ^{32}P-

containing residues in the pri-miRNA and pre-miRNA. *p* values were calculated using two-tailed Student's *t*-test and Mann-Whitney U-test.

Cellular pri-miRNA processing assay

The cellular assays were performed as described previously [15]. Briefly, cells were grown in heme-depleted media for 24 hours before splitting into smaller plates for both imaging and RNA analysis. Cells were transfected with the pri-miR-9-1 reporter. Eighteen hours posttransfection, 1 mM SA, either alone or with 0.2, 1 or 10 μM Co(III)PPIX, or 10 μM hemin, was added to the cells, and 1 μM doxycycline was also added to induce expression of reporters. Co(III)PPIX and hemin were dissolved in DMSO shortly before addition to the cell cultures. After 10 h of treatment, cells were used either for imaging or for total RNA extraction. Imaging and data analysis were performed as described [15]. Total RNAs were extracted using the miRNeasy mini kit (Qiagen). Taqman qRT-PCR assays (Life Technologies) were used to measure mature miR-9 and *β-actin* mRNA levels.

Treatment of mouse Dgcr8$^{+/-}$ neurons using Co(III)PPIX

All animal protocols used in this study are approved by Columbia University IACUC. *Dgcr8*$^{+/-}$ mice have been described previously [10] and have been backcrossed into C57BL/6J background for over ten generations. After embryonic dissection, dissociated neurons from individual pups were cultured. At DIV 3, cells were treated with Co(III)PPIX or DMSO (no porphyrin control) as indicated in Fig. 4-6. Co(III)PPIX was dissolved in DMSO. At DIV 5, total RNA was isolated from ~2 x 10^6 neurons per condition using miRNeasy mini kit (Qiagen). Taqman qRT-PCR assays (Life Technologies) were used to measure mature miR-185 and *Gapdh* mRNA levels, as described previously [28].

RESULTS

A metal ion is necessary for porphyrin to stably associate with DGCR8.

We examined potential interaction of porphyrin compounds with heme-free (apo) forms of DGCR8 via titration and electronic absorption spectroscopy. Size exclusion chromatography (SEC) was used to confirm the interaction and to estimate the stability of the complexes. Two apoDGCR8 proteins were used in the binding study: wild-type apoNC1 and the apoNC1-P351A mutant. NC1-P351A can be conveniently purified as a heme-free dimer (apoNC1-P351A) when recombinantly expressed in *E. coli* without the addition of δ-aminolevulinic acid (δ-ALA) to the media [20]. apoNC1-P351A can bind Fe(III) heme to form a stable complex similar to native Fe(III) heme-bound NC1. The porphyrin-binding assays using apoNC1-P351A were performed at pH 8 at which this protein is stable. This pH is close to physiological and is routinely used for our reconstituted pri-miRNA processing assays [25]. In contrast, the porphyrin-binding assays using wild-type apoNC1 were performed at pH 6 for this protein is not very soluble at pH 8. Wild-type NC1 is expressed in *E. coli* as the Fe(III) heme-bound form and it associates with Fe(III) heme very tightly [20]. Thus, the preparation of apoNC1 requires several additional steps after purification of NC1, including buffer exchange to pH 6, heme reduction, incubation with apomyoglobin to scavenge the Fe(II) (ferrous) heme fast-dissociating from NC1 and SEC to separate apoNC1 from myoglobin[21], thereby resulting in a lower yield. apoNC1 dimer prepared this way can bind Fe(III) heme and be activated for pri-miRNA processing [21]. Because of the comparative ease of preparation and handling, we chose to use apoNC1-P351A for initial binding assays with porphyrins. The binding or lack of binding for select porphyrins was confirmed using wild-type apoNC1.

We first tested protoporphyrin IX (PPIX), which does not contain a metal center (Fig. 4-

1A). Incubation of PPIX with apoNC1-P351A dimer resulted in a predominant Söret peak at 383 nm, which was slightly shifted from the 377 nm peak of PPIX without DGCR8 (Fig. S1A). The peak wavelengths and shape of the spectra did not change as the molar ratio of PPIX and apoNC1-P351A increased above 1:1, indicating that the PPIX did not bind specifically. Consistent with this notion, SEC analysis of the 1:1 mixture revealed little 383 nm absorbance associated with the NC1-P351A elution peak (Fig. S1B). Titration of PPIX to wild-type apoNC1 at pH 6.0 showed broadened split Söret peaks in the range of 300-500 nm with two maxima at 368 and 447 nm, respectively, and weaker Q bands at 535, 555, 592 and 643 nm (Fig. 4-2A). These features were similar to those of free PPIX [26] and no saturation behavior was observed (Fig 4-2B). Furthermore, the PPIX absorbance did not co-elute with apoNC1 in SEC analyses (Fig. 4-2C). Therefore, we conclude that a metal ion is required for strong DGCR8-porphyrin interaction.

Co(III)PPIX stably associate with DGCR8

We screened nine metalloporphyrins (Fig. 4-1) and found that at pH 8 only Co(III)PPIX is able to stably associate with apoNC1-P351A, that Zn(II)PPIX only weakly binds (Supplementary Results and Fig. S2), and that the others do not seem to bind. In the titration of Co(III)PPIX, we observed hyperporphyrin (split Söret) spectra with peaks appearing at 365, 456, and 563 nm, and a non-specific peak at 430 nm became prominent as Co(III)PPIX was added in excess (Fig. S3A). The 365 and 456 nm peaks are intense and of nearly equal heights, and the α/β band at 563 nm is much weaker. These features of the specific Co(III)PPIX-NC1-P351A complex are similar to those seen with Fe(III) heme titration [20]. Plotting of the specific and non-specific peak absorbance values over the Co(III)PPIX concentration revealed a common transition at 9 μM

(Fig. S3B), close to the 7.5 μM apoNC1-P351A concentration within experimental errors, indicating that the specific binding has a stoichiometry of one Co(III)PPIX per apoNC1-P351A dimer. SEC analyses showed that the Co(III)PPIX absorbance co-elutes with the protein, confirming that their association is stable (Fig. S3C).

Titration of Co(III)PPIX to wild-type apoNC1 at pH 8 resulted in electronic absorption spectra remarkably similar to those from titration to apoNC1-P351A. The peaks of the specific complex are at 368, 456, 563 nm and a non-specific peak at 432 nm became prominent when Co(III)PPIX is in excess (Fig. 4-3A). In SEC analyses, the A_{456} and slightly less intense A_{432} co-eluted with the 12.5 mL protein peak (Fig. 4-3B), indicating that Co(III)PPIX remains bound to NC1. Therefore, we conclude that Co(III)PPIX stably binds DGCR8 at both pH 6 and 8.

Co(II)PPIX does not strongly associate with DGCR8

The cobalt in Co(III)PPIX can be reduced to Co(II). We tested if the cobalt redox state affects the interaction with DGCR8. Co(II)PPIX was produced by reducing Co(III)PPIX using dithionite and was titrated to wild-type apoNC1. The electronic absorption spectra showed a prominent Söret peak at 398 nm and a relatively broad band at 563 nm, akin to the spectrum of free Co(II)PPIX (Fig. 4-3C). SEC analyses of the Co(II)PPIX-apoNC1 mixture showed little 398 nm absorbance in the protein elution peak (Fig. 4-3D). Therefore, we conclude that, in sharp contrast to Co(III)PPIX, Co(II)PPIX does not bind strongly to DGCR8. It is a common requirement for the metal ion in both CoPPIX and heme to be in a 3+ state to stably associate with DGCR8 (herein and published data [21]).

Co(III)PPIX increases pri-miRNA processing activity of DGCR8.

We next tested if Co(III)PPIX binding to apoNC1 can biochemically activate it for pri-miRNA processing. Uniformly ^{32}P-labeled pri-miRNAs were incubated with purified recombinant Drosha and various forms of DGCR8. The latter included native Fe(III) heme-bound NC1, apoNC1, and *in vitro* reconstituted NC1-Co(III)PPIX and NC1-Fe(III)-heme complexes. The subsequent denaturing gel and autoradiography analyses showed that, compared to native NC1, apoNC1 displayed a deficiency in pri-miRNA processing, with nearly no pre-miRNA produced for pri-miR-23a, a >60% reduction of processing for pri-miR-21 and pri-miR-380, and a modest reduction (~30%) for pri-miR-30a (Fig. 4-4, lanes 3 and 4 in all panels). Importantly, NC1 reconstituted with Co(III)PPIX and Fe(III) heme rescued pri-miRNA cleavage close to the levels of native NC1 for all four pri-miRNAs (Fig. 4-4, lanes 4 and 5 in all panels). These results clearly demonstrate that Co(III)PPIX is capable of activating DGCR8 for pri-miRNA processing, most likely by forming a complex similar to that containing Fe(III) heme.

Co(III)PPIX activates pri-miRNA processing in cells

Unlike heme, CoPPIX is not degraded by heme oxygenases, the major heme degradation pathway in mammalian cells [27], making it potentially more useful as a pri-miRNA processing activator. We tested if Co(III)PPIX can activate pri-miRNA processing in human cells using a recently developed fluorescent live-cell reporter assay that specifically reflects changes in pri-miRNA processing efficiency [15]. The reporter plasmid contains an mCherry expression cassette with a pri-miRNA sequence inserted in the 3′-untranslated region, so that cleavage of the pri-miRNA by Drosha/DGCR8 reduces the expression of this red fluorescent protein. The plasmid also expresses eYFP, which serves a normalization purpose. The total mCherry and eYFP

fluorescent intensities of individual cells have a linear relationship over the wide range of expression levels usually seen in a transient transfection experiment. The eYFP vs mCherry slope indicates pri-miRNA processing efficiency. This assay has been extensively validated at both protein and RNA levels and was used to demonstrate that alternations in heme biosynthesis and availability modulate pri-miRNA processing efficiency [15].

We used our cellular assay to determine if Co(III)PPIX can activate pri-miRNA processing in mammalian cells. HeLa cells were adapted to grow in media with ~50% of heme removed from the serum and then transfected with the pri-miR-9-1 reporter. Eighteen hours posttransfection, cells were treated with succinylacetone (SA) to block heme synthesis, either alone, with 0.2, 1 or 10 μM Co(III)PPIX, or with 10 μM hemin for 10 h. Cellular fluorescence signals indicated that, as expected, SA treatment decreased the slope (and thus the pri-miRNA processing efficiency) from 1 ± 0.02 (95% CI which is used for all fluorescence data) to 0.89 ± 0.03 and 10 μM hemin rescued it back to 1.07 ± 0.03 (Fig. 4-5A). Importantly, Co(III)PPIX increased pri-miRNA processing efficiency in SA-treated cells in a dose-dependent manner. The fluorescence slope was reversed back to 0.96 ± 0.03, 1.06 ± 0.04 and 1.12 ± 0.04 by 0.2 μM, 1.0 μM and 10 μM of Co(III)PPIX, respectively (Fig. 4-5A). Even the change cause by the lowest concentration (0.2 μM) of CoPPIX was highly significant ($p = 0.0005$). We subsequently tested if the boost of pri-miRNA processing efficiency resulted in increased production of mature miR-9 using qRT-PCR. With SA treatment, the abundance of mature miR-9 was reduced to 0.64-fold (± 0.05, SD) that of the no treatment control (Fig. 4-5B). This defect was rescued by both Co(III)PPIX and hemin, with the miR-9 levels 1.15 ± 0.17 and 0.81 ± 0.25 folds that of the no treatment control, respectively. Treatment with any of these compounds is not toxic to cells, as indicated by cell viability measurements using an MTT assay (Fig. 4-5C). Altogether, our data

clearly demonstrate that Co(III)PPIX is able to enhance pri-miRNA processing in cells without obvious harmful side-effects.

Co(III)PPIX-mediated activation compensates miRNA processing deficiency caused by heterozygous deletion of *Dgcr8* in mouse neurons

We wondered if Co(III)PPIX may be used to correct the miRNA processing deficiency in cultured neurons. Previous studies showed that heterozygous deletion of the *Dgcr8* gene either alone or along with other genes in the Df(16)A region in mice (syntenic to the 1.5 Mb 22q11.2 DiGeorge microdeletion in humans) reduces both the mRNA and protein levels to ~50% those of the $Dgcr8^{+/+}$ wild type [10]. This in turn reduces the maturation of certain miRNAs in the brain, including miR-185 that has been shown to target the expression of a neuronal inhibitor Mirta22 [28]. We prepared primary cortical neurons from $Dgcr8^{+/-}$ pups and their littermate controls at embryonic day 17. These neurons were cultured for 3 days in vitro (DIV) and treated for 2 additional days with 0.2, 2 and 20 μM Co(III)PPIX. We then extracted total RNAs and measured the miR-185 abundance. Similar to what has been reported previously, the miR-185 levels in the $Dgcr8^{+/-}$ neurons decreased by 31% as compared to the $Dgcr8^{+/+}$ neurons (Fig. 4-6) [28]. Treatment with Co(III)PPIX at all three concentrations elevated the miR-185 expression to 84-98% of the wild type (Fig. 4-6). At 20 μM, Co(III)PPIX restored miR-185 to a level indistinguishable to that of the wild type. Even at the lowest concentration of 0.2 μM, the increase of miR-185 to 89% of wild type is statistically significant. This experiment demonstrates that Co(III)PPIX is capable of correcting the miRNA processing deficiency caused by reduced *Dgcr8* gene dosage and thus pave the way to further explore the value of this metalloporphyrin in treating DiGeorge syndrome and other diseases linked to deficient miRNA processing.

DISCUSSION

Here we identify Co(III)PPIX as an activator of pri-miRNA processing. This activator mimics the required heme cofactor of DGCR8 but is not subjected to degradation by heme oxygenases. DGCR8 and its homologs constitute a unique class of heme protein in that they use two cysteine side chains (Cys352 from both subunits in a dimer) to ligate the heme iron [20,21]. At least one (likely both) of the Cys352 side chains are in the deprotonated thiolate state. The electron-rich environment contributes to a tremendous preference for DGCR8 to bind Fe(III) heme over Fe(II) heme. The human DGCR8 does not dissociate with Fe(III) heme substantially even after incubation at room temperature for 4 days (k_{off} < 3 x 10^{-6} s^{-1}) with large excess of heme scavenger apomyoglobin [20]. In contrast, the dissociation rate of Fe(II) heme from DGCR8 cannot be measured using the stop flow method (k_{off} > 100 s^{-1}) [21]. Thus, a single electron (the difference between Fe(III) and Fe(II)) causes a >10^7-fold change in k_{off}. The reduction of the heme iron causes loss of both cysteine ligands [21], resulting in near elimination of DGCR8 binding and activation activities.

Among the metalloporphyrins with the central atoms highlighted in Figure 4-1B, only Co(III)PPIX and Fe(III)PPIX (heme) are capable of stably binding DGCR8 and activating its miRNA processing activity. Cobalt and iron in the 3+ state contain 5 and 6 electrons in their *d* shells respectively, leaving those orbitals approximately half empty and thereby favoring the octahedral coordination. Our previous EPR study indicated that the Fe(III) in DGCR8 is in a low-spin S = ½ state, with one unpaired electron [20]. The spin state of Co(III)PPIX in DGCR8 remains to be determined. Both Co and Fe are redox active with another most accessible state being 2+ when chelated by porphyrins. Similar to Fe(II)PPIX, the Co(II)PPIX does not stably bind DGCR8. The stringent metal ion and redox state requirements are likely to be demanded by

the dual cysteine-ligation of DGCR8 and the electron-rich environment.

A key difference between CoPPIX and heme is that CoPPIX is not degraded by the heme degradation enzymes heme oxygenases [24]. This property makes Co(III)PPIX much more stable in the body. Subcutaneous injection to rats results in retention of the compound in spleen, gonads, lung, and thymus for up to 4 weeks [29]. Furthermore, Kappa and colleagues treated rats with CoPPIX and observed a substantial decrease in body fat contents and overall bodyweight [30]. Either subcutaneous injection or intracerebroventricular injection into the brain was effective. The effects persisted over a long period of time, with those from a single intracerebroventricular dosage at 0.2 or 0.4 μmol per kg of body weight lasting strikingly for over 300 days. These effects were not produced by cobalt chloride, heme or other metalloporphyrins tested, therefore are quite specific to CoPPIX. No histological abnormalities were observed in the brain, suggesting that administration of CoPPIX at low dosages may be safe for treating diseases such as DiGeorge syndrome. Additionally, there has been a substantial body of works trying to identify the *in vivo* targets of CoPPIX that contribute to the "slimming" effects, including heme oxygenase-1 (HO-1) [31] and nitric oxide synthase [32]. Our study suggests that boost of miRNA processing is another major effect of CoPPIX.

CoPPIX has been shown to potently induce the expression of HO-1, even though the compound itself is a competitive inhibitor of heme oxygenase enzymes [33-35]. Previous studies showed that 5-10 μM of CoPPIX is needed to induce HO-1 expression [33-35]. In the current study, we show that Co(III)PPIX is effective in activating pri-miRNA processing in human cells at concentrations as low as 0.2 μM. Thus, it should be possible to activate DGCR8 without substantially inducing HO-1. On the other hand, induction of HO-1 has major cytoprotective and other beneficial physiological effects [36,37]. These effects are elicited by the products of the heme

degradation reaction—biliverdin is a potent antioxidant and carbon monoxide has anti-inflammatory and anti-apoptotic activities. Therefore, activation of HO-1 by CoPPIX has been proposed as a potential therapeutic strategy for treating cardiovascular diseases and obesity [31,38]. It may be beneficial to activate both pri-miRNA processing and HO-1 using modest dosages of Co(III)PPIX. Elevated heme oxygenase expression and activity would reduce the intracellular heme availability, which would in turn be expected to reduce pri-miRNA processing. At 10 or 20 μM of Co(III)PPIX, direct activation of DGCR8 appears to have a dominating effect on enhancing pri-miRNA processing efficiency over the potential indirect inhibition via HO-1 induction (Figs. 4-5 and 4-6). The tight interaction between DGCR8 and Co(III)PPIX must have contributed to this overall positive effect of Co(III)PPIX on pri-miRNA processing.

CoPPIX shares major chemical properties with heme, and thus is able to interact with additional heme proteins and possibly affect their respective biological pathways. For example, CoPPIX has been shown to inhibit the rate-limiting heme synthesis enzyme δ-aminolevulenic acid synthase [39]. The combination of heme synthesis inhibition and degradation (the latter from induction of HO-1) causes a reduction of cytochrome P-450 in the liver [40]. Cobalt-substituted cytochrome P-450cam, cystathionine β-synthase and horseradish peroxidase can be biochemically reconstituted using the corresponding apoproteins and CoPPIX [41-43], although it is not clear whether CoPPIX is incorporated to these heme proteins *in vivo*. Therefore, caution should be exercised when considering CoPPIX in long-term systemic treatments, especially at medium to high concentrations.

In summary, we found that Co(III)PPIX binds DGCR8 tightly and activates its pri-miRNA processing activity potently. We show that this compound is effective in correcting pri-miRNA processing defects by activating the DGCR8 protein in mouse neurons that mimic the

DGCR8 haploinsufficiency in DiGeorge syndrome [10,28]. Co(III)PPIX is not degraded by the heme degradation enzymes, thus has highly favorable pharmacokinetic half-lives [29,30]. It works at low concentration, allowing the interaction with other heme proteins and potential undesired effects to be limited. These properties qualify Co(IIII)PPIX as a potential therapeutic for diseases in which pri-miRNA processing deficiency is involved. As pri-miRNA processing is highly regulated in broad biological contexts [14,44], Co(III)PPIX will also be useful as a research tool.

SIGNIFICANCE

miRNAs are extensively involved in development and cell physiology, and reduced miRNA production has been linked to many diseases. In cancers, decreased expression of miRNA processing factors has been extensively documented. Another disease, DiGeorge syndrome, is caused by the most common human chromosome microdeletion, with an incidence of 1 in 2,000–4,000 live births. Concrete evidence has demonstrated that these miRNA processing defects directly contribute to pathogenesis. However, it has not been possible to correct them. Here using a combined biochemical and cellular approach, we identify a miRNA processing activator, cobalt (III) protoporphyrin IX. This compound binds and activates DGCR8 by mimicking its essential heme cofactor, but is not degraded by heme degradation enzymes. Co(III)PPIX corrects the miRNA processing deficiency caused by heterozygous deletion of *DGCR8* in mouse neurons. Our study demonstrates that it is possible to compensate miRNA processing defects by activating the processing proteins.

FIGURES AND LEGENDS

a

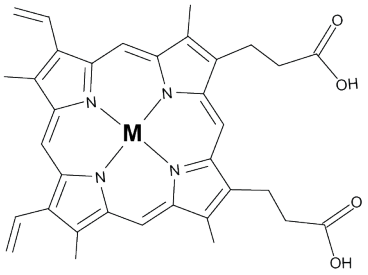

Metalloprotoporphyin IX

b

2	3	4	5	6	7	8	9	10	11	12	13	14
Mg											Al	Si
Ca	Sc	Ti	V	Cr	Mn (III)	Fe (III)	Co (III)	Ni (II)	Cu (II)	Zn (II)	Ga (III)	Ge
Sr	Y	Zr	Nb	Mo	Tc	Ru	Rh (II)	Pd	Ag	Cd	In (III)	Sn (IV)

Figure 4-1. Metalloporphyrins that were tested for association with DGCR8 and for activation of pri-miRNA processing. (a) Schematic of a metalloprotoporphyrin IX. The **M** at the center represents a metal ion. (**b)** A section of the periodic table showing the elements used in this study, with the group numbers labeled. The protoporphyrin IX complexes with the metals shown in red background stably bind to DGCR8, whereas the complexes with the elements in gray do not.

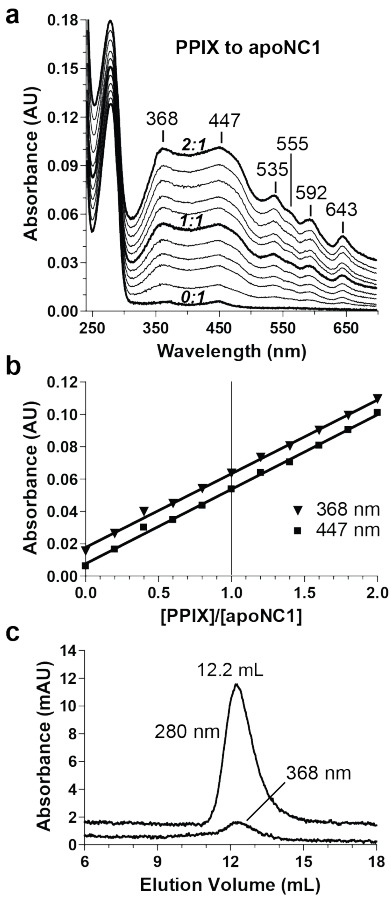

Figure 4-2. Protoporphyrin IX without a metal center does not stably associate with apoNC1. (**a**) Electronic absorption spectra of titration of PPIX into 1.25 μM apoNC1 dimer at 0.25 μM intervals, in 50 mM MES pH 6.0, 400 mM NaCl and 1 mM DTT. The PPIX:apoNC1-P351A ratios of the bold curves are indicated in italic. (**b**) Absorbance values at 368 nm and 447 nm obtained from the titration are plotted against PPIX:apoNC1 ratios. To avoid overlapping, the A_{368} values are nudged up by 0.01. In contrast to a similar titration experiment using Fe(III)PPIX [15], no saturation point is observed at 1:1 PPIX:apoNC1 ratio, indicating a lack of specific binding. (**c**) Size exclusion chromatogram of a mixture of apoNC1 and PPIX, both at 4 μM concentration shows little co-elution. The low 368 nm absorption in the elution peak was contributed by the ~10% heme remaining bound to the apoNC1 preparation. The chromatogram is indistinguishable from that of the apoNC1 alone.

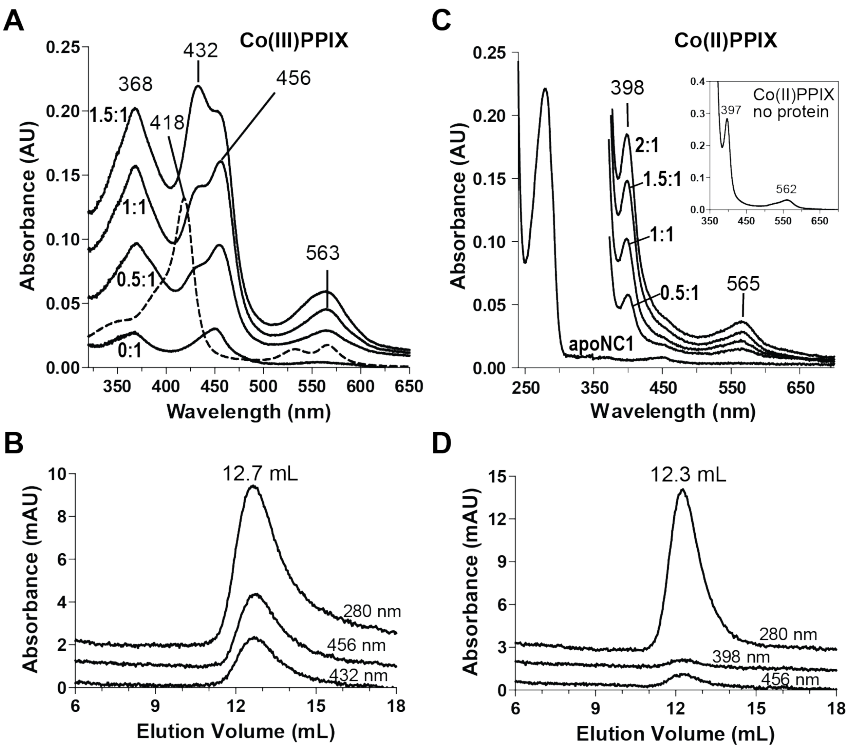

Figure 4-3. Co(III)PPIX, but not the Co(II) form, associates with apoNC1. (**A**) Electronic absorption spectra of Co(III)PPIX titrated into 2 μM apoNC1 dimer at 1 μM per step, in 50 mM MES pH 6.0, 400 mM NaCl and 1 mM DTT. The absorption peak at 432 nm results from a non-specific interaction. An absorbance spectrum of Co(III)PPIX alone is shown as a dashed line. (**B**) Size exclusion chromatogram of the reconstituted Co(III)PPIX-NC1 complex. (**C**) Co(II)PPIX was titrated into 2.5 μM apoNC1 in 50 mM MES pH 6.0, 400 mM NaCl and 2 mM sodium dithionite at 1.25 μM per step. Sodium dithionite obscures peaks below 350 nm due to its high absorbance. The apoNC1 spectrum before addition of sodium dithionite is also shown. The absorption spectrum of Co(II)PPIX without proteins is shown in the inset. (**D**) Size exclusion chromatogram of apoNC1 with Co(II)PPIX. The SEC buffer contained 50 mM MES pH 6.0 and 400 mM NaCl, and was degassed to remove O_2. The apoNC1 dimer elutes at an expected volume. However, there is no large accompanying absorbance at 398 nm (the Co(II)PPIX Söret wavelength) or 456 nm (potential re-oxidized Co(III)PPIX Söret wavelength).

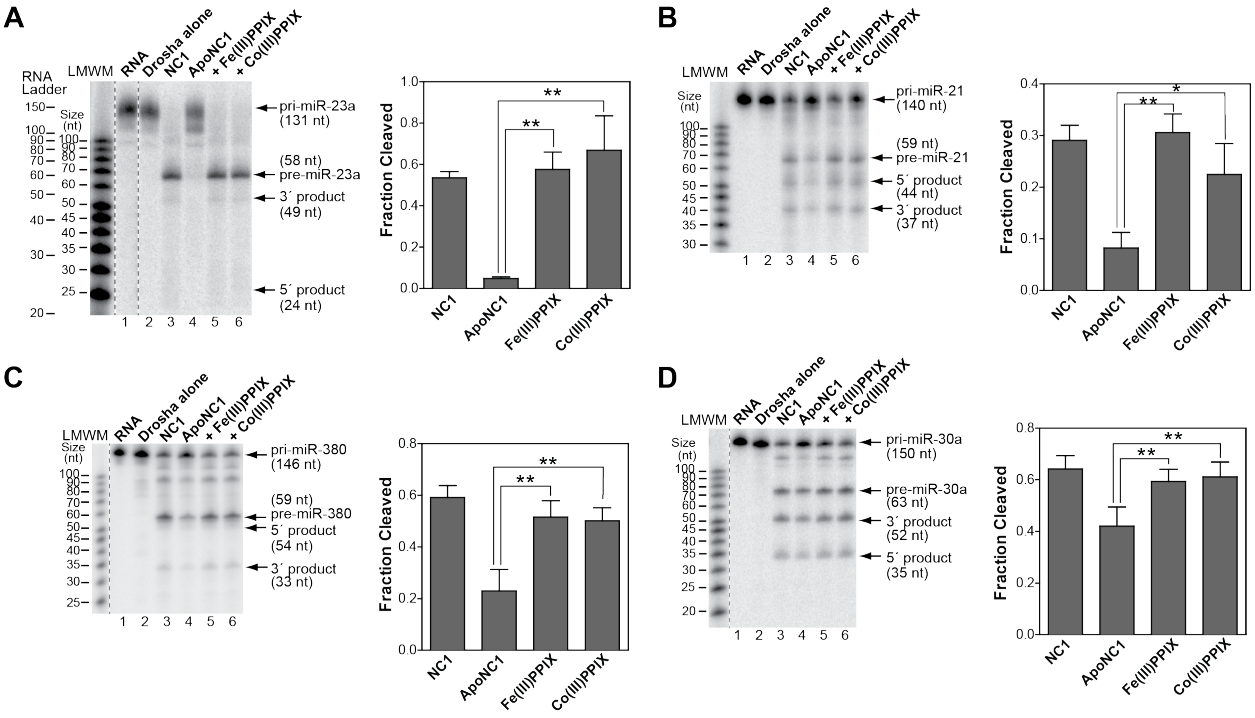

Figure 4-4. Co(III)PPIX activates DGCR8 for pri-miRNA processing *in vitro*. Denaturing gel analyses of cleavage assays of (**A**) pri-miR-23a, (**B**) pri-miR-21, (**C**) pri-miR-380 and (**D**) pri-miR-30a. The cleavage reactions contained trace amounts of uniformly ^{32}P-labeled pri-miRNAs, recombinant His_6-Drosha$^{390-1374}$ and the various forms of DGCR8 proteins (25 nM dimer). NC1 is the native Fe(III) heme-bound dimer. apoNC1 is NC1 with the >90% of heme removed. The reactions labeled with "+Fe(III)PPIX" and "+Co(III)PPIX" contained apoNC1 incubated with equimolar of Fe(III) heme or Co(III)PPIX, respectively. Fractions of pri-miRNAs converted to pre-miRNAs are plotted as means ± SD (n = 3 for pri-miR-23a, pri-miR-21 and pri-miR-380; n = 4 for pri-miR-30a). Asterisks indicate statistically significant activation of apoNC1 (**, $p \leq 0.01$; *, $0.01 < p \leq 0.05$).

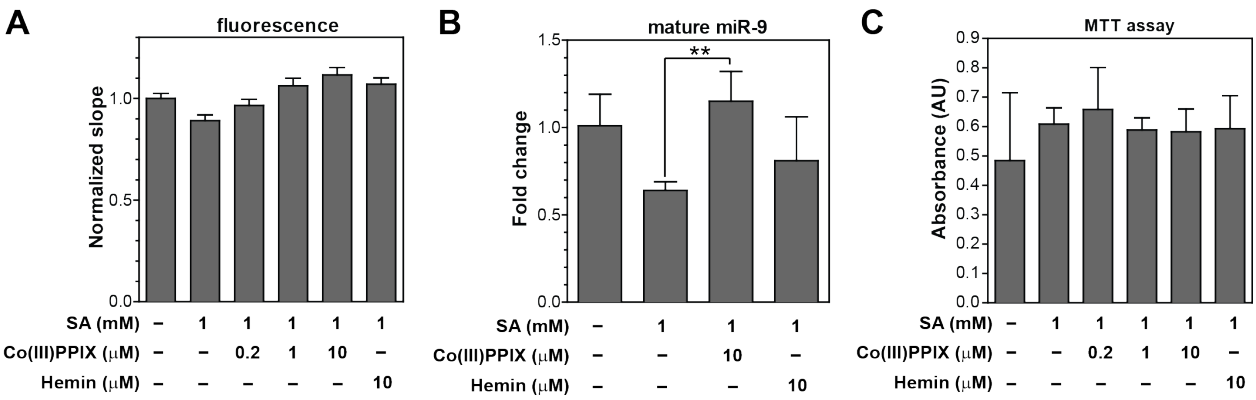

Figure 4-5. Live-cell pri-miRNA processing assay shows that Co(III)PPIX activates pri-miRNA processing without inducing cytotoxicity. Hela cells were cultured in heme-depleted media, transfected with the pri-miR-9-1 reporter, treated for 10 h with succinylacetone (1 mM) either alone or together with Co(III)PPIX or hemin at the indicated concentrations. (**A**) Normalized eYFP/mCherry fluorescence slopes (± 95% CI). (**B**) Abundance of mature miR-9 normalized by that of β-actin mRNA (mean ± SD, n = 4). (**C**) MTT assays showed little cytotoxicity.

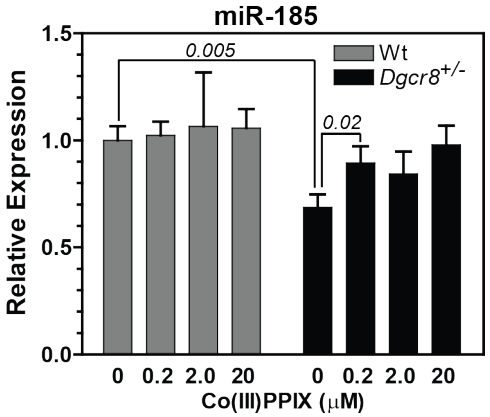

Figure 4-6. Co(III)PPIX restores deficient expression of miR-185 caused by heterozygous deletion of the *Dgcr8* gene in mice. Primary cortical neurons dissected from *Dgcr8*$^{+/-}$ mouse embryos and their wild-type littermates were treated with Co(III)PPIX at the indicated

concentrations between DIV 3 and 5, for 48 hr. Total RNAs were extracted and the miR-185 levels measured using RT-PCR. The abundance of miR-185 was normalized to that of the *GAPDH* mRNA. Each plotted value is average ± SEM from seven independent experiments using seven animals. Select *P* values are calculated using two-tailed Student's *t*-test and are indicated on the graph.

Table 4-1: DGCR8 binding properties of metalloporphyrins.

MPPIX	Soret peak, free (nm)	Soret peak, bound (nm)	Stably bind DGCR8	Activate pri-miRNA processing
Fe(III)	384	367, 450	Yes	Yes
Fe(II)	~390	N.D.	No	No
Co(III)	418	368, 456	Yes	Yes
Co(II)	397	398	No	N.D.

The properties of Fe(III) and Fe(II) heme were known from a previous study[14] and are shown for comparison. N.D., not determined.

References

1. Merritt, W.M. et al. Dicer, Drosha, and outcomes in patients with ovarian cancer. *N Engl J Med* 359, 2641-50 (2008).

2. Beveridge, N.J. & Cairns, M.J. MicroRNA dysregulation in schizophrenia. *Neurobiol Dis* 46, 263-71 (2012).

3. Kumar, M.S., Lu, J., Mercer, K.L., Golub, T.R. & Jacks, T. Impaired microRNA processing enhances cellular transformation and tumorigenesis. *Nat Genet* 39, 673-7 (2007).

4. Mori, M. et al. Hippo signaling regulates microprocessor and links cell-density-dependent miRNA biogenesis to cancer. *Cell* 156, 893-906 (2014).

5. Gregory, R.I. et al. The Microprocessor complex mediates the genesis of microRNAs. *Nature* 432, 235-240 (2004).

6. Denli, A.M., Tops, B.B., Plasterk, R.H., Ketting, R.F. & Hannon, G.J. Processing of primary microRNAs by the Microprocessor complex. *Nature* 432, 231-235 (2004).

7. Han, J. et al. The Drosha-DGCR8 complex in primary microRNA processing. *Genes Dev* 18, 3016-3027 (2004).

8. Landthaler, M., Yalcin, A. & Tuschl, T. The human DiGeorge syndrome critical region gene 8 and its *D. melanogaster* homolog are required for miRNA biogenesis. *Curr Biol* 14, 2162-2167 (2004).

9. Shiohama, A., Sasaki, T., Noda, S., Minoshima, S. & Shimizu, N. Molecular cloning and expression analysis of a novel gene DGCR8 located in the DiGeorge syndrome chromosomal region. *Biochem Biophys Res Commun* 304, 184-190 (2003).

10. Stark, K.L. et al. Altered brain microRNA biogenesis contributes to phenotypic deficits in a 22q11-deletion mouse model. *Nat Genet* 40, 751-60 (2008).

11. Fenelon, K. et al. Deficiency of Dgcr8, a gene disrupted by the 22q11.2 microdeletion, results in altered short-term plasticity in the prefrontal cortex. *Proc Natl Acad Sci USA* 108, 4447-52 (2011).

12. Schofield, C.M. et al. Monoallelic deletion of the microRNA biogenesis gene Dgcr8 produces deficits in the development of excitatory synaptic transmission in the prefrontal cortex. *Neural Dev* 6, 11 (2011).

13. Karayiorgou, M., Simon, T.J. & Gogos, J.A. 22q11.2 microdeletions: linking DNA structural variation to brain dysfunction and schizophrenia. *Nat Rev Neurosci* 11, 402-16 (2010).

14. Ha, M. & Kim, V.N. Regulation of microRNA biogenesis. *Nat Rev Mol Cell Biol* 15, 509-24 (2014).

15. Weitz, S.H., Gong, M., Barr, I., Weiss, S. & Guo, F. Processing of microRNA primary transcripts requires heme in mammalian cells. *Proc Natl Acad Sci U S A* 111, 1861-6 (2014).

16. Herbert, K.M., Pimienta, G., DeGregorio, S.J., Alexandrov, A. & Steitz, J.A. Phosphorylation of DGCR8 increases its intracellular stability and induces a progrowth miRNA profile. *Cell Rep* 5, 1070-81 (2013).

17. Wada, T., Kikuchi, J. & Furukawa, Y. Histone deacetylase 1 enhances microRNA processing via deacetylation of DGCR8. *EMBO Rep* 13, 142-9 (2012).

18. Gong, M. et al. Caspases cleave and inhibit the microRNA processing protein DiGeorge Critical Region 8. *Protein Sci* 21, 797-808 (2012).

19. Faller, M., Matsunaga, M., Yin, S., Loo, J.A. & Guo, F. Heme is involved in microRNA processing. *Nat Struct Mol Biol* 14, 23-9 (2007).

20. Barr, I. et al. DiGeorge Critical Region 8 (DGCR8) is a double-cysteine-ligated heme protein. *J Biol Chem* 286, 16716-16725 (2011).

21. Barr, I. et al. Ferric, not ferrous, heme activates RNA-binding protein DGCR8 for primary microRNA processing. *Proc Natl Acad Sci USA* 109, 1919-1924 (2012).

22. Senturia, R. et al. Structure of the dimerization domain of DiGeorge Critical Region 8. *Protein Sci* 19, 1354-1365 (2010).

23. Quick-Cleveland, J. et al. The DGCR8 RNA-binding heme domain recognizes primary microRNAs by clamping the Hairpin. *Cell Rep* 7, 1994-2005 (2014).

24. Kikuchi, G., Yoshida, T. & Noguchi, M. Heme oxygenase and heme degradation. *Biochem Biophys Res Commun* 338, 558-67 (2005).

25. Barr, I. & Guo, F. Primary microRNA processing assay reconstituted using recombinant Drosha and DGCR8. *Methods Mol Biol* 1095, 73-86 (2014).

26. Scolaro, L.M. et al. Aggregation behavior of protoporphyrin IX in aqueous solutions: Clear evidence of vesicle formation. *J Phys Chem B* 106, 2453-2459 (2002).

27. Kappas, A. & Drummond, G.S. Control of heme metabolism with synthetic metalloporphyrins. *J Clin Invest* 77, 335-9 (1986).

28. Xu, B., Hsu, P.K., Stark, K.L., Karayiorgou, M. & Gogos, J.A. Derepression of a neuronal inhibitor due to miRNA dysregulation in a schizophrenia-related microdeletion. *Cell* 152, 262-75 (2013).

29. Rosenberg, D.W. Pharmacokinetics of cobalt chloride and cobalt-protoporphyrin. *Drug Metab Dispos* 21, 846-849 (1993).

30. Galbraith, R.A. & Kappas, A. Regulation of food intake and body weight by cobalt porphyrins in animals. *Proc Natl Acad Sci U S A* 86, 7653-7657 (1989).

31. Csongradi, E., Docarmo, J.M., Dubinion, J.H., Vera, T. & Stec, D.E. Chronic HO-1 induction with cobalt protoporphyrin (CoPP) treatment increases oxygen consumption,

activity, heat production and lowers body weight in obese melanocortin-4 receptor-deficient mice. *Int J Obes* 36, 244-253 (2012).

32. Li, M.Y., Vizzard, M.A., Jaworski, D.M. & Galbraith, R.A. The weight loss elicited by cobalt protoporphyrin is related to decreased activity of nitric oxide synthase in the hypothalamus. *J Appl Physiol* 100, 1983-1991 (2006).

33. Shan, Y. et al. Induction of the heme oxygenase-1 gene by metalloporphyrins. *Arch Biochem Biophys* 380, 219-27 (2000).

34. Shan, Y., Lambrecht, R.W., Donohue, S.E. & Bonkovsky, H.L. Role of Bach1 and Nrf2 in up-regulation of the heme oxygenase-1 gene by cobalt protoporphyrin. *FASEB J* 20, 2651-3 (2006).

35. Dercho, R.A., Nakatsu, K., Wong, R.J., Stevenson, D.K. & Vreman, H.J. Determination of in vivo carbon monoxide production in laboratory animals via exhaled air. *J Pharmacol Toxicol Methods* 54, 288-95 (2006).

36. Motterlini, R. & Foresti, R. Heme oxygenase-1 as a target for drug discovery. *Antioxid Redox Signal* 20, 1810-26 (2014).

37. Wu, M.L., Ho, Y.C., Lin, C.Y. & Yet, S.F. Heme oxygenase-1 in inflammation and cardiovascular disease. *Am J Cardiovasc Dis* 1, 150-8 (2011).

38. Galbraith, R.A. & Kappas, A. Cobalt-protoporphyrin suppresses expression of genetic obesity in homozygous (fa/fa) Zucker rats. *Pharmacology* 41, 292-298 (1990).

39. Schoenfeld, N. et al. The effects of metalloporphyrins, porphyrins and metals on the activity of delta-aminolevulinic acid synthase in monolayers of chick embryo liver cells. *Biochem Pharmacol* 33, 2783-8 (1984).

40. Drummond, G.S. & Kappas, A. The cytochrome P-450-depleted animal: an experimental model for in vivo studies in chemical biology. *Proc Natl Acad Sci U S A* 79, 2384-8 (1982).

41. Wagner, G.C., Gunsalus, I.C., Wang, M.Y. & Hoffman, B.M. Cobalt-substituted cytochrome P-450cam. *J Biol Chem* 256, 6266-73 (1981).

42. Smith, A.T. et al. Cobalt cystathionine beta-synthase: a cobalt-substituted heme protein with a unique thiolate ligation motif. *Inorg Chem* 50, 4417-27 (2011).

43. Wang, M.Y., Hoffman, B.M. & Hollenberg, P.F. Cobalt-substituted horseradish peroxidase. *J Biol Chem* 252, 6268-75 (1977).

44. Davis, B.N. & Hata, A. Regulation of MicroRNA Biogenesis: A miRiad of mechanisms. *Cell Commun Signal* 7, 18 (2009).

CHAPTER 5

Fe(III) protoporphyrin IX derivatives activate DGCR8 for microRNA processing

The work described in this chapter was initiated by Jose Paul Jacob. The project is a spin off from Ian Barr's metalloporphyrin screen. Jose used purified DGCR8 to test Fe(III) heme protoporpyrin ring derivatives for their ability to activate DGCR8. I then took these compounds and tested then using my cellular assay. We both contributed to writing the results.

ABSTRACT

Heme has recently been identified as an essential component of the miRNA biogenesis pathway. In the first step of the pathway, primary transcripts of miRNA (pri-miRNA) are recognized by the RNA-binding protein DGCR8. DGCR8 binds an Fe(III) heme cofactor which is required for its activity. To gain insight into the structural function of the heme in DGCR8 we tested a series of Fe(III) protoporphyrin derivatives modified at the porphyrin ring. We classify the derivatives as either strong or weak activators based on their ability to bind to DGCR8 and activate its processing activity both *in vitro* and in cells. Our results show that DGCR8 tolerates only small changes to the protoporphyrin ring. This suggests that DGCR8 makes tight connections with the porphyrin ring, which are important for its function.

INTRODUCTION

Heme serves a variety of functions in the cell. It aids in oxygen transport, serves as an enzymatic cofactor, and functions as a signaling molecule[1–3]. In the miRNA processing pathway, heme is a cofactor for the RNA binding protein DGCR8 (DiGeorge Critical Region gene 8)[4]. miRNAs are initially transcribed as long primary transcripts of miRNA (pri-miRNA)[5]. Pri-miRNA form a characteristic hairpin structure which is specifically recognized by DGCR8[6–9]. Pri-miRNAs are then cleaved by the RNase III enzyme Drosha and continue on the maturation pathway until they are finally loaded into the RNA-induced silencing complex (RISC).

The first step of pri-miRNA recognition is essential for the correct production of mature miRNA. DGCR8 binds to the pri-miRNA hairpin through the coordinated use of its RNA-binding heme domain (Rhed) and its two double-stranded RNA binding domains (dsRBD)[10,11]. Heme is required for DGCR8 activity both *in vitro* and in cells[12]. An active recombinant construct of

DGCR8 call NC1 (residues 276-751) binds Fe(III) heme by dimerizing and using one Cys residue from each subunit of the dimer as the axial ligand[13,14]. The heme free form (apoNC1) can be made by reducing the heme and incubating with excess apomyglobin. Though many hemoproteins use Cys residues to ligate heme, DGCR8 is the first example of a double Cys ligated hemoprotein.

Figure 5-1 shows the structure of heme. In the most common form of heme, heme *b*, the C_3 and C_8 positions (R1 in the figure) both contain vinyl functional groups. In hemoglobin and myoglobin these vinyl groups point in toward the interior of the protein and are surrounded by apolar aliphatic and aromatic side chains[15]. These interactions contribute to hemoglobin's and myoglobin's affinity for heme. Without a structure of heme-bound DGCR8, it is unknown how the porphyrin ring contributes to heme affinity. To investigate the structural contribution of the porphyrin ring in DGCR8 we tested the following Fe(III) protoporphyrin IX derivatives: Fe(III) mesoporphyrin IX , Fe(III) 2,4-dimethyl deuteroporphyrin IX, Fe(III) deuteroporphyrin IX, Fe(III) isohematoporphyrin IX, and Fe(III) hematoporphyrin IX. Each derivative was synthesized by replacing the vinyl groups of hemin at the C_3 and C_8 positions on the ring with a different functional group (Fig 5-1a). Herein, we characterize each Fe(III) porphyrin IX derivative as either a strong or weak/transient activator of DGCR8 on the basis of the following criteria : 1) their ability to bind stochiometrically with apoNC1 2) Co-elution with apoNC1 3) ability to activate miRNA processing *in vitro* and in cells.

METHODS

Materials

Hemin was purchased from Sigma (St. Louis, MO, USA). All other metalloporphyrins were obtained from Frontier Scientific (Logan, UT, USA).

Expression and purification of recombinant DGCR8

Fe(III) NC1 and apoNC1 proteins were purified as described previously[13,14]. Briefly, the constructs were expressed in the pET-24a$^+$ vector in *E. coli* and purified using cation exchange chromatography followed by size-exclusion chromatography (SEC). The SEC buffer contained 20 mM Tris pH 8.0, 400 mM NaCl, and 1 mM DTT. Reduction of the Fe(III) NC1 was accomplished using 2 mM sodium dithionite in 50 mM 2-(*N*-morpholino)ethanesulfonic acid (MES) pH 6.0, 400 mM NaCl, and 1 mM DTT.

DGCR8-porphyrin binding assay

All porphyrin solutions were made fresh on the day of use and stored at ≤ 4°C. Metalloporphyrins were initially dissolved in 0.1 M NaOH, and then diluted to 100 μM stocks using binding buffer. The concentrations were determined using published extinction coefficients.

The porphyrin-binding reaction buffer contained 1 mM DTT, 400 mM NaCl, and the buffer 50 mM MES pH 6.0. Absorbance spectra were collected using either a Varian Cary 300 Bio spectrophotometer with bandwidth set to 1 nm or a DU800 spectrophotometer (Beckman-Coulter, bandwidth ≤ 1.8 nm).

Reconstituted pri-miRNA processing assays

The assays were done as described previously[13]. The reactions were incubated at 37°C for 45 min, and were analyzed using 15% acrylamide, 7 M urea denaturing gels and autoradiography. The bands were quantified using the ImageQuant software (GE Healthcare). The intensities of pre-miRNAs were converted to the equivalents of pri-miRNAs by multiplying the ratio of the numbers of ^{32}P-containing residues in the pri-miRNA and pre-miRNA. *p* values were calculated using two-tailed Student's *t*-test and Mann-Whitney U-test.

Cellular pri-miRNA processing assay

The cellular assays were performed as described previously. Briefly, cells were grown in heme-depleted media for 24 hours before splitting into smaller plates for both imaging and RNA analysis. Cells were transfected with the pri-miR-9-1 reporter. Eighteen hours post-transfection, 1 mM SA, either alone or with 10 μM Fe(III) isohematoporphyrin IX, Fe(III) mesoporphyrin IX, Fe(III) 2,4-methyl deuteroporphyrin IX or Hemin, was added to the cells, and 1 μM doxycycline was also added to induce expression of reporters. Fe(III) isohematoporphyrin IX, Fe(III) mesoporphyrin IX, and Fe(III) 2,4-methyl deuteroporphyrin IX were dissolved in NaOH. Hemin was dissolved in DMSO shortly before addition to the cell cultures. After 10 h of treatment, cells were used either for imaging or for total RNA extraction. Imaging and data analysis were performed as described. Total RNAs were extracted using the miRNeasy mini kit (Qiagen). Taqman assays (Life Technologies) were used to measure mature miR-9 and *eYFP* mRNA levels.

RESULTS

Fe(III) mesoporphyrin IX and Fe(III) 2,4-dimethyl deuteroporphyrin IX are strong activators

Each derivative was first tested to see whether it could bind heme free apoNC1. DGCR8 wt protein has characteristic Soret peaks at 450 nm and 366 nm in its absorption spectra. We have previously shown that NC1 protein dimerizes and stochiometrically binds Fe(III) heme at 1:1 ratio. We incubated apoNC1 with increasing concentrations of Fe(III) mesoporphyrin IX and Fe(III) 2,4-dimethyl deuteroporphyrin IX and monitored the absorption spectrum. Both derivatives displayed characteristic Soret peaks suggesting reconstitution of the DGCR8 protein to an active heme-bound form (Figs. 5-2A,B; 5-3A,B). The 436 nm peak for both derivatives

increased steadily until saturating at a 1:1 ratio, which demonstrates stoichiometric binding. Fe(III) mesoporphyrin IX and Fe(III) 2,4-dimethyl deuteroporphyrin IX were then incubated with apoNC1 for 30 minutes before running the complex on a size-exclusion column. Both of the derivatives co-eluted with NC1, suggesting a strong interaction (Figs. 5-2C, 5-3C).

Fe(III) deuteroporphyrin IX, Fe(III) isohematoporphyrin IX, and Fe(III) hematoporphyrin IX are weak/transient activators

The absorption spectrum for the mixture of apoNC1 with Fe(III) deuteroporphyrin IX, Fe(III) isohematoporphyrin IX, and Fe(III) hematoporphyrin IX did not display the typical split Soret peak (Fig. 5-4A). For Fe(III) deuteroporphyin IX, a small peak at 357 nm was present at lower concentration but disappeared as the concentration increased. The interaction of Fe(III) isohematoporphyrin IX and Fe(III) hematoporphyrin IX with apoNC1 was even less stable and the Soret peaks were completely absent. Additionally, all three derivatives did not co-elute with apoNC1 during size exclusion chromatography (Fig. 5-4B).

Strong derivatives activate miRNA processing efficiently

We next tested the derivatives' ability to activate DGCR8 in an *in vitro* processing assay. Radiolabeled primary microRNAs pri-miR-9-1 and pri-miR-21 were incubated with Drosha, apoNC1 and the individual derivatives. The cleavage products were then visualized using gel electrophoresis (Fig. 5-5). Both Fe (III) mesoporphyrin IX and Fe(III) 2,4-dimethyl deuteroporphyrin IX activated miRNA processing similar to heme, whereas Fe(III) deuteroporphyrin IX, Fe(III) isohematoporphyrin IX, and Fe(III) hematoporphyrin IX only partially activated processing. The *in vitro* processing assays were also consistent with the

classification of strong and weak activators.

Fe(III) mesoporphyrin IX activates DGCR8 activity in cells

We tested if the protoporphyrin ring modified hemes were able to activate pri-miRNA processing in human cells using our previously described live-cell processing assay[12]. The reporter plasmid used in this assay co-expresses eYFP and an mCherry which contains a pri-miRNA within its 3′-untranslated region. Processing of the pri-miRNA by DGCR8/Drosha reduces mCherry protein expression. eYFP is used for normalization. Plots of eYFP vs mCherry fluorescent intensities for individual cells are best fit with a linear regression with the slope indicating processing efficiency.

HeLa cells were grown in heme-depleted media (HDM) and transfected with the pri-miR-9-1 reporter. Eighteen hours post-transfections the reporter was induced and cells were treated with succinylacetone (SA) to block heme synthesis. In addition to SA, cells were also treated with Fe(III) isohemato-, meso-, 2,4 dimethyl deutero- porphyrin IX or hemin for 10 h. Treatment with SA resulted in the expected decrease in normalized slope (from 1.0 ± 0.02 (no treatment) to 0.89 ± 0.03 (SA)) (Fig. 5-6A). Hemin, meso-, and 2,4dimethyl deutero- were all able to rescue this processing defect, increasing the slope to 1.06 ± 0.03, 1.09 ± 0.03, and 1.07 ± 0.03 respectively. A smaller rescue was observed for treatment with isohematoporphyrin IX (slope = 0.95 ± 0.02, $p = 0.0025$ for change between SA and SA+isohemato). To clarify the results we also tested the cellular activity of the porphyrin derivatives while overexpressing DGCR8. HeLa cells are missing one copy of chromosome 22, which codes for DGCR8[16]. As a result these cells have a reduced expression level of DGCR8. Therefore, overexpressing DGCR8 makes the cellular assay more sensitive (manuscript in preparation). We tested the same porphyrin

derivatives using the pri-miR-9-1 reporter and the N-terminal flag tagged overexpression construct (N-flag-DGCR8). Even though the cells were grown in HDM, overexpression of DGCR8 still increased the slope from 1.00 ± 0.06 to 1.91 ± 0.13. Treatment with SA reduced DGCR8 activity resulting in a slope = 1.53 ± 0.10. Similar to the previous experiment, both meso- and 2,4 dimethyl deutero- were able to rescue DGCR8 activity (slope = 2.48 ± 0.18 and 2.39 ± 0.17, respectively). Isohemato- again was able to rescue but to a lesser extent (slope = 2.00 ± 0.16). Altogether, the cellular experiments demonstrate that both mesoporphyrin and 2,4 dimethyl deuterophorphyrin are tolerable substitutions to hemin and are potent activators of DGCR8. On the other hand, isohematoporphyrin is a less potent activator and may only form a transient complex with DGCR8.

DISCUSSION

In this study we have gained further insight into the structure of the DGCR8 heme-binding pocket. We show that in addition to Fe(III) heme, DGCR8 can stably bind Fe(III) mesoporphyrin IX and Fe(III) 2,4-dimethyl deuteroporphyrin IX. These two derivatives can activate DGCR8 processing activity both *in vitro* and in cells. Compared to the other derivatives that were tested, meso- and 2,4-dimethyl deuteroporphyrin present the smallest chemical deviation from the natural hemin cofactor. These two derivatives maintain the non-polar environment that is also characteristic of the vinyl group in heme. These porphyrin modifications are also tolerated by hemoglobin and myoglobin[17]. It is likely that similar to hemoglobin and myglobin, the side of the DGCR8 heme-pocket that contacts the vinyl group of heme is composed non-polar and aromatic residues. In support of this hypothesis, substitutions with the polar derivatives hemato- and isohemato- are not tolerated. Isohemato and hemato also

provide bulk to the heme cofactor and might result in steric hindrance. Unlike hemoglobin, DGCR8 does not tolerate substitution with deuteroporphyrin. This suggests that the presence of an aliphatic group at the C_3 and C_8 position on heme is required for DGCR8 heme recognition.

Another interesting result from our study is the difference in activating potential of isohemato- in our *in vitro* studies versus in cells. *In vitro* isohemato- and apoNC1 are unable to form a stable complex and isohemato- is unable to activate apoNC1's processing activity in the reconstituted processing assay. However, in cells isohemato- is able to partially rescue the DGCR8 activity defect associated with SA treatment. DGCR8 and Drosha are the minimal components necessary to form an active pri-miRNA processing complex. However, it has been demonstrated that in cells many other proteins associate with this complex[18]. It is possible that in cells DGCR8 can accept a wider range of porphyrin derivatives due to the increased stability provided by binding partners. Alternatively, the crowded environment of the cell may strengthen the DGCR8 isohemato- complex.

FIGURES AND LEGENDS

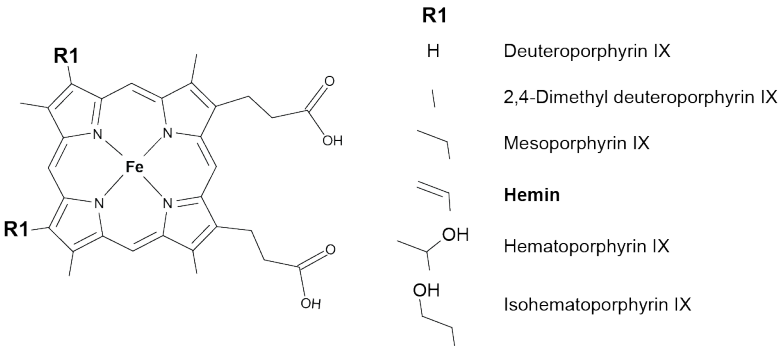

Figure 5-1. Fe(III) porphyrin IX derivatives that were tested for association with DGCR8 and for activation of pri-miRNA processing. (a) Schematic of a Fe(III) porphyrin IX derivative. The **R1** represents a functional group listed on the right.

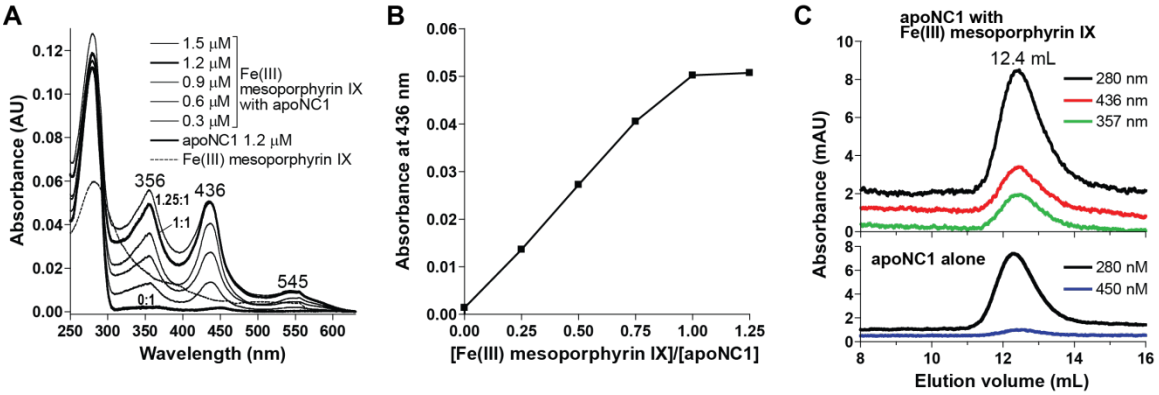

Figure 5-2. Fe(III) mesoporphyrin IX stably associates with apoNC1. (**A**) Electronic absorption spectra of titration of Fe(III) mesoporphyrin IX into 1.2 μM apoNC1 dimer at indicated concentrations, in 50 mM MES pH 6.0, 400 mM NaCl and 1 mM DTT. The porphyrin:apoNC1 ratios of select curves are indicated in bold. An absorbance spectrum of Fe(III) mesoporphyrin IX alone is shown as a dashed line. (**B**) Absorbance values at the 436 nm Söret peak are plotted against porphyrin:apoNC1 ratios. (**C**) Size-exclusion chromatogram of a mixture of Fe(III) mesoporphyrin IX and apoNC1 (top), both at 1.2 μM concentration, shows co-elution. The chromatogram of apoNC1 alone is shown below for comparison.

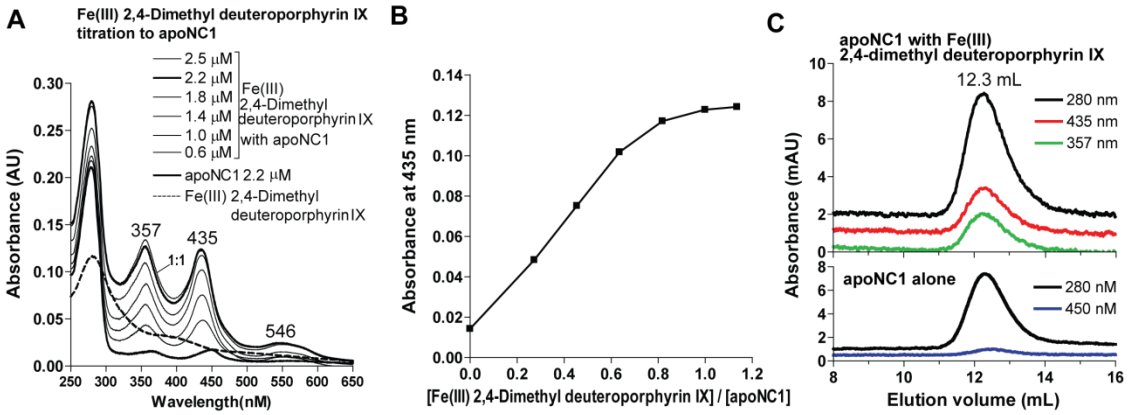

Figure 5-3. Fe(III) 2,4-dimethyl deuteroporphyrin IX associates with apoNC1. (**A**) Electronic absorption spectra of Fe(III) 2,4-dimethyl deuteroporphyrin IX titrated into 2.2 μM apoNC1 dimer at the indicated concentrations, in 50 mM MES pH 6.0, 400 mM NaCl and 1 mM DTT. (**B**) Absorbance values at the 435 nm Söret peak are plotted against the porphyrin:apoNC1 ratios. (**C**) Size-exclusion chromatogram of a mixture of Fe(III) 2,4-dimethyl deuteroporphyrin IX and apoNC1 (top), both at 2.2μM concentration, shows co-elution. The chromatogram of apoNC1 alone is shown below for comparison.

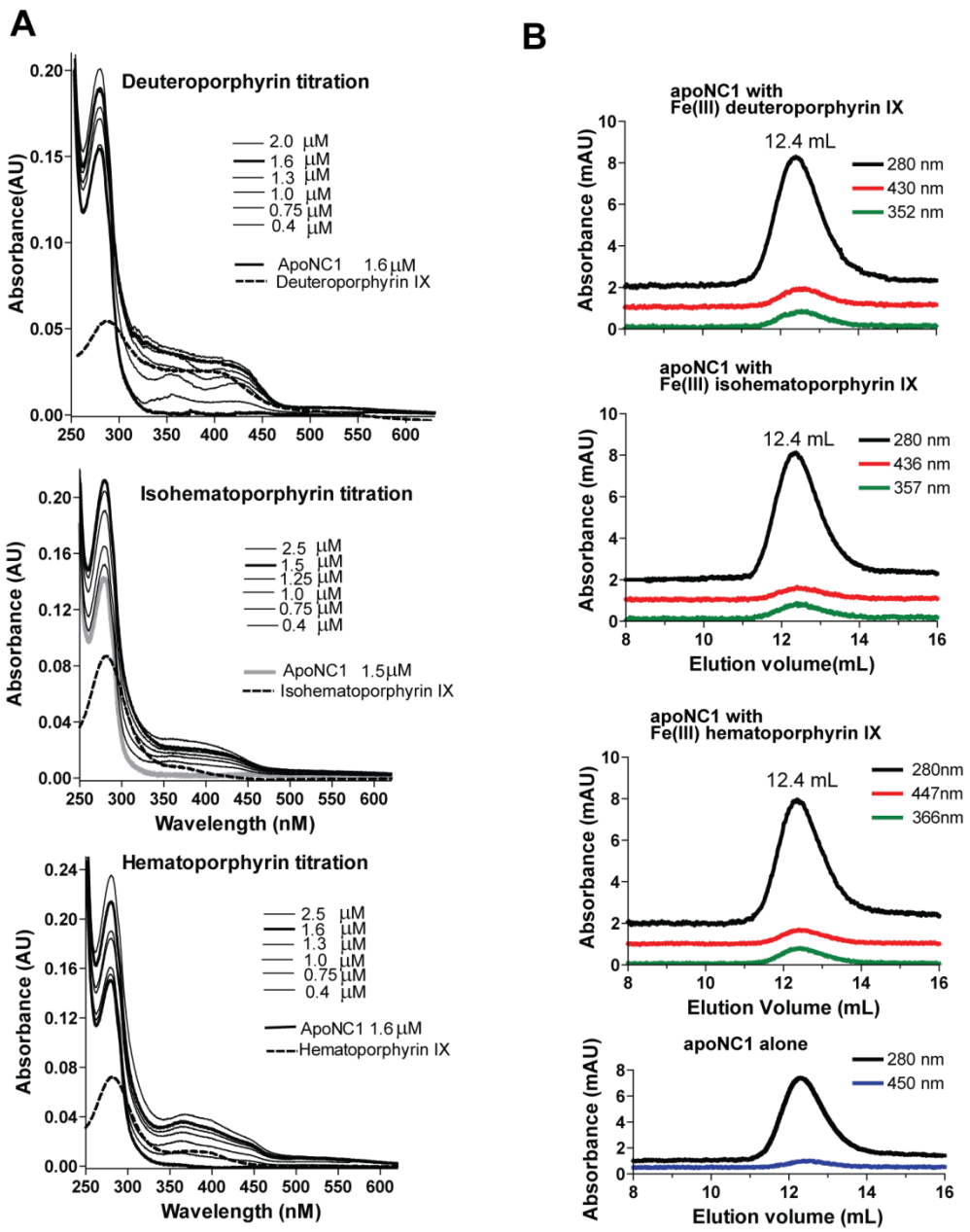

Figure 5-4. Fe(III) deuteroporphyrin IX, Fe(III) isohematoporphyrin IX and Fe(III) hematoporphyrin IX loosely associates with apoNC1. (**A**) Electronic absorption spectra of Fe(III) deuteroporphyrin IX, Fe(III) isohematoporphyrin IX and Fe(III) hematoporphyrin IX titrated into apoNC1 dimer at the indicated concentrations, in 50 mM MES pH 6.0, 400 mM NaCl and 1 mM DTT. (**B**) Size-exclusion chromatogram of a mixture of each one of the Fe(III) deuteroporphyrin IX, Fe(III) isohematoporphyrin IX and Fe(III) hematoporphyrin IX with

apoNC1 (top). The chromatogram of apoNC1 alone is shown below for comparison.

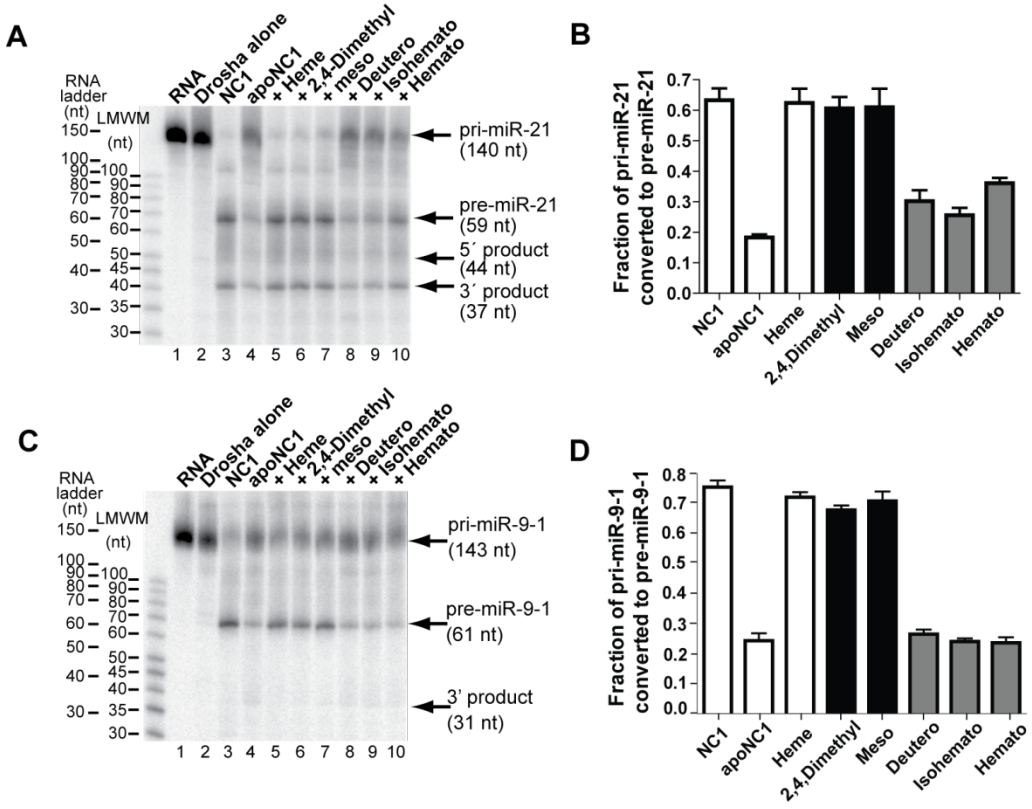

Figure 5-5. Fe(III) mesoporphyrin IX and Fe(III) 2,4-methyl deuteroporphyrin IX activates DGCR8 for pri-miRNA processing *in vitro*. Trace amounts of uniformly ^{32}P-labeled pri-miR-21 and ^{32}P-labeled pri-miR-9-1was incubated with recombinant His_6-Drosha$^{390-1374}$ and the various forms of DGCR8 proteins (25 nM dimer). NC1 is the native Fe(III) heme-bound dimer. apoNC1 is NC1 with the >90% of heme removed. apoNC1 pre-incubated with porphyrin compounds are labeled with the compound's names. (**A, C**) A representative denaturing gel image of the cleavage assays. (**B,D**) Fractions of pri-miRNAs converted to pre-miRNAs are plotted as means ± SD (n = 3).

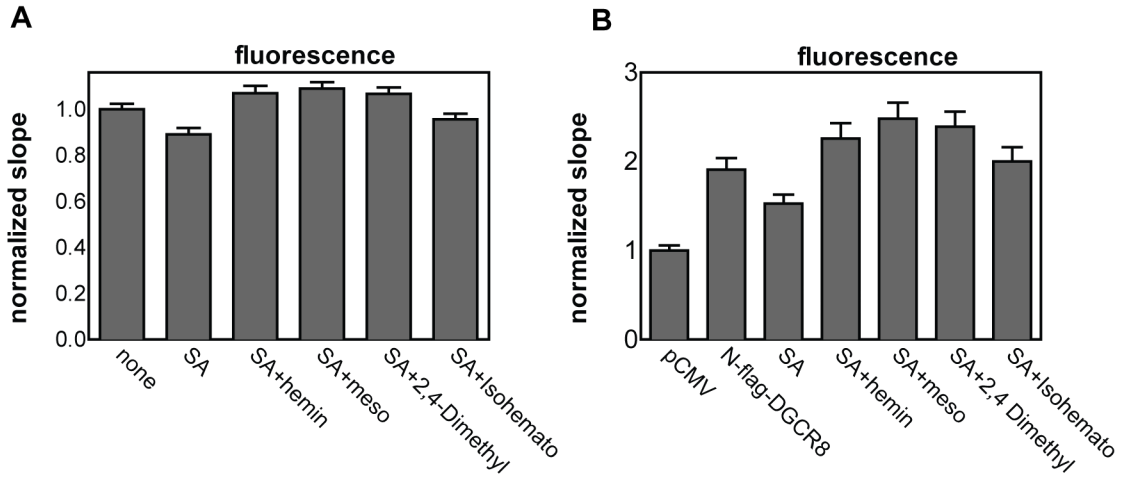

Figure 5-6. Live-cell pri-miRNA processing assay shows that Fe(III) mesoporphyrin IX and Fe(III) 2,4-methyl deuteroporphyrin IX activates pri-miRNA processing. Hela cells were cultured in heme-depleted media, transfected with the pri-miR-9-1 reporter, treated for 10 h with succinylacetone (1 mM) either alone or together with the indicated porphyrin compounds at 10 □M concentration. (**A**) Normalized eYFP vs mCherry fluorescence slopes (± 95% CI). (**B**) Normalized fluorescence slope of HeLa cells transfected with pri-miR-9-1 reporter plus either empty pCMV-tag2a vector (v.c.) or N-flag-DGCR8 expression constructs as indicated. Error bars represent 95% confidence interval from the linear fit.

References

1. Thöny-meyer, L. in *Tetrapyrroles: Birth, Life, and Death* (Warren, M. & Smith, A.) 149–159 (Springer, 2009).

2. McCoubrey Jr., W. K. Heme Oxygenase-2 Is a Hemoprotein and Binds Heme through Heme Regulatory Motifs That Are Not Involved in Heme Catalysis. *J. Biol. Chem.* **272,** 12568–12574 (1997).

3. Tracz, M. J., Alam, J. & Nath, K. a. Physiology and pathophysiology of heme: implications for kidney disease. *J. Am. Soc. Nephrol.* **18,** 414–20 (2007).

4. Faller, M., Matsunaga, M., Yin, S., Loo, J. A. & Guo, F. Heme is involved in microRNA processing. *Nat. Struct. Mol. Biol.* **14,** 23–9 (2007).

5. Kim, V. N., Han, J. & Siomi, M. C. Biogenesis of small RNAs in animals. *Nat. Rev. Mol. Cell Biol.* **10,** 126–39 (2009).

6. Faller, M. *et al.* DGCR8 recognizes primary transcripts of microRNAs through highly cooperative binding and formation of higher-order structures. *RNA* **16,** 1570–83 (2010).

7. Shiohama, A., Sasaki, T., Noda, S., Minoshima, S. & Shimizu, N. Molecular cloning and expression analysis of a novel gene DGCR8 located in the DiGeorge syndrome chromosomal region. *Biochem. Biophys. Res. Commun.* **304,** 184–190 (2003).

8. Han, J. *et al.* The Drosha-DGCR8 complex in primary microRNA processing. *Genes Dev.* **18,** 3016–27 (2004).

9. Yeom, K.-H., Lee, Y., Han, J., Suh, M. R. & Kim, V. N. Characterization of DGCR8/Pasha, the essential cofactor for Drosha in primary miRNA processing. *Nucleic Acids Res.* **34,** 4622–9 (2006).

10. Quick-Cleveland, J. *et al.* The DGCR8 RNA-binding heme domain recognizes primary microRNAs by clamping the hairpin. *Cell Rep.* **7,** 1994–2005 (2014).

11. Sohn, S. Y. *et al.* Crystal structure of human DGCR8 core. *Nat. Struct. Mol. Biol.* **14,** 847–53 (2007).

12. Weitz, S. H., Gong, M., Barr, I., Weiss, S. & Guo, F. Processing of microRNA primary transcripts requires heme in mammalian cells. *Proc. Natl. Acad. Sci. U. S. A.* **111,** 1861–6 (2014).

13. Barr, I. *et al.* Ferric, not ferrous, heme activates RNA-binding protein DGCR8 for primary microRNA processing. *Proc. Natl. Acad. Sci. U. S. A.* **109,** 1919–24 (2012).

14. Barr, I. *et al.* DiGeorge critical region 8 (DGCR8) is a double-cysteine-ligated heme protein. *J. Biol. Chem.* **286,** 16716–25 (2011).

15. Hargrove, M. S., Barrick, D. & Olson, J. S. The association rate constant for heme binding to globin is independent of protein structure. *Biochemistry* **35,** 11293–9 (1996).

16. Macville, M. *et al.* Comprehensive and Definitive Molecular Cytogenetic Characterization of HeLa Cells by Spectral Karyotyping Comprehensive and Definitive Molecular Cytogenetic Characterization of HeLa Cells by Spectral Karyotyping. 141–150 (1999).

17. Yonetani, T., Yamamoto, H. & Woodrow, G. Studies on cobalt myoglobins and hemoglobins: I. Preparation and optical properties of myoglobind and hemoglobind

containing cobalt proto-, meso-, and deuteroporphyrins and thermodynamic characterization of their reversible oxygenation. *J. Biol. Chem.* **249,** 582–600 (1974).

18. Ha, M. & Kim, V. N. Regulation of microRNA biogenesis. *Nat. Rev. Mol. Cell Biol.* **15,** 509–524 (2014).

CHAPTER 6

The pool of available Fe(III) heme in mammalian cells

One of the final applications of my cellular assay was to use it to determine Fe(III) heme availability. This project began with the characterization of heme binding defective DGCR8 mutants that were discovered by Jen Quick-Cleveland. Jen performed the *in vitro* characterization of the mutant while I performed the cellular analysis. This was one of the first times that we found DGCR8 mutants with altered heme binding *in vitro* that were still active in cells. We were able to use these mutants to analyze the cellular heme availability. Jose Paul Jacob and Rachel Senturia also helped with this study by performing *in vitro* processing assays and cloning. Ian Barr performed the stop-flow heme association measurements. This chapter is our unpublished manuscript.

ABSTRACT

Heme is an essential biological cofactor for many proteins. While heme is synthesized in the Fe(II) form, Fe(III) heme is specifically required for processing primary transcripts of microRNAs (pri-miRNAs) by binding the RNA-binding protein DGCR8. However, it is unknown how readily available Fe(III) heme is in human cells. Here we address this question by characterizing a set of DGCR8 mutants with various degrees of heme-binding deficiency. We observed a strikingly simple correlation between Fe(III) heme affinity in vitro and pri-miRNA processing activity in HeLa cells. The results are consistent with a model in which the available Fe(III) heme concentration sets the threshold for determining if DGCR8 is successfully loaded with Fe(III) heme and thereby activated for pri-miRNA processing. These results suggest that available Fe(III) heme is present in mammalian cells in a tightly controlled state. Our study has important implications to the mechanisms of heme trafficking and redox regulation.

INTRODUCTION

Heme is an essential cofactor for life. It participates in numerous biological pathways, by serving as a prosthetic group for heme proteins, or as a signaling molecule to regulate cellular processes [1-3]. For cells to function normally, a fine balance is maintained between heme synthesis and degradation through feedback and feedforward mechanisms [4-6]. Over-abundance of heme causes severe cell and tissue damages. Conversely, heme deficiency results in anemia or porphyria. Most heme molecules in cells and tissues are already bound to their host proteins. Therefore, it is the pool of "available" heme (sometimes called "free heme" or "regulatory heme") that determines whether newly synthesized heme proteins are loaded with heme and whether a

signaling pathway is turned on or off. The available heme in cells is transient and is dynamically regulated, leading to technical challenges in measuring its concentration [7]. Based on characterization of the heme degradation enzymes, heme oxygenases (K_M = ~1 μM), it was proposed that the concentration of available heme may be just below the K_M, probably around 100 nM. Another theory suggests that available heme molecules are bound to heme transporter proteins and there is little to no free heme in cells [8].

Heme activates miRNA maturation by binding to DGCR8 (*D*i*G*eorge *c*ritical *r*egion gene *8*, also called Pasha in flies and worms) [9-11]. DGCR8 and the ribonuclease III Drosha form the Microprocessor complex, which recognize and cleave pri-miRNAs to produce the processing intermediates, precursor miRNAs (pre-miRNAs) [12-15]. DGCR8 contains an RNA-binding heme domain (Rhed, residues 276-498 in humans) that binds to the ends of pri-miRNA hairpins and collaborates with the two double-stranded RNA-binding domains (dsRBDs) of DGCR8 to achieve high pri-miRNA-binding affinity and specificity (Fig. 6-1A) [16]. At steady state, the heme iron may adopt either 2+ or 3+ oxidation state. Only the Fe(III) heme availability directly affects pri-miRNA processing, as DGCR8 strongly prefers binding Fe(III) heme over Fe(II) heme and only Fe(III) heme can activate DGCR8 [10,17]. DGCR8 binds heme as a dimer using Cys352 from each subunit as the coaxial ligands [9,17,18]. The electron-rich dual cysteine ligation is key to the extraordinary specificity of DGCR8 for Fe(III) heme.

The available Fe(III) heme concentration may be determined by characterizing DGCR8 mutants with various affinities for Fe(III) heme. The intracellular Fe(III) heme availability should be between the dissociation constants (K_d) of an active DGCR8 with the lowest Fe(III) heme affinity and an inactive DGCR8 mutant with the highest Fe(III) heme affinity. Cys352 and the surrounding residues, including Ile350, Pro351, and Leu353, generate the "IPCL" motif that

is critical for heme binding. Mutation of any single one of these residues to alanine abolishes DGCR8 activity in cells [11]. Out of these mutants, only P351A is still capable of binding Fe(III) heme in vitro, though with much reduced affinity [17]. The heme-binding affinities of heme proteins may be compared by measuring their dissociation rates (k_{off}) [19]. The k_{off} of P351A-heme complex is around 5 x 10^{-4} s^{-1} at room temperature, whereas the k_{off} of wild-type DGCR8 is very slow with no Fe(III) heme dissociation observed in 4 days ($k_{off} << 3 \times 10^{-6}$ s^{-1}) [17]. The large gap between the Fe(III) heme affinities of the active wild-type DGCR8 and the inactive P351A mutant leaves it uncertain what the available Fe(III) heme concentration is in cells.

Here we identified DGCR8 mutants that have reduced affinities for Fe(III) heme but maintain their activity. In combination with the inactive mutants described above, our results suggest that Fe(III) heme availability in HeLa cells falls in a surprisingly narrow and low concentration range. We validated this estimate by manipulating the cellular heme environments. These findings have important implications as to how Fe(III) heme is produced and transported in mammalian cells.

METHODS

Expression, purification and characterization of DGCR8 (NC1) proteins

Expression, purification and reconstituted pri-miRNA processing assays were done as described [29]. Proteins were expressed in the presence of 1 mM δ-ALA. The proteins were stored in 20 mM Tris pH 8.0, 400 mM NaCl and 1 mM dithiothreitol. Heme off-rate measurements were performed as previously described [17].

Cellular pri-miRNA processing assays

The assay has been described previously [11]. Succinylacetone and hemin stock solutions were prepared in water and DMSO, respectively. Cells were grown either in heme-depleted media or complete media and then split into glass-bottom plates for imaging. Cells were treated for 2 hr with 1 mM SA either alone or with hemin. Cells were cotransfected with the pri-miR-9-1 reporter and the indicated N-flag-DGCR8 construct. We used twice the amount of N-flag-DGCR8 mutant plasmid as the wild type in the cotransfections. Doxycycline was added to a final concentration of 1 μM to induce reporter expression. Cells were imaged 20-24 hr post-induction.

RESULTS and DISCUSSION

The DGCR8 G2 mutant does not bind heme

In a systematic mutagenesis of basic residues within the C-terminal region of Rhed, designed for the purpose of another study [16], we identified a group mutant G2 (containing R441A, K446A and R447A) that is severely defective in heme binding. The mutations were introduced to NC1, a truncated construct of DGCR8 (a.a. 276-751) that includes all functionally important regions for pri-miRNA processing, namely the Rhed, the dsRBDs and the C-terminal tail (CTT) (Fig. 6-1A). We overexpressed the mutants in *E. coli*, purified them to homogeneity and examined the presence of heme using electronic absorption spectroscopy. No intense absorption was observed in the 400-500 nm region (Fig. 6-1B). The minor residual Söret peak was mostly at 424 nm, not the 450 nm characteristic for Fe(III) heme ligated by two cysteine residues of DGCR8 (Fig. 6-1B inset). These results indicate that one or more of the residues mutated in G2 are necessary for DGCR8-heme association.

Next, we measured the activity of the DGCR8 G2 mutant using *in vitro* and cellular assays. In reconstituted pri-miRNA processing assays, we incubated ^{32}P-labeled pri-miRNAs

with purified NC1 G2 and His_6-$Drosha^{390-1374}$ proteins. Denaturing polyacrylamide gel analyses indicated that the pri-miRNA processing activity of G2 was abolished (Fig. 6-1C,D). To test the cellular activity of G2, we used a fluorescent-based live-cell pri-miRNA processing reporter assay [11]. In this assay, a pri-miRNA (pri-miR-9-1) is inserted into the 3′UTR of mCherry so that processing of the pri-miRNA results in degradation of the fusion mRNA and thereby a reduction of mCherry fluorescence. The reporter plasmid simultaneously transcribes *eYFP* and the *mCherry-pri-miRNA* fusion through the use of a bi-directional inducible promoter. The eYFP and mCherry fluorescence signals are measured for individual cells and the slope of eYFP vs mCherry indicates the cellular pri-miRNA processing efficiency. Co-transfection of the reporter with the expression plasmid for full-length DGCR8 (N-flag-DGCR8) increases pri-miRNA processing efficiency, with the fluorescent slope increased by ~2 fold in HeLa cells cultured in complete medium (Fig. 6-1E). This assay allows us to measure the activity of DGCR8 mutants in cells. Because endogenous DGCR8 is expressed at very low levels in HeLa cells, changes in fluorescence slope mostly reflect the activity of ectopically expressed N-flag-DGCR8 proteins. All inactive DGCR8 mutants characterized in our previous studies give fluorescence slopes similar to the vector control [11,16]. Here we found that expression of N-flag-DGCR8 G2 in HeLa cell cultured in complete medium resulted in a fluorescent slope close to that of the vector control and much lower than wild-type DGCR8 (Fig. 6-1E). Quantification of mature miR-9 produced from the reporter supported the conclusion that G2 is inactive in cells (Fig. 6-1F). Western blot analysis showed that G2's lack of activity was not due to reduced protein expression relative to the wild type (Fig. 6-1G). Altogether, our results suggest that the G2 mutations cause DGCR8 to lose Fe(III) heme binding and thereby the pri-miRNA processing activity.

G2 single mutants show reduced affinity for heme, but are active in pri-miRNA processing

To determine which residue is responsible for the heme-binding defect of G2, we engineered the individual mutations in the context of NC1 and tested their ability to bind heme when expressed in *E. coli*. As Lys446 and Arg447 are immediately next to each other, we also tested if these two residues function together by characterizing the double mutant K446A/R447A. Similar to G2, the purified NC1 K446A/R447A protein did not contain Fe(III) heme (Fig. S1), suggesting that simultaneous mutation of these residues to a large extent accounts for the heme-binding defect. Somewhat surprisingly, NC1 R441A, K446A, and R447A single mutants were all capable of binding Fe(III) heme (Fig. 6-2A-C). These results suggest that Lys446 and Arg447 serve a redundant function in heme binding. These basic residues may stabilize heme by directly contacting one or both propionate groups, as has been shown in other heme proteins such as myoglobin, human catalase I and hemopexin [20].

We then examined whether the single mutants have reduced heme affinity by measuring their rates of heme dissociation. We incubated the mutants with a five-fold excess of apomyoglobin, which has a high affinity for heme and serves as a heme scavenger. The Fe(III) heme dissociation from DGCR8 is indicated by a reduction in the 450-nm Söret peak with a concurrent appearance of a 409-nm peak indicative of Fe(III) heme transferring to myoglobin. Among the three NC1 mutants, R441A had the strongest association with Fe(III) heme, with the half-life of heme loss ($t_{1/2}$) >8 hr (k_{off} = 2.3 × 10^{-5} s^{-1}) (Fig. 6-2A). K446A lost its heme faster with $t_{1/2}$ ≈ 3.3 hr (k_{off} = 8.7 × 10^{-5} s^{-1}) (Fig. 6-2B). The dissociation of heme from NC1-R447A was very slow in the initial 4 hr, but subsequently sped up with most of the Fe(III) heme transferred by the 8th hr (Fig. 6-2C). The R447A data could not be fit using a single exponential

function, suggesting that the mutant loses heme through a multi-step process. Compared to the previously characterized heme-binding mutations, the three G2 single mutations more modestly reduce the affinity for Fe(III) heme.

We subsequently engineered the G2 double and single mutations in the context of N-flag-DGCR8 and measured their cellular activity. In HeLa cells cultured in the complete medium, K446A/R447A is inactive in pri-miRNA processing, whereas the three single mutants were as active as wild-type N-flag-DGCR8, as indicated by both fluorescence slopes and mature miR-9 production (Fig. 6-2D,E). Western blots showed that the mutant proteins express well in HeLa cells (Fig. 6-2F), ruling out the possibility that the lack of activity for K446A/R447A was caused by reduced expression. Furthermore, similar fluorescence slopes and miR-9 expression levels were obtained when the mutants were expressed at levels higher than or similar to the wild type (the latter data not shown). Therefore, the Fe(III) heme affinity of the G2 single mutants must be sufficient to acquire heme and to process pri-miRNAs under this experimental condition.

K446A and P351A provide an estimate of intracellular Fe(III) heme availability

Among the three G2 single mutants, K446A has the lowest affinity for Fe(III) heme. The k_{off} of NC1-K446A is only five fold slower than that of P351A, the inactive mutant with the highest affinity for Fe(III) heme. Assuming this dramatic change in activity is caused solely by differences in Fe(III) heme affinities, this pair of DGCR8 mutants allow the intracellular available Fe(III) heme concentration to be estimated with great precision.

To determine the affinity of K446A and P351A for Fe(III) heme, we attempted to measure their Fe(III) heme association rate k_{on} (as $K_d = k_{off} / k_{on}$). We previously reported that purified heme-free (apo) NC1-P351A dimer can bind Fe(III) heme to reconstitute a complex

with an absorption spectrum very similar to that of the native complex [17]. In these measurements, we monitored over time the growth of the Söret peak at 447 nm as an indicator of complex formation. This binding reaction went to completion quickly, so we employed the stop flow method. The data were best fit to a two-phase association curve, giving two pseudo-first-order rates k_1 and k_2 (Fig. S3A). To obtain the rate for this second-order reaction, we measured the association rates at four apoNC1-P351A concentrations, all in large excess of the Fe(III) heme concentration (Fig. S3B). The pseudo-first-order rates should have a linear relationship with the protein concentration and the slope gives k_{on}. However, both k_1 and k_2 remained roughly unchanged over the apoNC1-P351A concentration range. This is most likely because Fe(III) heme tends to stack in aqueous solutions, forming a variety of oligomers [21]. Unstacking of heme from oligomers may be the rate-limiting step of the binding reaction. Imidazole can unstack Fe(III) heme to produce monomers, but it appeared to interfere with the DGCR8-Fe(III)-heme interaction. It is currently not possible to measure the second-order k_{on} for DGCR8 and monomeric Fe(III) heme. Nevertheless, our measurements indicate that association between DGCR8 and Fe(III) heme is very fast.

Previous characterization of many heme proteins revealed that their k_{on}'s for heme are very similar and thus the K_d values are largely determined by the k_{off} [19,22-26]. The k_{on}'s for 35 globins, BSA, and bacterial heme uptake proteins IsdA and Rv0203 are all about 1×10^8 M^{-1} s^{-1}. Assuming DGCR8 binds Fe(III) heme with a similar k_{on}, we estimate that the K_d of P351A for Fe(III) heme is ~5 pM, whereas that for K446A is ~1 pM. Therefore, the Fe(III) heme concentration available to support pri-miRNA processing within HeLa cells may be between 1 and 5 pM.

Validation of the Fe(III) heme availability model

Our estimated range of intracellular Fe(III) heme availability rests on the assumption that the differing affinities of K446A and P351A for Fe(III) heme is responsible for the observed change in activity. However, it is possible that mutational effects unrelated to heme binding are involved. We therefore tested our model by monitoring the pri-miRNA processing activity of these DGCR8 mutants while altering heme availability in cells. Four different heme conditions were used, including (1) the complete medium (CM) with a final heme concentration of ~10 μM, (2) complete medium containing 1 mM heme biosynthesis inhibitor succinylacetone (CM+SA), (3) heme-depleted medium (HDM) in which the heme in serum is partially (~50%) removed so that the final heme concentration in the medium is reduced to ~5 μM, and (4) heme-depleted media containing 1 mM SA (HDM+SA). The pri-miRNA processing activity of wild-type N-flag-DGCR8 was not sensitive to a reduced amount of heme in the medium or inhibition of endogenous heme synthesis alone (Fig. 6-3A). However, a more severe heme deficiency, caused by combination of the two treatments, rendered the activity of N-flag-DGCR8 greatly reduced (Fig. 6-3A). Measurements of mature miR-9 produced were generally consistent with the fluorescence slopes, although the larger errors limited further insight (Fig. 6-3B). We were able to rescue the pri-miRNA processing defect under the HDM+SA condition by adding increasing concentrations of hemin to the media (Fig. 6-3C). A full rescue was achieved at 1 and 10 μM hemin. Even 0.2 μM hemin was able to slightly but significantly rescue the defect. The dose-dependent rescue excluded the possibility that the reduced N-flag-DGCR8 activity is an unintended effect of depleting heme from the serum or the heme biosynthesis inhibitor. Anti-DGCR8 immunoblotting ruled out another possibility that reduced N-flag-DGCR8 expression level is responsible for the pri-miRNA processing deficiency (Fig. 6-3D). Overall, these results

suggest that, under typical culture conditions, Fe(III) heme is not limiting pri-miRNA processing in HeLa cells. Similar effects, but to much less extents, have been observed in HeLa cells without ectopic expression of N-flag-DGCR8 [11]. Co-expression of N-flag-DGCR8 in HeLa cells provides a sensitive system for testing the effect of Fe(III) heme availability on the activity of DGCR8 mutants.

In our model, the K_d of K446A for Fe(III) heme is close to the concentration of available Fe(III) heme in HeLa cells cultured in complete media. Thus, the activity of this mutant should be more sensitive to heme depletion than the wild type. Indeed, in the cellular assays for N-flag-DGCR8 K446A, even the heme-depleted medium alone caused a large reduction of the fluorescence slope, from 2.21 ± 0.07 in CM to 1.67 ± 0.07 in HDM (Fig. 6-4A). Combination of HDM and SA treatments further deactivated K446A, with the fluorescence slope decreased to 1.15 ± 0.05, also lower than that (1.31 ± 0.06) of the wild type (Fig. 6-4A). These changes are likely to be direct effects of altering Fe(III) availability, as addition of hemin rescued the K446A activity in a dose-dependent manner.

In a parallel experiment, we tested the N-flag-DGCR8 P351A mutant. Not surprisingly, P351A remained largely inactive under all conditions tested (Fig. 6-4A). We tried to rescue the P351A defect by titrating in 0.2, 1, and 10 μM hemin. Indeed, when 10 μM hemin was added to the medium, the fluorescence slope for P351A increased modestly from 0.99 ± 0.04 (HDM+SA) to 1.23 ± 0.02 and this increase was statistically significant ($p < 0.001$). It is likely that the presence of 10 μM hemin in the medium raised the intracellular Fe(III) heme availability so that P351A was able to partially or transiently associate with heme.

In addition to reducing affinity for Fe(III) heme, the P351A mutation may inactivate DGCR8 in cells by other mechanisms, i.e. by affecting the Fe(III) heme-induced conformational

change. We found that purified apoNC1-P351A is activated for pri-miRNA processing by Fe(III) heme (Fig. S4) in a way very similar to wild-type apoNC1 [10], thereby ruling out this possibility. Overall, this series of validation experiments strongly supports our model that the intracellular Fe(III) heme availability in HeLa cells under typical culture conditions is between the K_d's of the K446A and P351A mutants for Fe(III) heme.

Implications to Fe(III) heme production and transport

The presence of an available Fe(III) heme pool that sharply determines miRNA maturation efficiency suggests that relevant processes are cross-regulated. Heme is synthesized in the Fe(II) form [27] and has to be oxidized to the Fe(III) state when activating miRNA maturation. The heme iron oxidization must occur during trafficking from mitochondria, the site of synthesis, to its destination, which could be the cytoplasm where DGCR8 is translated or the nucleus where pri-miRNA processing occurs. The interconversion between the Fe(II) and Fe(III) forms is presumably regulated by the redox environment of the cell, including metabolic rates, cell growth and oxygen availability. Redox regulation of available heme may also be linked to heme degradation, and import and export across cellular membranes [4,8].

The ultra-low effective concentration (1-5 pM) of available Fe(III) heme seems to present a paradox. Considering that the volume of a typical HeLa cell is ~2,000 μm^3, this concentration means that only a few Fe(III) heme molecules exist within each cell cultured in the complete medium, leaving little room for further reduction under heme deficient conditions. Additionally, it may be challenging for these few Fe(III) heme molecules to "find" the apo DGCR8 proteins whether they are in the nucleus or cytoplasm. While the value of 1-5 pM is only a rough estimate, the paradox may be resolved by an intriguing possibility that a currently unknown

Fe(III) heme-specific transporter (or chaperone) loads and activates DGCR8. In this scenario, the effective available Fe(III) heme concentration we observed may reflect an affinity requirement for a DGCR8 protein to receive Fe(III) heme from the transporter. The actual available Fe(III) concentration may be higher and heme deficient conditions result in fewer transporter molecules loaded with Fe(III) heme.

The function of the tightly controlled pool of available Fe(III) heme is not limited to miRNA maturation. A class of heme proteins that have been proposed to be heme sensors also used electron-rich cysteine side chain thiolate for axial ligation, and thus generally prefers Fe(III) heme over Fe(II) heme [28]. These sensors are involved in circadian rhythm, transcription regulation of metabolic pathways, heme catabolism, ion channel activities and protein degradation. The pool of available Fe(III) heme may be a common link that coordinates these pathways important for cell physiology.

FIGURES AND LEGENDS

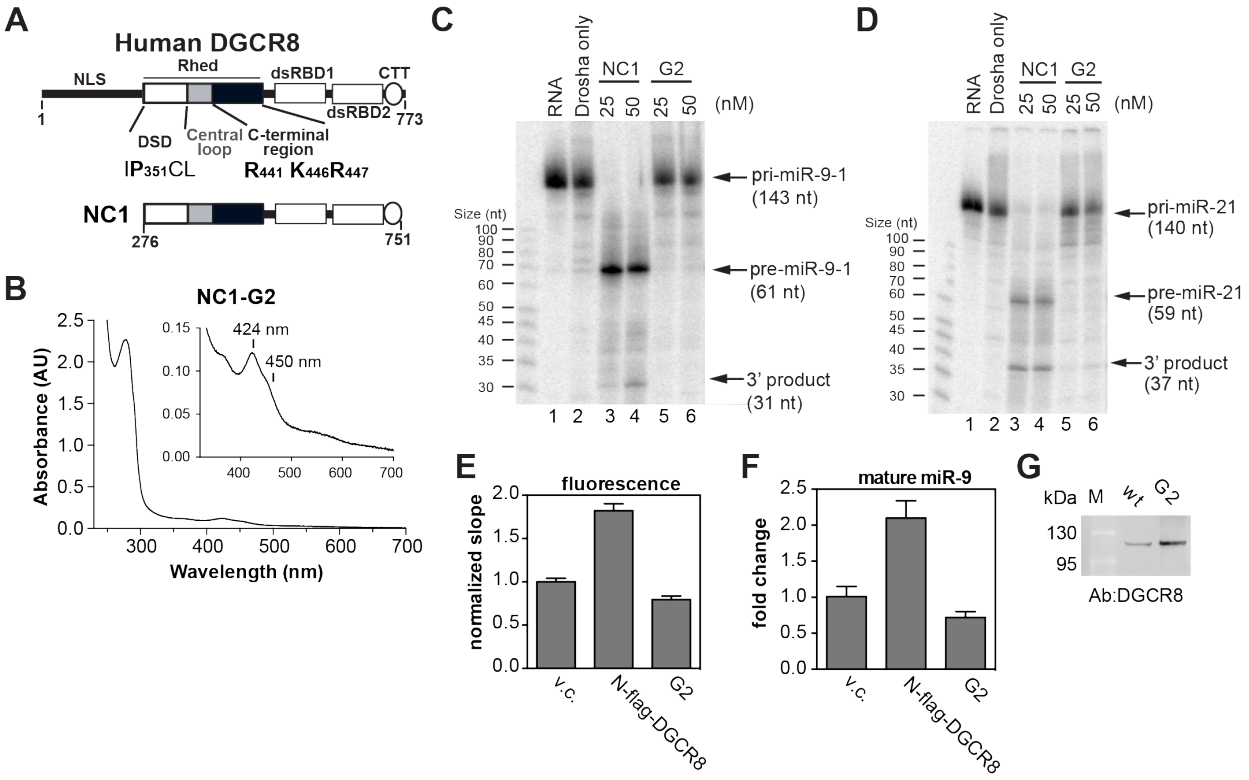

Figure 6-1. The DGCR8 G2 mutant fails to bind heme and is inactive in pri-miRNA processing. (A) Domain structure of human DGCR8, with relevant residues labeled. The NC1 construct is indicated underneath. (B) Electronic absorption spectrum of purified NC1 G2 with an inset showing a zoom-in. No intense 450 nm Söret peak was observed. (C,D) pri-miRNA processing assays reconstituted using purified Drosha and 25 nM NC1 dimers. (E) HeLa cells cultured in complete medium were transfected with pri-miR-9-1 reporter plus either pCMV-tag2a (vector control, v.c.) or N-flag-DGCR8 expression plasmids as indicated. Normalized fluorescence slopes are plotted. Error bars represent 95% confidence interval from the linear fit. (F) The abundance of mature miR-9 (mean ± SD, n = 3) from (E) measured using qRT-PCR. (G) An anti-DGCR8 immunoblot with equal amounts of nuclear extracts loaded.

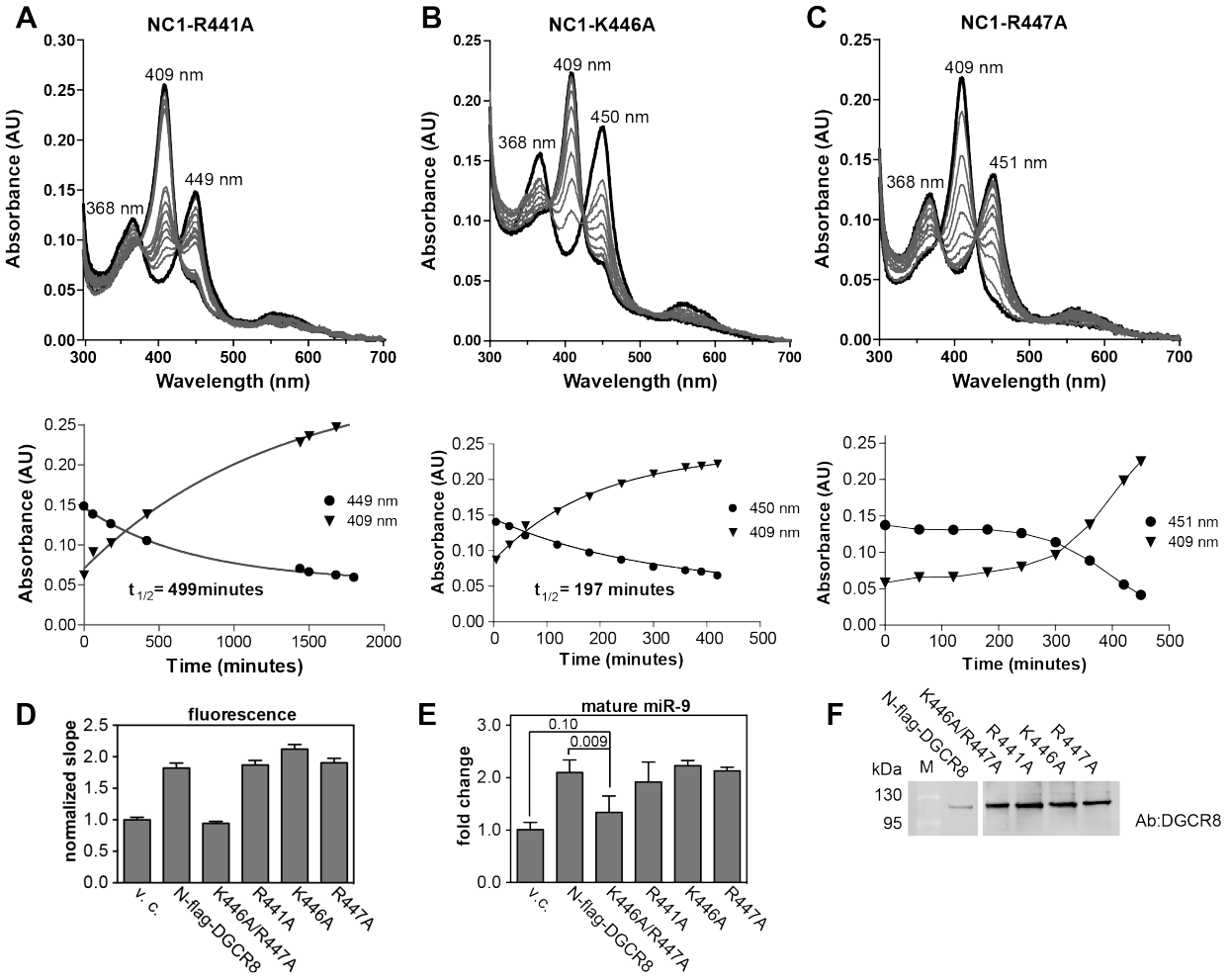

Figure 6-2. K446A and R447A modestly reduce affinity for Fe(III) heme but remain active in pri-miRNA processing. Fe(III) heme bound NC1 R441A (A) K446A (B) or R447A (C) was incubated with 6 fold excess of apomyoglobin. Top: electronic absorption spectra obtained at different time points. Bottom: A_{409} (aquametmyoglobin) and A_{450} (Fe(III) heme-bound NC1) time points were fit to a single exponential (A, B) or simply connected by lines (C). (D) Cellular pri-miR-9-1 processing assays in complete culture media. Error bars represent 95% CI from the linear fit. (E) Abundance of mature miR-9 (mean ± SD, n = 3). (F) An anti-NC1 immunoblot with equal amounts of nuclear extracts loaded.

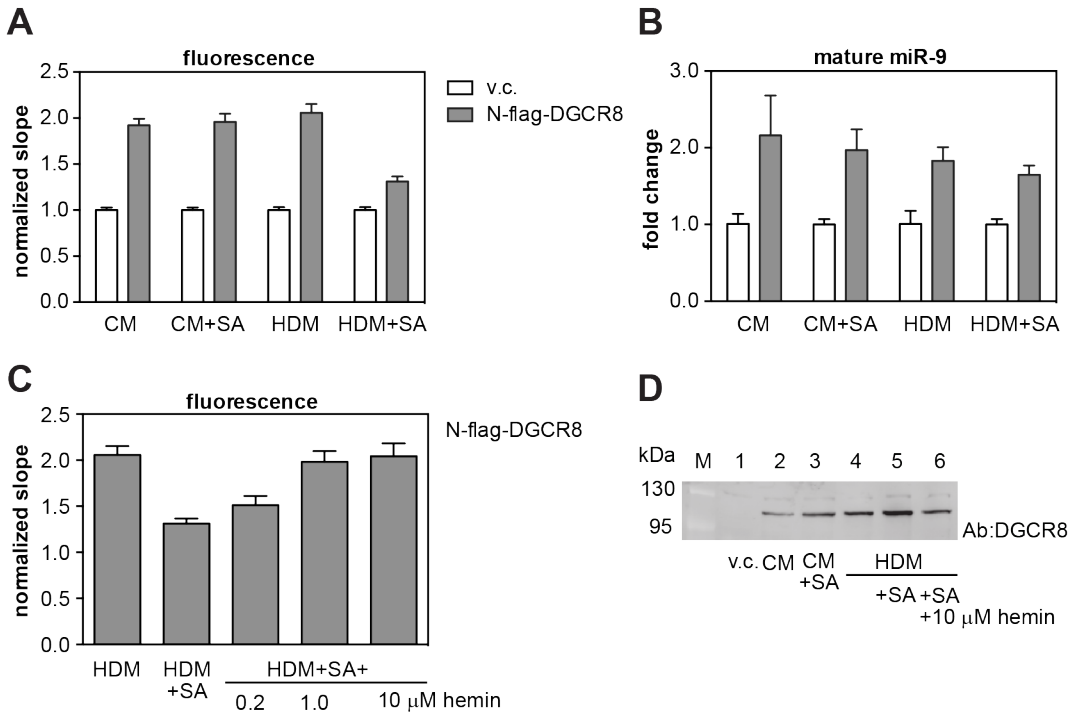

Figure 6-3. Only severe heme deficiency influences pri-miRNA processing efficiency of wild-type N-flag-DGCR8 in HeLa cells. Cellular pri-miR-9-1 processing assays were performed with the N-flag-DGCR8 expression plasmid cotransfected with the reporter. CM: complete media, CM+SA: complete media plus 1 mM succinylacetone, HDM: heme depleted media, HDM+SA: heme depleted media plus 1 mM succinylacetone. (A) Normalized fluorescence slopes. Error bars represent 95% CI from the linear fit. (B) Abundance of mature miR-9 (mean ± SD, n = 3). (C) Cellular pri-miR-9-1 processing assays in which HDM+SA treatment was rescued by adding 0.2, 1, or 10 μM hemin to the media. Error bars represent 95% CI from the linear fit. (D) Anti-DGCR8 immunoblots with equal amounts of nuclear extracts loaded.

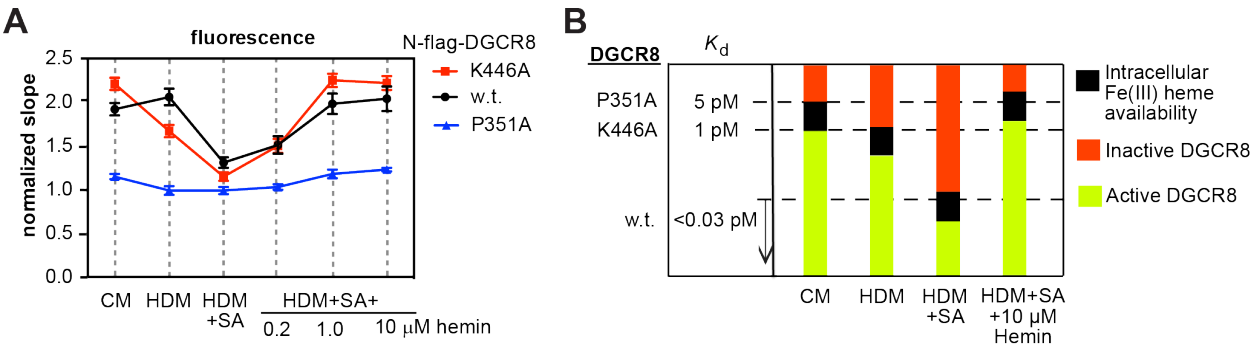

Figure 6-4. Validation under various heme conditions supports our model of estimating intracellular Fe(III) heme availability.

(A) Cellular pri-miR-9-1 processing assay for N-flag-DGCR8 wild-type, P351A and K446A under varying heme conditions as described in Fig. 6-3. (B) Schematic of how intracellular Fe(III) heme availability determines DGCR8 activity. The estimated K_d for wild-type, P351A and K446A N-flag-DGCR8 are plotted in an exponential scale. The black box represents the range of intracellular Fe(III) heme availability. The red and green bars represent the K_d ranges in which DGCR8 is inactive and active, respectively.

References

1. Ponka, P. Cell biology of heme. *Am J Med Sci* 318, 241-256 (1999).

2. Zhang, L. (ed.) *Heme Biology: The secret life of heme in regulating diverse biological processes*, (World Scientific, Singapore, 2011).

3. Tracz, M.J., Alam, J. & Nath, K.A. Physiology and pathophysiology of heme: implications for kidney disease. *J Am Soc Nephrol* 18, 414-20 (2007).

4. Khan, A.A. & Quigley, J.G. Control of intracellular heme levels: heme transporters and heme oxygenases. *Biochim Biophys Acta* 1813, 668-82 (2011).

5. Ryter, S.W. & Tyrrell, R.M. The heme synthesis and degradation pathways: role in oxidant sensitivity. Heme oxygenase has both pro- and antioxidant properties. *Free Radic Biol Med* 28, 289-309 (2000).

6. Ye, W. & Zhang, L. Heme deficiency causes apoptosis but does not increase ROS generation in HeLa cells. *Biochem Biophys Res Commun* 319, 1065-71 (2004).

7. Sassa, S. Why heme needs to be degraded to iron, biliverdin IXalpha, and carbon monoxide? *Antioxid Redox Signal* 6, 819-824 (2004).

8. Severance, S. & Hamza, I. Trafficking of heme and porphyrins in metazoa. *Chem Rev* 109, 4596-616 (2009).

9. Faller, M., Matsunaga, M., Yin, S., Loo, J.A. & Guo, F. Heme is involved in microRNA processing. *Nat Struct Mol Biol* 14, 23-9 (2007).

10. Barr, I. et al. Ferric, not ferrous, heme activates RNA-binding protein DGCR8 for primary microRNA processing. *Proc Natl Acad Sci USA* 109, 1919-1924 (2012).

11. Weitz, S.H., Gong, M., Barr, I., Weiss, S. & Guo, F. Processing of microRNA primary transcripts requires heme in mammalian cells. *Proc Natl Acad Sci U S A* 111, 1861-6 (2014).

12. Denli, A.M., Tops, B.B., Plasterk, R.H., Ketting, R.F. & Hannon, G.J. Processing of primary microRNAs by the Microprocessor complex. *Nature* 432, 231-235 (2004).

13. Gregory, R.I. et al. The Microprocessor complex mediates the genesis of microRNAs. *Nature* 432, 235-240 (2004).

14. Han, J. et al. The Drosha-DGCR8 complex in primary microRNA processing. *Genes Dev* 18, 3016-3027 (2004).

15. Landthaler, M., Yalcin, A. & Tuschl, T. The human DiGeorge syndrome critical region gene 8 and its *D. melanogaster* homolog are required for miRNA biogenesis. *Curr Biol* 14, 2162-2167 (2004).

16. Quick-Cleveland, J. et al. The DGCR8 RNA-binding heme domain recognizes primary microRNAs by clamping the Hairpin. *Cell Rep* 7, 1994-2005 (2014).

17. Barr, I. et al. DiGeorge Critical Region 8 (DGCR8) is a double-cysteine-ligated heme protein. *J Biol Chem* 286, 16716-16725 (2011).

18. Senturia, R. et al. Structure of the dimerization domain of DiGeorge Critical Region 8. *Protein Sci* 19, 1354-1365 (2010).

19. Hargrove, M.S., Barrick, D. & Olson, J.S. The association rate constant for heme binding to globin is independent of protein structure. *Biochemistry* 35, 11293-11299 (1996).

20. Smith, L.J., Kahraman, A. & Thornton, J.M. Heme proteins--diversity in structural characteristics, function, and folding. *Proteins* 78, 2349-68 (2010).

21. Brown, S.B., Hatzikonstantinou, H. & Herries, D.G. The dimerization of ferrihaems. I. The effect of buffer ions and specific cations on deuteroferrihaem dimerization. *Biochim Biophys Acta* 539, 338-51 (1978).

22. Bhakta, M.N. & Wilks, A. The mechanism of heme transfer from the cytoplasmic heme binding protein PhuS to the delta-regioselective heme oxygenase of Pseudomonas aeruginosa. *Biochemistry* 45, 11642-9 (2006).

23. Gaudin, C.F., Grigg, J.C., Arrieta, A.L. & Murphy, M.E. Unique heme-iron coordination by the hemoglobin receptor IsdB of Staphylococcus aureus. *Biochemistry* 50, 5443-52 (2011).

24. Liu, M. et al. Direct hemin transfer from IsdA to IsdC in the iron-regulated surface determinant (Isd) heme acquisition system of Staphylococcus aureus. *J Biol Chem* 283, 6668-76 (2008).

25. Nygaard, T.K. et al. The mechanism of direct heme transfer from the streptococcal cell surface protein Shp to HtsA of the HtsABC transporter. *J Biol Chem* 281, 20761-71 (2006).

26. Owens, C.P., Du, J., Dawson, J.H. & Goulding, C.W. Characterization of heme ligation properties of Rv0203, a secreted heme binding protein involved in Mycobacterium tuberculosis heme uptake. *Biochemistry* 51, 1518-31 (2012).

27. Dailey, H.A. Terminal steps of haem biosynthesis. *Biochem Soc Trans* 30, 590-5 (2002).

28. Shimizu, T. Binding of cysteine thiolate to the Fe(III) heme complex is critical for the function of heme sensor proteins. *J Inorg Biochem* (2011).

29. Barr, I. & Guo, F. Primary microRNA processing assay reconstituted using recombinant Drosha and DGCR8. *Methods Mol Biol* 1095, 73-86 (2014).

CHAPTER 7

A protocol for measuring pri-miRNA processing efficiency in live cells

ABSTRACT

MicroRNA (miRNA) are small regulatory RNA, 20-22 nt in length, that are produced by a series of truncations. The primary transcript of miRNA (pri-miRNA) forms a hairpin structure that is recognized by the Microprocessor, a complex of the RNA-binding protein DiGeorge Critical Region gene 8 (DGCR8) and the RNase-III enzyme Drosha. The Microprocessor cleaves pri-miRNA at the base of the hairpin to produce precursor miRNA (pre-miRNA). We have developed a fluorescence-based assay for determining pri-miRNA processing efficiency in live cells. Here we provide a detailed protocol for performing the pri-miRNA live-cell assay. The protocol includes cloning, cellular transfection and imaging, data analysis, and validation with qPCR. The assay produces a robust and reproducible signal with a simple fluorescence microscope. The protocol can be used to answer a multitude of questions about pri-miRNA processing and regulation.

INTRODUCTION

miRNA are non-coding RNAs that regulate gene expression via mRNA degradation and translation inhibition[1]. They have been found to function in a variety of biological activities such as development and are related to many diseases including cancer[2–5]. The initial transcripts of miRNA, pri-miRNA, have been a target of interest because of their diversity and regulation[6,7]. The standard method for studying pri-miRNA processing involves synthetic RNA's and immunoprecipitated Microprocessor. Though this method can reconstruct a pri-miRNA processing reaction *in vitro* it does not offer information about what is going on inside cells. Two cellular reporter assays for pri-miRNA processing have been previously described; one is based on a fluorescent protein while the other luciferases[8,9]. The fluorescence assay is composed

of a GFP-pri-miRNA fusion construct that is infected into various cell lines[8]. This assay suffers from the lack of a normalization factor to overcome variability in fluorescent protein expression due to processes unrelated to pri-miRNA processing. The second system utilizes a firefly luciferase-pri-miRNA fusion and normalizes the firefly luciferase signal to that of Renilla luciferase expressed from a co-transfected plasmid[9]. However, single cell resolution and the possibility for real time experiments are lost with the use of luciferase assays. We have developed a cellular pri-miRNA assay using a bi-directional fluorescence reporter that allows for detection of miRNA processing in live cells.

Advantages and disadvantages of the procedure

The advantage of our procedure is the robustness and reproducibility of the data. For each experimental condition at least one hundred different cells are imaged and analyzed. Therefore, much of the experimental noise associated with cellular experiments is filtered out. Additionally, a majority of the data follows a linear trend so outliers are easy to recognize.

One disadvantage of our protocol is the use a Tet-system cell line. Because of the Tet-controlled promoter, only a cell line that expresses the reverse tetracycline transcription factor can be used. Therefore, the current assay is not applicable to primary cell culture.

Application of the method

Our protocol has been applied to study the role of heme in pri-miRNA processing and dissecting how DGCR8 recognizes and binds pri-miRNA hairpins[10,11]. Because the assay is highly sensitive to DGCR8 overexpression, mutants that have altered cellular activity can be easily detected. We also can study changes in processing resulting from changes in the cellular environment. For example, by growing cells in heme-depleted media and blocking endogenous heme synthesis, we were able to detect a decrease in pri-miRNA processing. Additionally, this

assay can be used to study how regulatory proteins influence the pri-miRNA processing machinery. For example, using our assay Grace Xiao's lab was able to show that ADAR can either increase or decrease the processing of different pri-miRNA (manuscript under review).

Experimental design

The reporter construct is based on a plasmid containing a bi-directional tetracycline-inducible promoter that simultaneously drives the expression of two fluorescent proteins mCherry and eYFP[12]. Mukherji, Sharp and colleagues generated this plasmid for examining interactions between mature miRNAs and 3′-untranslated regions (UTR). In our reporter, pri-miRNA sequences were inserted into the 3′-UTR of the mCherry expression cassette whereas the eYFP 3′-UTR was left unaltered. Thus, this construct expresses a mCherry/pri-miRNA fusion RNA. Processing of the pri-miRNA moiety of the fusion RNA results in removal of the polyadenylation (poly-A) tail along with a portion of the 3′-UTR, which leads to degradation of the mCherry mRNA and hence a loss of mCherry protein expression and fluorescent signal. This loss of mCherry signal is determined with respect to the eYFP fluorescence whose signal allows for normalization of individual cells' transcriptional activity.

When the mCherry and eYFP intensities of individual cells were plotted, the data appeared to be linear over a wide range of fluorescent intensities. The slope obtained from linear regression should negatively correlate with the efficiency of pri-miRNA processing. We have validated the assay by overexpression and knockdown of DGCR8. As expected, overexpression of DGCR8 continually resulted in a 50% decrease in slope whereas knock down resulted in a 2-fold increase in slope. An inactive DGCR8 mutant that is deleted in the C-terminal tail region (**Δ**CTT) was used as a negative control. We detected no change in processing after the overexpression of **Δ**CTT. These results indicated that our assay was able to detect modifications in expression of

both endogenous and ectopic DGCR8. Changes in eYFP and mCherry mRNA levels have been confirmed with RT-qPCR. We also used RT-qPCR to monitor the fluctuations in mature miRNA levels. Overexpression of our reporter construct resulted in an increase in the mature miRNA verifying that our synthetic construct is properly processed.

PROCEDURE

Step 1: Cloning pri-miRNA reporter

1. Design primers to amplify your pri-miRNA of choice from human genomic DNA. Find the miRNA sequences in the miRNA database miRBase. Use blast to find the miRNA sequence in the human genome. Choose how long to make your primary pri-miRNA, our standard is 140-150 nt total. Include the restriction sites ClaI and SalI in your primer design to clone the pri-miRNA into the 3'UTR of mCherry. Use standard cloning procedures to ligate PCR amplified primary miRNA sequence into ptre-bi red/yellow vector. The insert band might be hard to see on the gel because of its size, so you can run a 2% gel. Measure concentration of all minipreps before sending for sequencing. Ptre-bi can have trouble being amplified by E. coli (see troubleshooting tip)

Step 2-3: Transfection

2. Grow HeLa tet-on cells in glass bottom plates to 80-90% confluency. The confluency of the cells is very important, it is better to be too confluent then not enough. It is best to use tetracycline-system approved FBS.
3. Transfect cells with Effectene (Qiagen) according to manufacture's protocol. When testing a new reporter include:
    1. Reporter + pCMV (empty vector)

2. Reporter + wt DGCR8
3. Reporter + ΔCTT (DGCR8 mutant)

Keep the total amount of DNA the same for all transfections. Add 1 μg/mL doxycycline. Our standard stock concentration is 1 mg/mL. I typically image the cells 14-18 hrs. post induction so it is best to add doxycycline in the evening and then image the next morning

Step 4: Imaging

4. Before imaging wash cells 2-3 times with 1X PBS and add warmed clear media. Turn on Nikon microscope, lamp, and camera. Check for the proper color of light seen coming out of the objective for the YFP and TxRed channel. YFP: turquoise bluish color. TxRed: bright lime green. If the wrong color or no color is seen, check for the correct filters. Find cells using white light then switch to the lamp and filter cubes. Take pictures of the cells starting with the YFP channel followed by the TxRed channel using the Andor software. I typically take 10 pictures per plate. Look for areas that contain many cells but are spread out and not in clumps. Make sure you move the objective around so you image different areas of the plate. When done imaging use the batch conversion function to convert all images to tiff. There will be two options when you export. Choose 16 bit and 0 – 5600.

Step 5-6: Data analysis and Graphing

5. Open MATLAB and the program called "cell segmentation raw coor" (the code is in the appendix). Change your MATLAB directory to the location of your cell images. Run the cell segmentation program. The program will bring up the eYFP and mCherry images and convert them to binary images. Compare the original images with binary

images. You want to find as many cells as possible but keep cells that are close together separate.

The program will ask you if you like the threshold settings used to make the binary images. If you like the binary images enter "0". If you want to change them enter "1". To find more cells decrease the threshold, to find less increase the threshold. Choose any number between 0.0019 – 0.0035. Once you find a good binary image and enter "0" the program will generate many numbers. These are the two sets of numbers that are important: tot_intensity: total intensity of pixels for each cell found (mCherry, eYFP) and center cell: coordinates for the center of each cell (y,x)

Copy the average intensity and center cell numbers to an excel spreadsheet. Examine original cell image and remove any data generated from a dead cell or a clump of cells. Make a scatter plot of eYFP vs mCherry and fit with a linear regression that passes through the origin. For the final data plot, calculate the distance from the origin for each point. Remove the furthest 10% of the data.

6. The final graphing and organization is done in GraphPad Prism. Copy the data from excel into Prism and fit with a non-linear regression → line through the origin. Use 95% confidence interval to calculate error. To calculate statistical significance copy the two data sets that you wish to compare into one spreadsheet. Make sure the y values are in two different columns. Perform two non-linear regressions. Under compare → do the

best-fit values of selected parameters differ between different data sets? → choose slope. The results will give you a p-value.

Step 7-14: Mature miRNA analysis

7. Grow cells in 12 well dishes to 80-90% confluency. Grow enough cells so that you can perform 4 biological repeats for each condition. Transfect cells with the miRNA reporter and/or desired plasmid using Effectene. Follow the Effectene protocol. Add 1 μg/mL doxycycline after transfection if using miRNA reporter.
8. ~20-24 hours post transfection extract RNA using miRNeasy kit (Qiagen). Follow miRNeasy protocol. Add qiazol reagent to cells and pipet up and down about 5 times or until the solution appears homogeneous. I do not perform a DNase digestion. Wash the column one time with Buffer RWT and two times with Buffer RPE. Spin at full speed in empty tube to dry column. Elute with 30 μL water. Wait 1 min. after adding water before spinning down. The RNA can be stored at -80°C until you are ready to continue the protocol.
9. To determine the concentration of the RNA run 2μL of RNA on a 1% agarose gel for 30 min. at 80 V. Take one sample that you loaded somewhere near the center of the gel and measure the absorbance at 260 nm. Quantify the gel using Quantity One or your program of choice. Use the absorbance reading and the gel quantification to determine all RNA concentrations. Typical RNA concentration for Hela cells grown in 12 well dishes is 200-400 ng/μL.
10. For mature miR-9 analysis I use the miR-9 miRNA expression assay from ABI. I also use the ABI RT-PCR kit. Follow the manufacturer's instructions.

11. Originally I used β-actin to normalize miR-9 expression but more recently have switched to using eYFP. Whichever you decide the random primer RT-PCR stays the same. The random primer is ordered from Invitrogen. I recommend using SSII since that was what the protocol was optimized for but SSIII also works. Follow the manufacture's instructions.

12. I use Taqman Gene Expression kit and the Taqman Universal MM for qPCR. This protocol is very similar to the miR9 qPCR except that 4 technical repeats are performed instead of 3. Follow the manufacture's instructions.

13. The program used for data analysis is MXPro. The first thing to check when analyzing new data is that all of the qPCR curves for the same primer platue to the same level. If this is not the case then some sort of inhibition is happening and the experiment should be repeated. The software automatically calculates the threshold and this is the threshold I usually use. If you have too many samples to analyze in one round of qPCR make sure to pick a threshold value and use it for all samples. Export all C_t values to an excel spread sheet. Calculate the average C_t from the technical repeats for each sample. For each sample calculate miR9 C_t – eYFP C_t (or whatever you are using for normalization). To calculate $\Delta\Delta C_t$ I typically normalize the data to reporter + empty vector control:

    i. Calculate the average ΔCt for empty vector control

    ii. $\Delta\Delta Ct = \Delta Ct$ (control) – ΔCt (sample)

    iii. I also calculate this for the individual empty vector control samples

    iv. Calculate $2^{\Delta\Delta Ct}$ for each sample (this is considered the "fold change")

    v. Calculate average of the $2^{\Delta\Delta Ct}$ for each sample and the standard deviation

14. You can then determine if the difference between two samples is statistically significant by calculating the p-value using a Student's *t*-test. In excel: =ttest(values of interest 1, values of interest 2, 2, 2). The first 2 designates the tails, two-tailed distribution means that your second set of numbers can be higher or lower than the first set, you don't have any expectations. The second 2 designates a two-sample equal variance test, this means that the two samples are independent (as apposed to a paired *t*-test) also that each sample set is equally distributed and both samples have the same standard deviation.

Troubleshooting

1. Low concentration of ptre-bi plasmid when purified from E. coli: The ptre-bi plasmid has the tendency to have a low replication level in E. coli. Once I have the correct construct that I want to use for transfection, I perform a maxiprep. For the final step I perform an isopropanol precipitation. Then I resuspend the pellet in 200 μL of water. This should give a high enough concentrated plasmid to be used in transfection.
2. Low transfection efficiency: Most often problems with transfection are related to cell density. Make sure cells are between 80-90% confluent when transfecting.
3. Most often the results from the assay are straightforward, there is either a decrease or an increase in processing. Sometimes though only small changes are observed. Because the data sets are large and linear fits generally very good, the error, even the 95% confidence interval, tends to be small. Therefore, even small changes in slope can be calculated as significant. If the changes in slope are less than 10% it is important to repeat the experiment to make sure the change is real.

References

1. Ambros, V. The functions of animal microRNAs. *Nature* **431,** 350–5 (2004).

2. Yi, R. *et al.* DGCR8-dependent microRNA biogenesis is essential for skin development. *Proc. Natl. Acad. Sci. U. S. A.* **106,** 498–502 (2009).

3. Santa, F. De, Iosue, I., De Santa, F., Del Rio, A. & Fazi, F. microRNA biogenesis pathway as a therapeutic target for human disease and cancer. *Curr. Pharm. Des.* **19,** 745–64 (2013).

4. Croce, C. M. Causes and consequences of microRNA dysregulation in cancer. *Nat. Rev. Genet.* **10,** 704–14 (2009).

5. Pegoraro, M. & Tauber, E. The role of microRNAs (miRNA) in circadian rhythmicity. *J. Genet.* **87,** 505–511 (2008).

6. Winter, J., Jung, S., Keller, S., Gregory, R. I. & Diederichs, S. Many roads to maturity: microRNA biogenesis pathways and their regulation. *Nat. Cell Biol.* **11,** 228–34 (2009).

7. Blahna, M. T. & Hata, A. Regulation of miRNA biogenesis as an integrated component of growth factor signaling. *Curr. Opin. Cell Biol.* **25,** 233–40 (2013).

8. Tsutsui, M. *et al.* Establishment of cells to monitor Microprocessor through fusion genes of microRNA and GFP. *Biochem. Biophys. Res. Commun.* **372,** 856–61 (2008).

9. Allegra, D. & Mertens, D. In-vivo quantification of primary microRNA processing by Drosha with a luciferase based system. *Biochem. Biophys. Res. Commun.* **406,** 501–5 (2011).

10. Weitz, S. H., Gong, M., Barr, I., Weiss, S. & Guo, F. Processing of microRNA primary transcripts requires heme in mammalian cells. *Proc. Natl. Acad. Sci. U. S. A.* **111,** 1861–6 (2014).

11. Quick-Cleveland, J. *et al.* The DGCR8 RNA-binding heme domain recognizes primary microRNAs by clamping the hairpin. *Cell Rep.* **7,** 1994–2005 (2014).

12. Mukherji, S. *et al.* MicroRNAs can generate thresholds in target gene expression. *Nat. Genet.* **43,** 854–9 (2011).

CHAPTER 8

Single molecule detection of pri-miRNA processing in live-cells

This chapter describes the progress I made in developing a single molecule assay for studying pri-miRNA processing in live cells. The approach is based on the MS2 system, which has been used to label mRNA in cells. I would like to acknowledge Rob Singer for the pSL-MS2-24 plasmid containing 24 repeats of the MS2 binding site and the pCR4-24XPP7SL plasmid containing 24 repeats of the PP7 binding site. I would like to acknowledge Melissa Jurica who sent me a plasmid containing the PP7 coat protein sequence. Finally, I acknowledge Yaron Shav-Tal for providing me with three fluorescent MS2 construct: MS-eYFP, MS2-GFP, and MS2-mCherry and providing me with guidance during my two-month internship in his lab. I experienced many technical difficulties with this project that I will describe briefly in this chapter. The project is currently unfinished but may be picked up by a future student.

INTRODUCTION

MS2 is a bacteriophage coat protein that binds to phage RNA and forms the phage capsid[1]. It recognizes a specific RNA hairpin sequence with a K_D of ~1 nM. Rob Singer's group was the first to use MS2 to label single mRNA molecules inside cells[2]. They conjugated 24 repeats of the MS2 RNA binding site to their mRNA of interest. The 24 repeats are necessary to have a signal that is strong enough above the background. Overexpression of fluorescently labeled MS2 protein enabled them to track single mRNAs in real time. This method has been very useful in studying mRNA localization and dynamics[3–6]. Another protein that is similar in structure and function is PP7[7]. This protein also binds to a specific stem loop with high affinity. Studies have shown that PP7 binds with very low affinity to the MS2 loop and vice versa[8]. Since there is very little cross binding observed for these two proteins, I used both proteins to label a pri-miRNA with two different colors.

To create a single molecule reporter, I fused one side of a pri-miRNA with 24 repeats of the MS2 binding site and the other side with 24 repeats of the PP7 binding site. The plan was to express the MS2 protein fused to mCherry and the PP7 protein fused to GFP. Induction of the pri-miRNA reporter construct will be detected by the co-localization of the fluorescent signals from the two fusion proteins (Fig. 8-1). The fluorescent proteins are not expected to be fluorescence energy transfer (FRET) pairs. During the first pri-miRNA cleavage event the overhangs containing the MS2 and PP7 multiple repeats will be cleaved off and the co-localization no longer detected. We can then monitor the cellular fluorescence in real time and track single processing events.

RESULTS

Cloning of the MS2/PP7 pri-miRNA construct

The first step of this project was to clone the pri-miRNA MS2/PP7 reporter. I received a construct containing 24 repeats of the MS2 binding site from Rob Singer's lab. The original plan was to PCR out the 24 repeats and then clone them into the pTre2 vector. The full 24 repeat sequence should be around 1500 kb. However, when I tried to perform PCR I kept getting a smear and several non-specific bands. I tried for several months to optimize the PCR but was never able to get a specific band of the right size. The 24 repeats of the MS2 binding site were adjacent to a BamHI and a BglII site. Though not within the multiple cloning site, the pTre plasmid did have a BamHI site upstream from where I had cloned in the pri-miRNA. I cut and pasted the 24 repeats of the MS2 binding site into the BamHI site in the pTre2 vector already containing either pri-miR-9 or pri-miR-30a. Sequencing results and test digests of these two constructs confirmed the presence of the MS2 binding site.

To clone the 24 repeats of the PP7, I obtained a plasmid containing the sequence for two repeats of the binding site from Melissa Jurica. I first tried PCR amplifying the two sites with primers containing restriction sites with compatible ends. I purified the PCR product, setup a large-scale ligation, ran the result on a gel, and tried to purify a band that was the approximate size of 24 repeats. However, there was never a high enough yield of the high molecular weight bands.

Another approach that I tried was using synthesized oligos that contained two copies of the binding site plus 12 bp of compatible overhang. I annealed the oligos, ligated them together and then fill in the gaps with T4 polymerase. Our rational was that the larger overhang would promote more frequent ligation. However, this approach still didn't produce a high yield of the

correct molecular weight product. I tried to PCR amplify the product to increase the yield but had no success.

After struggling for a long time to make multiple repeats of the PP7 binding site, Rob Singer published a paper using PP7 to image RNA in cells[9]. In this paper, they used a construct containing 24 repeats of the PP7 binding site so I requested the plasmid. Since I knew that I couldn't PCR amplify the repeats, I cut the repeats out using BamHI and BglII. I then blunted the repeat insert and cloned it into an EcoRV site. Somehow this worked and I now have a pTre2 plasmid containing pri-miR-9 flanked by 24 repeats of MS2 and 24 repeats of PP7.

To verify that the construct was capable of being processed and producing mature miRNA, I transfected HeLa tet-on cells with the miR-9 MS2/PP7 reporter. HeLa cells do not express miR-9 endogenously so any miR-9 signal that I detected must have come from the reporter. RNA from the transfected cells was extracted and mature miR-9 qPCR performed. I also extracted RNA from non-transfected cells for comparison. Mature miR-9 signal was observed for the cells expressing the reporter whereas no signal was seen for the non-transfected cells. This result showed that my MS2/PP7 reporter was able to be processed and produce mature miRNA.

Cloning and initial testing of MS2 and PP7 fluorescent fusions

I received three MS2 fluorescent protein fusion constructs from Yaron Shav-Tal's lab: MS2-mCherry, MS2-YFP, and MS2-GFP. These proteins contain a nuclear localization signal, followed by MS2 and finally the fluorescent protein. I was never given vector maps for these constructs and am unsure which vector they are in but they are optimized for lower expression to minimize the background. I received a plasmid containing the PP7 protein coding sequence from Melissa Jurica. I subcloned PP7 into the pCMV-tag2A vector for mammalian expression.

I then cloned in several different fluorescent proteins including Crimson, eGFP, and mCherry. My constructs are all in following order: fluorescent protein, PP7, nuclear localization signal.

I transfected all of the fluorescent fusion proteins to check their transfections efficiency, nuclear localization and fluorescent signal. Many of the constructs had either very low signal or seemed to aggregate within the cell. After screening all of the constructs the best results were seen with MS2-mCherry, MS2-YFP, Crimson-PP7 and eGFP-PP7.

Initial attempts at capturing images of single pri-miRNA

I first tried co-transfecting the pri-miRNA PP7/MS2 reporter plasmid with the four fluorescent fusion proteins that had the best signal after the first screen. Since the reporter plasmid is tetracycline inducible, I added 1 μg/mL of doxycycline at the time of transfection. I imaged the cells ~18 hours post-transfection and induction. Out of the three fluorescent proteins that I tested, I occasionally observed small spots in the cells for three of them: MS2-YFP, Crimson-PP7 and eGFP-PP7. Figure 8-2 is an example of cells transfected with MS2-eYFP and Crimson-PP7 and the spots I occasionally observed. Even though some of the images of Crimson-PP7 looked promising, I was unable to reproducibly obtain good transfection efficiency and see spots within the cells. The only fluorescent protein that gave me consistent fluorescent spots was eGFP-PP7 and MS2-YFP. I took some time lapsed images of eGFP-PP7 but observed little movement before the spots photobleached. Unfortunately, the spectrum for YFP and eGFP are two close and the two cannot be imaged together.

Potential Next Steps

The biggest hurdle that needs to be overcome for this project to continue is finding two fluorescent protein fusions that are spectrally separate and bind the reporter plasmid. I did try replacing the eGFP in the eGFP-PP7 construct with mCherry. The mCherry-PP7 construct expressed will in HeLa cells but I was not able to observe spots in cell, which most likely indicates no reporter binding.

There are several steps that could be done to optimize this assay and possibly get it working. I spent some time working in Yaron Shav-Tal's lab trying to optimize the assay. From their experience, the multiple repeat plasmid can be unstable in mammalian cells. They recommended making stable cell lines with the MS2/PP7 reporter. I tried doing this but was never able to get a positive clone. It might be worthwhile putting the reporter into a lentiviral plasmid and using viruses to make stable cell lines. Viral stable cell line generation is much more efficient.

Another test that I wanted to perform but never got a chance to do, was to perform RNA-FISH on cells expressing the MS2/PP7 reporter. Both Yaron Shav-Tal and Rob Singer have RNA-FISH probes for the MS2 binding site and most likely the PP7 binding site that can be ordered. Performing FISH on the MS2/PP7 reporter would confirm that enough of the binding site repeats are being expressed in the cells to detect a signal. Additionally co-staining could be performed to see if the reporter associates with any specific region of the cell.

Overall, I think the project has potential but a lot of work still needs to be done. The imaging itself needs to be optimized in order to see spots for PP7 and MS2 simultaneously. We also need to verify that the individual spots observed are in fact individual molecules of RNA. Once the imaging is working, we need to optimize the imaging conditions in order to perform time-lapse imaging experiments on the cells while minimizing cell death and photobleaching. Additionally, I have not worked out a way to analyze the data once movies are acquired. Xavier Michelet has

software to perform single particle tracking analysis on time-lapsed images. A problem with this type of analysis is that is does not take into account movement in the z-direction. It might be better to move the data collection to a microscope that is capable of taking z-stacks while doing time-lapsed imaging. Yaron Shav-Tal's lab has sophisticated imaging analysis software that they use for tracking RNA molecules. Another option would be to purchase/borrow the software from Shav-Tal's lab or try to collaborate with them for data analysis.

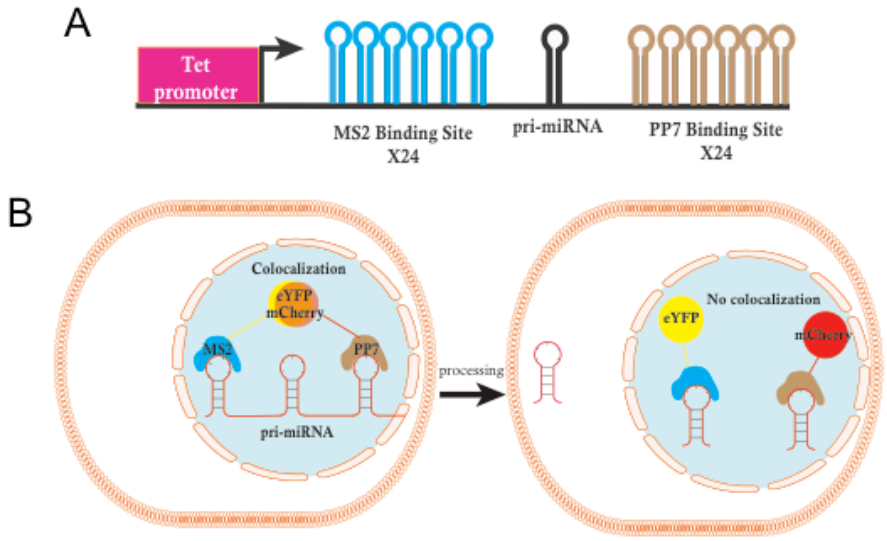

Figure 8-1. Schematic for the single molecule pri-miRNA processing assay. A. Schematic of single molecule reporter B. Diagram of cells expressing single molecule fluorescent assay

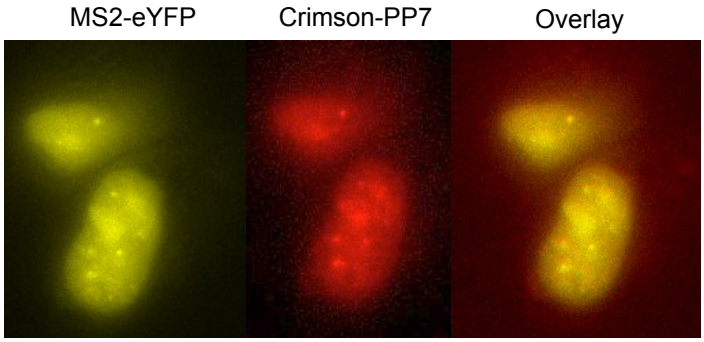

Figure 8-2. Example of MS2-eYFP and Crimson-PP7 transfected with single molecule reporter. HeLa tet-on cells were transfected with the pri-miR-9-1 single molecule reporter and either MS2-eYFP or Crimson-PP7.

References

1. Peabody, D. S. The RNA binding site of bacteriophage MS2 coat protein. *EMBO J.* **12,** 595–600 (1993).

2. Bertrand, E. *et al.* Localization of ASH1 mRNA particles in living yeast. *Mol. Cell* **2,** 437–45 (1998).

3. Shav-Tal, Y. *et al.* Dynamics of single mRNPs in nuclei of living cells. *Science* **304,** 1797–800 (2004).

4. Mor, A. *et al.* Dynamics of single mRNP nucleocytoplasmic transport and export through the nuclear pore in living cells. *Nat. Cell Biol.* **12,** 543–552 (2010).

5. Fusco, D., Bertrand, E. & Singer, R. H. Imaging of Single mRNAs in the Cytoplasm of Living Cells Rationale for Live Cell Imaging of mRNA. *Cell* (2003).

6. Zenklusen, D., Larson, D. R. & Singer, R. H. Single-RNA counting reveals alternative modes of gene expression in yeast. *Nat. Struct. Mol. Biol.* **15,** 1263–71 (2008).

7. Chao, J. A., Patskovsky, Y., Almo, S. C. & Singer, R. H. Structural basis for the coevolution of a viral RNA-protein complex. *Nat. Struct. Mol. Biol.* **15,** 103–5 (2008).

8. Gesnel, M.-C., Del Gatto-Konczak, F. & Breathnach, R. Combined use of MS2 and PP7 coat fusions shows that TIA-1 dominates hnRNP A1 for K-SAM exon splicing control. *J. Biomed. Biotechnol.* **2009,** 104853 (2009).

9. Larson, D. R., Zenklusen, D., Wu, B., Chao, J. A. & Singer, R. H. Real-time observation of transcription initiation and elongation on an endogenous yeast gene. *Science* **332,** 475–8 (2011).

APPENDIX A

Appendices

A.1 Protocol of nuclear extraction and western blot

Buffer A:

	Final Concentration	Stock Concentration	Volume Added
Hepes KOH pH = 7.9	10 mM	1 M	100 uL
MgCl2	1.5 mM	1 M	15 uL
KCl	10 mM	1 M	100 uL
DTT	0.5 mM	1 M	5 uL
PMSF	0.2 mM	100 mM	20 uL
H2O			9.76 mL

Buffer C (high salt):

	Final Concentration	Stock Concentration	Volume Added
Hepes KOH pH = 7.9	20 mM	1 M	200 uL
glycerol	25%	100%	2.5 mL
NaCl	500 mM	4 M	1.25 mL
MgCl2	1.5 mM	1 M	15 uL
DTT	0.5 mM	1 M	5 uL
PMSF	0.2 mM	100 mM	20 uL
H2O			6.21 mL

20X PBS:

1. 800 mL of ddH_2O
2. 80 g of NaCl
3. 2 g of KCl
4. 26.8 g of Na_2HPO_4 - 7 H_20
5. 2.4 g of KH_2PO_4
6. Adjust pH to 7.4 with 1M HCl
7. Adjust volume to 1 L with ddH_2O

1X PBST:

1X PBS + 0.02% Tween-20

1. Transfection
    a. Grow cells in a 6-well dish to 80-90% confluency
    b. Transfect cells with DGCR8 wt and mutants of interest
        i. For western blot I don't transfect the reporter
        ii. I always start transfecting equal amounts of DGCR8 wt and mutants. After finishing the blot if the mutant expression is less than the wild-type, repeat the whole procedure doubling the amount of mutant plasmid used in the transfection
    c. 18-24hrs. post-transfection the cells are ready for nuclear extraction
2. Nuclear Extraction
    a. Keep all buffers and cells on ice during the procedure
    b. Wash cells 2X with 1 mL/well of cold PBS
    c. Add 200 µL of cold PBS to the cells and scrape into 1.7 mL tube
    d. Spin down cells at 1000xg for 2 min at 4°C
    e. Aspirate out PBS
    f. Resuspend cells in 80 µL cold Buffer A
        i. Do not pipet up and down. Flick the tube to resuspend
    g. Incubate on ice for 10 min.
    h. Add 5 µL of NP-40, mix, and incubate on ice for 1 min.
    i. Spin down at 16,000xg for 10 sec.
    j. Pipet out supernatant into new tube (cytoplasmic fraction)
    k. Resuspend pellet in 50 µL Buffer C
        i. Flick to resuspend
    l. Incubate on ice for 20 min.
    m. Spin at 16,000xg for 2 min. at 4°C
    n. Pipet supernatant into new tube (nuclear fraction)
    o. The pellet is the nuclear envelope
        i. I usually throw this away but if interested you can also run this on the western

p. Add 2x SDS loading dye with fresh DTT to all samples
q. Store samples at -80°C until ready to do western

3. Western Blot (takes 3 days to complete)
    a. Protein gel for sample loading normalization
        i. Load a 12% SDS gel with 10 µL of each protein sample
            1. I usually use a homemade gel for this
        ii. Run at 180V for 1 hour
        iii. Stain with coomasie for 10 min.
        iv. Destain overnight
    b. Quantify protein gel
        i. Calculate how much sample to load based on what type of gel you will run
            1. 10 well commercial gel → 15 µL of lowest concentrated sample
            2. 15 well commercial gel → 10 µL of lowest concentrated sample
    c. Gel for western
        i. Load a commercial 12% SDS gel based on the above calculation
        ii. Also load 8 µL of pre-stained protein ladder
        iii. Run gel 150V for 1 hour
    d. Sandwich
        i. While the gel is running make 1X transfer buffer
            1. 700 mL H2O, 100 mL 10X Transfer buffer, 200 mL Methanol
                a. Make sure to add the water first
            2. Put in 4°C to cool while gel is running
        ii. Cut filter paper (2 pieces) and nitrocellulose membrane to the approximate size of the gel
            1. Always use tweezers when handling the membrane directly
        iii. Soak sponges, filter paper, and nitrocellulose in 1X transfer buffer for ~1 min before assembling sandwich
            1. This can be done in the glass tray
        iv. Assemble the sandwich in the glass tray with 1X transfer buffer
            1. clear side of the clamp, sponge, filter paper, membrane, gel, filter paper, sponge, black side of clamp

2. Center the sandwich so that the sponges or filter paper do not hang out the side
3. Place sandwich in western running box
    a. Align black side of sandwich with the black side of the box

v. Run transfer at 250 mAmps for 3 hours

e. Blocking
    i. Disassemble blot
        1. The pre-stained ladder should be clearly seen on the membrane
        2. Place the membrane with the protein side up in a clean small box
    ii. Add 5% milk in PBST to the membrane
    iii. Shake gently at RT for 1 hour
f. Primary antibody
    i. If you are using a new aliquot of anti-NC1 serum antibody make sure to freeze thaw a few times before use
        1. This is a weird superstition that I learned from Feng/Ming but it seems to work
    ii. Add anti-NC1 1:7,000 to the milk
    iii. If using a different primary follow manufacture's instructions
    iv. Shake gently at 4°C overnight
g. Secondary antibody
    i. Wash blot 3X for 10 min. with 20 mL PBST
    ii. Add secondary (anti-rabbit HRP 1:30,000 if using anti-NC1) to 20 mL of PBST
    iii. Shake gently at RT for 1 hour
    iv. Wash blot 3X for 10 min with 20 mL PBST
h. Detection
    i. I use ECL2 blotting solution
    ii. Mix 37.5 uL of Sol B with 1.5 mL of Sol A
    iii. Put membrane on one side of a clear envelope with the protein side up
    iv. Add the ECL buffer to the edge of the blot

v. Slowly close the envelope to spread the buffer over the entire blot and check for bubbles
vi. Cover with foil and let sit for 45 min.

i. Imaging
    i. Rinse blot 2X with water
    ii. Keep blot in water to keep wet
    iii. Image blot on the typhoon
        1. Make sure to place the blot with the protein side down on the Typhoon

A.2 Protocol for making heme depleted media

1. Thaw conical of serum
2. Make 1M ascorbic acid stock:
    a. 1.76 g into 10 mL H2O
3. Remove 1 mL of serum for hemochromogen assay
4. Add ascorbic acid to media 100 mM final concentration
    a. For 20 mL of FBS: 2 mL ascorbic acid + 18 mL FBS
5. Vortex and leave at RT for 2 hrs
6. Make 2 L of 1X of PBS
7. Dialyze overnight exchanging PBS after 2 hours
8. Remove 1 mL of serum for hemochromogen assay
9. Add to media and filter sterilize
    a. 20mL of FBS into 200mL of media
    b. add 2 mL of penicillin/streptomycin

A.3 Code for MATLAB for cellular pri-miRNA assay

```
clear all
clc

% 1. Load two data images
info = imfinfo('mcherry_5.tif');
Ia=imread('mcherry_5.tif');
Ib=imread('yfp_5.tif');
frame = size(info,1);
row=info(1,1).Height;    % row size of the image
column=info(1,1).Width;  % column size of the image
% 1. end

% 2. Generate original file
max_a=max(Ia(:));
min_a=min(Ia(:));
max_b=max(Ib(:));
min_b=min(Ib(:));

if max_a >=  max_b;
    max_val= max_a;
else
    max_val= max_b;
end

if min_a <= min_b;
    min_val = min_a;
else
    min_val = min_b;
end

%imtool(Ia, [min_val max_val]);
%imtool(Ib, [min_val max_val]);
% 2. end

% 3. generate two image's perimeter and label them
I_eq_a = adapthisteq(Ia);  % enhances the contrast of the grayscale image
I_eq_b = adapthisteq(Ib);
bw_a = im2bw(I_eq_a, graythresh(I_eq_a)); %converts the grayscale image I to
a binary image
bw_b = im2bw(I_eq_b, graythresh(I_eq_b));
bw2_a = imfill(bw_a,'holes'); % fill the small dot
bw2_b = imfill(bw_b,'holes');
bw3_a = imopen(bw2_a, ones(5,5)); % morphological opening, size 5 X 5
bw3_b = imopen(bw2_b, ones(5,5));
bw4_a = bwareaopen(bw3_a, 80);  % removes images which have fewer than 40
pixel
bw4_b = bwareaopen(bw3_b, 80);
bw4_perim_a = bwperim(bw4_a);  % return perimeter
bw4_perim_b = bwperim(bw4_b);
overlay1_a = imoverlay(I_eq_a, bw4_perim_a, [.3 1 .3]); % overlay a binary
mask onto an I_eq_a
overlay1_b = imoverlay(I_eq_b, bw4_perim_b, [.3 1 .3]);
imtool(overlay1_a);
imtool(overlay1_b);
fprintf('threshold of image 1 is %d.\n', graythresh(I_eq_a));
fprintf('threshold of image 2 is %d.\n', graythresh(I_eq_b));
```

```
val=input('If you want to use those value, press 0. Otherwise press anything
: ');

while val~= 0;
    threshold_a=input('Assign threshold for image 1 : ');
    threshold_b=input('Assign threshold for image 2 : ');
    I_eq_a = adapthisteq(Ia);  % enhances the contrast of the grayscale image
    I_eq_b = adapthisteq(Ib);
    bw_a = im2bw(I_eq_a, threshold_a); %converts the grayscale image I to a
binary image
    bw_b = im2bw(I_eq_b, threshold_b);
    bw2_a = imfill(bw_a,'holes'); % fill the small dot
    bw2_b = imfill(bw_b,'holes');
    bw3_a = imopen(bw2_a, ones(5,5)); % morphological opening, size 5 X 5
    bw3_b = imopen(bw2_b, ones(5,5));
    bw4_a = bwareaopen(bw3_a, 80);  % removes images which have fewer than 40
pixel
    bw4_b = bwareaopen(bw3_b, 80);
    bw4_perim_a = bwperim(bw4_a);  % return perimeter
    bw4_perim_b = bwperim(bw4_b);
    overlay1_a = imoverlay(I_eq_a, bw4_perim_a, [.3 1 .3]); % overlay a
binary mask onto an I_eq_a
    overlay1_b = imoverlay(I_eq_b, bw4_perim_b, [.3 1 .3]);
    imtool(overlay1_a);
    imtool(overlay1_b);
    val=input('If you want to use those value, press 0. Otherwise press
anything : ');
end

Im_or = bw4_a .* bw4_b;
Im_and = bw4_a + bw4_b;
Label_or=bwlabeln(Im_or);
Label_and=bwlabeln(Im_and);
% 3. end

% 4. Generate adequate perimeter for both images
% 2 criteria to choose cell
% 1) If two chosen cells are common for both images, choose smaller one
% (Intersection of cells)
% 1) is performed above in  Im_or = bw4_a .* bw4_b;

% 2) If either one cell is chosen, select it and
% 2) process is in below
% Label cells in Im_and = bw4_a + bw4_b;
% Drop cells by label it by Label_and=bwlabeln(Im_and);
for i=1:row;
    for j=1:column;
        if Im_and(i,j) == 2; % if cells are common, drop it
            X=Label_and(i,j); % Label the cell, common for both images
            Label_and2=Label_and-X; % dropping labeled cell
            Label_and3=Label_and2 .* Label_and; % Multiply two images to drop
both backGND and the cell you want to drop
            Label_and4=bwlabeln(Label_and3); % Label again for next dropping
            Label_and5=im2bw(Label_and4);
            Im_and=Im_and.*Label_and5;
        end
    end
```

```
end

Im_tot=Im_or+Im_and;
Im_tot_perim= bwperim(Im_tot);
overlay1_c = imoverlay(I_eq_b, Im_tot_perim, [.3 1 .3]);
imtool(overlay1_c);
Label_Im_tot=bwlabeln(Im_tot);
cell_number=max(Label_Im_tot(:));
fprintf('%d cells are detected.\n', cell_number);
% 4. end

% 5. Background correction (didn't count cell's intensity but only count BG's
average)
Ia=double(Ia);
Ib=double(Ib);
BGsum_a=0;
BGsum_b=0;
BGcount_a=0;
BGcount_b=0;
for i=1:row
    for j=1:column
        if Label_Im_tot(i,j) == 0;
            BGsum_a=BGsum_a + Ia(i,j);
            BGcount_a=BGcount_a + 1;

            BGsum_b=BGsum_b + Ib(i,j);
            BGcount_b=BGcount_b + 1;
        end
    end
end
BG_avg_a=BGsum_a/BGcount_a;
BG_avg_b=BGsum_b/BGcount_b;

BG_crt_Ia=Ia-BG_avg_a;
BG_crt_Ib=Ib-BG_avg_b;
% 5. end

% 6. Get average intensity of each cell
sum=zeros(cell_number,2);
count=zeros(cell_number,2);
avg_intensity=zeros(cell_number,2);

for i=1:max(Label_Im_tot(:));
    for j=1:row
        for k=1:column
            if Label_Im_tot(j,k) ==i
                sum(i,1)=sum(i,1)+BG_crt_Ia(j,k);
                count(i,1)=count(i,1)+1;

                sum(i,2)=sum(i,2)+BG_crt_Ib(j,k);
                count(i,2)=count(i,2)+1;
            end
        end
    end
    avg_intensity(i,1)=sum(i,1)/count(i,1);
    avg_intensity(i,2)=sum(i,2)/count(i,2);
end
```